Université du Québec

Institut national de la recherche scientifique

INRS-Énergie Matériaux et Télécommunications

Millimeter-wave Electromagnetic Band-gap Structures for Antenna and Antenna Arrays Applications

by

Mu'ath J. Al-Hassan

A dissertation submitted in partial fulfillment of the requirements
for the degree of Doctor of Philosophy (Ph.D.) in Telecommunication Engineering

Evaluation Jury

External examiner	Prof. Chan-Wang Park Université de Québec à Rimouski (UQAR)
External examiner	Prof. Khelifa Hettak Communication Research Center Canada (CRC)
Internal examiner	Prof. Serioja Ovidiu Tatu INRS-Énergie Matériaux et Télécommunications
Research co-director	Prof. Abdel Razik Sebak Concordia University
Research director	Prof. Tayeb A. Denidni INRS-Énergie Matériaux et Télécommunications

ABSTRACT

Recently, communication systems and applications have been driven toward the millimeter-wave band (MMW). In addition to the emerging demands of compact, high-speed, and large bandwidth systems, the crowd of RF bands, and the commercial availability of MMW components have made the MMW band a suitable choice for many short-range wireless applications. Moreover, compared to the ultra-wide band (UWB), MMW bands are free of major interference sources that UWB systems may suffer from.

However, and from antenna designers' point of view, MMW bands suffer from the high attenuation characteristics associated with these bands. Therefore, researchers have proposed several techniques to overcome this problem. Nevertheless, most of these techniques have proven major drawbacks that negatively affect the antenna performance.

Furthermore, and due to the compact sizes of the circuits and components at the MMW bands, the mutual coupling between antenna array elements has becomes a big concern that deteriorates the efficiency of the communications systems, especially in multiple-input-multiple output (MIMO) systems, where it has been proven that mutual coupling strongly affects the systems capacity.

Therefore, the main research in this thesis work consists of several investigations and techniques on increasing the gain and improving the radiation characteristics of complex-structured MMW antennas by using Electromagnetic Band-Gap (EBG) structures. Experimental results show the advantages of these techniques over those exist in the literature.

Moreover, the applications of Mutual-coupling reduction in Antenna arrays at MMW wave bands new compact EBG unit-cell is introduce in this work. It has been proven to effectively reduce the mutual coupling between antenna array elements at MMW bands.

Reconfigurable radiation pattern antennas are in the scope of this work. Their ability to meet the demands of emerging communication systems and applications by producing diversity in radiation pattern, polarization, and frequency made them very attractive to be used in the MMW bands.

To my parents; Rima and Jodei;

To my brothers Moayyad & Mohammed, and my sisters Ruba & Rahaf.

ACKNOWLEDGMENT

First and foremost, I would like to express my deepest gratitude to my supervisor, Prof. Tayeb A. Denidni who has been a tremendous mentor for me. I really appreciate his continues support, aspiring guidance, invaluably constructive criticism, and immense knowledge. I would like to thank you for encouraging my research and allowing me to grow up as a researcher.

Beside my supervisor, I would like to acknowledge with much appreciation my co-supervisor Prof. Abdel Razik Sebak. He continually and persuasively helped me in all the time of research and writing this thesis.

In addition, I would like to thank the rest of my committee: Prof. Chan-Wang Park, Prof. Khelifa Hettak, and Prof. Serioja Ovidiu Tatu for their encouragements, insight comments and suggestions. I also want to thank you for letting my defense be an enjoyable moment.

Special thanks to my family. Words cannot express how grateful I am to my mom, father, brothers and sisters for all the sacrifices that you have made on my behalf. Your prayers for me were what sustained me thus far.

Last but not the least, my sincere thanks go to my colleagues for our constructive discussions, exchanges of knowledge and venting of frustration during my PhD program.

Finally special thanks to those who helped me in developing this thesis.

Table of Contents

List of Figures

List of Tables

RESUME

Ce chapitre résume les travaux de recherche effectués dans le cadre de ma thèse en commençant par présenter les motivations de mon projet de recherche. Ensuite, les problèmes et les objectifs des travaux sont identifiés avec des solutions proposées et discutées. Puis, les contributions du projet sont présentées. Enfin, les grandes lignes du projet de recherche sont établies.

Motivations

Les bandes millimétriques (MMW) ont attiré beaucoup l'attention des chercheurs au cours des dernières années. D'ailleurs ils ont un grand potentiel pour répondre aux besoins émergents des systèmes de communication sans fil. À part de la communication à grande vitesse et la largeur de bande, les systèmes de communication sans fil dans la bande des 60 GHz permettent l'intégration des antennes compactes et à haut rendement. Ces attributs font d la bande 60 GHz un choix approprié pour de nombreux applications sans fil à courte portée.
Selon une étude récente [2], les communications à 60 GHz présentent plusieurs avantages par rapport aux communications UWB:

- La coordination internationale pour les spectres de fréquences est difficile pour l'exploitation UWB par rapport aux communications à 60 GHz.

- Les systèmes UWB peuvent causer des interférences pour les systèmes WLANs à 2,4 GHz et 5 GHz (bandes sans licence), tandis que les bandes à 60 GHz sont libres des principales sources d'interférence.

- Pendant que les systèmes UWB peuvent fournir des débits de données jusqu'à 480 Mbps, les appareils à 60 GHz sont capables de fournir des débits de l'ordre de plusieurs Gbps.
- En raison de la perte de trajet qui dépend fortement de la fréquence centrale, la

puissance du signal reçu peut montrer beaucoup plus de variations dans le spectre de signaux UWB (où le spectre peut varier entre 3,1 GHz et 10,6 GHz), tandis que la gamme dynamique de perte du trajet sur les fréquences à 60 GHz est considérablement plus faible.

Cependant, certains obstacles se dressent dans l'application commerciale des bandes MMW. Les fortes pertes de conducteur des bandes MMW détériorent l'efficacité de radiation des antennes métalliques classiques. Un autre obstacle auquel fait face l'application des bandes MMW est la caractéristique d'atténuation élevée. Étant donné que la longueur d'onde de la bande à 60 GHz se trouve au voisinage de 5 mm, on peut s'attendre à un taux élevé d'atténuation due aux pertes sur le trajet. En outre, aux bandes MMW, l'atténuation due à l'absorption des molécules d'oxygène est importante.

En passant à des réseaux d'antennes opérant dans bandes MMW, le couplage mutuel entre les éléments rayonnants dans les réseaux devient sévère en raison de la compacité des systèmes. Le couplage mutuel a des effets négatifs sur la capacité et l'efficacité des systèmes de communications en ondes millimétriques.

Dans ce contexte, on propose dans cette thèse plusieurs solutions originales pour surmonter les difficultés dans les systèmes de communication en ondes millimétriques.

Problèmes et Objectifs de Recherche

Plusieurs techniques ont été proposées afin d'augmenter le gain d'une antenne et réduire les lobes secondaires. Parmi ces techniques, on peut citer l'utilisation d'un conducteur électrique parfait (PEC) en tant que support réflecteur pour minimiser le niveau du lobe arrière et accroitre le gain [3-7]. Habituellement, le réflecteur PEC est placé à un quart de la longueur d'onde guidée par rapport à l'antenne source. Dans une antenne, combiner une couche à fente avec un réflecteur PEC forme un guide d'onde. Ceci provoque une fuite d'énergie entre les plaques parallèles; par conséquent l'apparition des lobes secondaires et la dégradation du rendement de l'antenne [5-8]. En

outre, une couche arrière de support avec des cavités métalliques fermées [9] ou l'insertion des broches autour de l'ouverture [10] sont considérées comme des techniques conventionnelles afin de réduire le lobe arrière et augmenter le gain de l'antenne. Cependant, ces techniques constituent un véritable défi en bandes millimétriques à cause de la complexité de fabrication et à la réduction de la largeur de bande à travers les résonances qui peuvent en survenir [3].

Pour faire face à ces problèmes, une nouvelle approche scientifique s'est dirigée vers l'utilisation des matériaux à base de surface à haute impédance HIS (High Impédance Surface) [11]. Les HIS sont des matériaux composites artificiels qui présentent de nouvelles et uniques caractéristiques qui ne sont pas réalisables à partir de matériaux conventionnels. Ils sont généralement formés par des motifs métalliques périodiques, comme un réseau de patch ou de ruban, imprimés sur des substrats diélectriques. Plus spécifiquement, les matériaux à bande interdite électromagnétique (BIE) forment un sous-ensemble des matériaux HIS. Ils ont la propriété de contrôler la propagation des ondes électromagnétiques. Ces structures peuvent jouer un rôle de filtre fréquentiel et de filtre spatial [3]. Ces caractéristiques ont permis l'utilisation des matériaux BIE dans la conception d'antennes avec une bonne efficacité, un gain plus élevé et des lobes secondaires réduites [12, 13]. Les BIE sont également connues d'avoir une bande de fréquence dans laquelle une onde plane incidente est réfléchie avec une phase de réflexion égale à zéro degré [8, 14-18].

Cette caractéristique unique permet aux BIE d'avoir un comportement similaire à un conducteur magnétique parfait (CMP) sur une bande de fréquence limitée [8]. Les CMP, qui n'existent pas dans la nature, possèdent trois caractéristiques intéressantes. Premièrement, les courants d'image sont en phase avec ceux d'origine; par conséquent, ils peuvent remplacer les réflecteurs PEC et améliorer l'efficacité de l'antenne dans le champ lointain [8]. Deuxièmement, dans le cas où ils sont utilisés comme des réflecteurs, les modes de plaques parallèles d'ordres supérieurs peuvent être supprimés en choisissant la bonne distance entre l'antenne et le CMP, tout en gardant le mode dominant non affecté [8, 19-22]. Troisièmement, les CMP éliminent la propagation et la diffusion des ondes de

surface en fournissant une haute impédance de surface équivalente, et par conséquent, ils améliorent le rayonnement de l'antenne et réduisent les effets de diffusion de bord [8]. La réalisation physique d'un CMP sur une bande de fréquence finie est connue comme conducteur magnétique artificiel (CMA) [20]. Les CMA ont récemment eu une énorme attention dans la littérature [18, 19, 23, 24].

L'utilisation d'une couche de support en matériaux HIS pour les antennes filaires a été un sujet de recherche très intéressant dans la littérature. Dans [19], une antenne dipôle directionnel soutenue avec une surface BIE a été proposée. L'antenne proposée a une large bande passante et des caractéristiques de rayonnement améliorées. Une antenne dipôle avec une couche support BIE avec de meilleures performances en termes de bande passante et de rayonnement a également été étudiée dans [7]. Dans [4], une antenne à guide d'ondes coplanaires alimentée à travers une fente et soutenue avec une couche AMC a été présentée. Les résultats montrent que le maintien d'une antenne annulaire à fente avec un réflecteur BIE augmente le gain et améliore le rapport entre le lobe principal et le lobe arrière. Il a été également démontré que les réflecteurs CMA augmentent le gain de l'antenne par 3 dB. Une antenne annulaire à fente utilisant un réflecteur BIE avec un lobe unidirectionnel et un gain amélioré a également été proposée dans [3]. Dans les études précédentes, le principe essentiel de l'amélioration des caractéristiques de l'antenne était l'utilisation des structures périodiques comme plan de masse pour améliorer l'adaptation d'impédance et rediriger le rayonnement de l'arrière vers l'avant. Passant aux antennes planaires, les caractéristiques de rayonnement d'une antenne patch sur une surface EBG ont été étudiées dans [25]. Un réseau d'antennes à résonateur diélectrique (DRA) sur une surface CMP a été introduit dans [26], dans lequel il a été montré que l'utilisation d'une couche CMP pour un DRA réduit le couplage mutuel et augmente la directivité du réseau. Les travaux du projet mentionné ci-dessus ont été appliqués à des structures d'antenne simple à une seule couche.

Les problèmes mentionnés précédemment concernent principalement les antennes en ondes millimétriques avec un seul élément. Cependant, pour les réseaux d'antennes, le problème de couplage mutuel apparait à cause de la grande proximité entre les éléments

du réseau. Le couplage mutuel se réfère aux interactions électromagnétiques entre les éléments d'un réseau d'antennes. Le couplage mutuel apparait lorsque les éléments d'antenne sont étroitement espacés causant ainsi des effets négatifs sur l'intégrité du signal et sur la capacité du canal [27]. Dans [28, 29], il a été démontré que le couplage mutuel entre les éléments d'antenne a un impact négatif sur la capacité des canaux sans fil MIMO. Le niveau de couplage mutuel dépend de plusieurs paramètres tels que la distance entre les éléments, la forme du rayonnement de l'élément, et la géométrie du réseau. Plusieurs techniques ont été rapportées sur la réduction du couplage mutuel dans les réseaux d'antennes. Une de ces techniques est l'utilisation des structures BIE.

L'objectif de ce travail est d'étudier de manière approfondie l'utilisation des BIE pour améliorer les caractéristiques du rayonnement des antennes multicouches dans la bande millimétrique. Jusqu'à présent, le support des réseaux d'antennes complexes et multicouches par des surfaces CMA fait l'objet d'un nombre limité de travaux de recherche. À titre d'exemple, le travail publié dans [8] est la première étude où l'application des surfaces CMA dans une structure multicouche a été considérée. En effet, une antenne patch alimentée par une ligne micro ruban à travers une fente soutenue avec une couche CMA a été proposée. L'objectif principal du [8] était donc d'étudier la relation entre les propriétés de réflexion de la surface CMA et le diagramme de rayonnement du réseau d'antennes patch. Notre objectif se concentre principalement sur l'augmentation du gain et la réduction du niveau du lobe arrière en utilisant une nouvelle surface AMC plus stable et avec une bande passante large.

Notre démarche s'appuie sur les deux propriétés des BIE, à savoir la réflexion en-phase et l'écart de la bande. Cette dernière propriété n'autorise aucune propagation des ondes électromagnétiques et ceci afin d'éliminer la propagation des ondes de surface dans les antennes multicouches dans la bande millimétrique. Les travaux [11, 32] ont proposé de placer une structure BIE compacte et uni-planaire (UC- BIE) autour d'une antenne micro-ruban avec ouverture couplée. Les résultats n'ont montré aucune amélioration de gain, ou de réduction du lobe arrière. Ces résultats sont expliqués par le fait que les UC- BIE peuvent supprimer seulement les ondes de surface TE lorsque TM_{00} est le mode

dominant dans les ondes de surface avec une fréquence de coupure égale à zéro. Par conséquent, une structure UC-EBG ne fonctionnera jamais avec une antenne qui excite les ondes de surface TM et TE [34]. Cependant, dans ce travail, nous utilisons une nouvelle structure BIE en forme de « Mushroom », avec des trous « vias » pour supprimer les ondes de surface [11].

Le couplage mutuel (MC) fait référence aux interactions électromagnétiques entre les éléments d'un réseau d'antennes. Le MC a un effet sur les performances du réseau d'antennes ; ceci se fait en changeant l'impédance de l'entrée des éléments rayonnants, le gain, le niveau des lobes secondaires ainsi que le diagramme de rayonnement. Afin de maximiser la capacité du canal et d'améliorer le rapport signal-sur-bruit dans un système multi-entrée-multi-sortie (MIMO), où les signaux subissent des différents évanouissements, l'espacement inter-antennes doit être égale à la moitié de la longueur d'onde. Toutefois, cette condition donne un couplage mutuel fort et nécessite un haut niveau d'isolation entre les antennes pour réduire la cécité du balayage «scan blindness ». En effet, le couplage mutuel doit être réduit de manière efficace afin d'obtenir une meilleure performance des systèmes où les antennes d'émission et de réception fonctionnent dans la même bande de fréquence et aussi sont placées l'un à coté de l'autre.

Dans le régime des ondes millimétriques (MMW), en raison de la courte distance entre les éléments du réseau, le processus de fabrication est plus difficile, et les tolérances seront plus sévères. Par conséquent, la présence d'une structure BIE devient très difficile. De plus, la largeur de bande associée à la bande MMW a besoin d'une structure BIE avec une large "band-gap" pour supprimer efficacement les ondes de surface et améliorer l'isolation sur toute la largeur de la bande. Par conséquent, un autre objectif de ce travail est de concevoir une nouvelle et compacte structure BIE opérant en ondes millimétriques et avec une grande largeur de bande pour réduire le MC entre des antennes rapprochées.
Un autre objectif principal de cette thèse est de concevoir une antenne MMW à diagramme de rayonnement reconfigurable en utilisant la technologie EBG. La reconfiguration du diagramme de rayonnements réfère à la capacité de l'antenne à

modifier ses caractéristiques en utilisant des moyens électroniques, mécaniques et etc. Ça peut être réalisé par plusieurs techniques comme des diodes à commutation, des charges réactives variables, MEMS, etc. Cette approche permet d'avoir plusieurs avantages comme la possibilité de réduire le niveau des interférences, l'économie d'énergie, la réduction de la taille de l'antenne, l'augmentation du gain, et fabrication à un cout moindre. De plus, la reconfigurabilité du diagramme de rayonnement est utile pour couvrir des angles de balayage assez importants dans un système de communication sans fil et peut être utilisée pour maintenir une meilleure qualité de transmission dans des conditions difficiles et imprévisibles.

D'autre part, pour la conception des antennes reconfigurables avec un diagramme de rayonnement variable, de nombreux défis sont présents dont on peut citer:

- Avoir la fonctionnalité souhaitée du mécanisme qui permet la reconfiguration (par exemple l'utilisation des diodes à commutation).
- L'intégration de cette fonctionnalité avec l'antenne d'une façon efficace et rentable.
- L'orientation de la direction du diagramme de rayonnement vers des angles importants nécessite de grandes structures d'antennes.
- Incorporation des dispositifs actifs en ondes millimétriques exige une conception minutieuse.
- À cause de la proximité entre le circuit de commutation et l'élément de rayonnement aux ondes millimétriques, les interactions électromagnétiques puissent changer radicalement les caractéristiques opérationnelles des dispositifs actifs et aussi celles de l'antenne.

Dans ce contexte, notre objectif principal est de concevoir une antenne compacte, efficace et reconfigurable opérant ondes millimétriques avec un grand balayage du faisceau principal et aussi avec un nombre minimal de dispositifs actifs.

Contribution des travaux de thèse

Récemment, les systèmes de communication sans fil et leurs applications en ondes millimétriques ont connu un intérêt considérable. En plus de nombreuse demandes pour des systèmes compacts, à grande vitesse, et à grandes largeurs de bande ont fait des ondes millimétriques un choix approprié pour plusieurs applications sans fil. Cependant, les caractéristiques de rayonnement et du couplage mutuel restent des préoccupations majeures. Pour surmonter le problème d'atténuation associée à ces bandes, les antennes à gain élevé pourraient être utilisées. Quant au couplage mutuel en ondes millimétriques, qui affecte considérablement la capacité du canal de propagation de ces systèmes, les structures EBG pourrait considérées comme une solution efficace.

Pour surmonter ces problèmes, ce projet étudie l'utilisation des propriétés des structures BIE. Donc, le travail dans le cadre de cette thèse vise à développer des points suivants:

- L'utilisation des structures BIE avec des antennes à une seule couche. Ce travail est considéré comme l'un des premières contributions scientifiques basées sur l'utilisation des structures BIE dans les d'antenne multicouches en vue d'augmenter le gain et améliorer les caractéristiques de rayonnement.
- Ce projet examine également la réduction du couplage mutuel entre les éléments d'un réseau d'antennes à 60 GHz utilisant des structures BIE. Ceci est considéré comme une tâche difficile accuse de la proximité des éléments d'antennes en ondes millimétriques. Pour cela, on a proposé une nouvelle cellule compacte de BIE pour réduire efficacement le couplage mutuel. À notre connaissance, cette idée n'a jamais encore été explorée, ce qui représente une contribution très importante dans le cadre de cette thèse.
- Ce projet examine également la conception des antennes reconfigurables avec un diagramme de rayonnement variable. Le but est de produire une diversité en termes de diagrammes de rayonnement. Pour cela, on a effectué des travaux de recherche visant à exploiter les structures EBG pour contrôler le diagramme de

rayonnement afin d'assurer un balayage électronique du faisceau principale, ce qui constitue une autre contribution dans le domaine des antennes millimétriques.

Organisation de la thèse

Cette thèse est organisée en sept chapitres. Le premier chapitre présente l'introduction du projet de recherche effectué dans le cadre de cette thèse. Ensuite la thèse suit l'organisation suivante :

Le **chapitre** 2 présente une nouvelle antenne à résonateur diélectrique à ouverture couplé (ACDR) soutenue avec surface AMC et un gain élevé. Cette antenne génère de meilleures caractéristiques en termes de radiation. La méthodologie de conception et les résultats expérimentaux sont présentés et discutés.

Chapitre 3 présente une autre approche pour augmenter le gain et renforcer les caractéristiques de radiation de l'antenne ACDR utilisant les techniques BIE. Encore une fois, l'approche de cette conception et les résultats expérimentaux sont présentés.

Dans le **chapitre** 4, une nouvelle structure BIE est présentée. La structure BIE proposée n'utilise pas de trous d'interconnexion métalliques ou des composantes verticales, et elle est formé par la gravure de deux fentes et l'ajout de deux ponts reliés à une cellule unitaire classique uni-planaire BIE.

Les résultats démontrent que la structure BIE proposée a une taille compacte par rapport aux autres structures BIE rapportées dans la littérature. Ils montrent aussi une diminution significative du niveau de couplage.
Dans le **chapitre** 5, un nouvel isolateur hybride est présenté pour réduire le couplage mutuel (MC) entre deux antennes à résonateur diélectrique (DR) rapprochées. L'isolateur hybride proposé comprend une nouvelle structure uni-plane BIE et un absorbant.

Le **chapitre** 6 présente une nouvelle antenne reconfigurable utilisant un résonateur

diélectrique (DR) et une structure BIE qui permet de produire un balayage électronique. Six secteurs BIE sont placés symétriquement autour de l'antenne DR. Les résultats montrent le balayage du faisceau.

Chapitre 7 présente les conclusions et traite les travaux futurs.

References

[1] A. Perron, T. A. Denidni and A. R. Sebak, "High Gain Hybrid Dielectric Resonator Antenna for Millimeter-Wave Applications: Design and Implementation", IEEE Trans. Antennas and Propag., vol. 57, no. 10, pp. 2882-2892, Oct. 2009.

[2] S. K. Yong, P. Xia, and A. V. Garcia, 60 GHz Technology for Gbps WLAN and WPAN: From Theory to Practice, 1st edition, Wiley, 2011.

[3] F. Elek, R. Abhari, and G. V. Eleftheriades, "A uni-directional ring-slot antenna achieved by using an electromagnetic band-gap surface," IEEE Trans. Antennas Propag., vol. 53, no. 1, pp. 181–190, Jan. 2005.

[4] J. Joubert, J. C. Vardaxoglou, W. G. Whittow, and J. W. Odendaal, "CPW-fed cavity-backed slot radiator loaded with an AMC reflector, IEEE Trans. Antennas Propag., vol. 60, no. 2, pp. 735–742, Feb. 2012.

[5] Y. Yoshimura, "A microstrip line slot antenna," IEEE Trans. Microwave Theory and Techniques, vol.20, issue 11, pp.760-762, Nov. 1972.

[6] M. Qiu, M. Simcoe, and G. V. Eleftheriades, "Radiation efficiency of printed slot antennas backed by a ground reflector," in Proc. 2000 IEEE AP-S Symp. Dig., pp. 1612–1615.

[7] D. Dawn, Y. Ohashi, and T. Shimura, "A novel electromagnetic bandgap metal plate for parallel plate mode suppression in shielded structures," IEEE Microwave Wireless Compon. Lett., vol. 12, no. 5, pp. 166–168, May 2002.

[8] J. Y. Zhang, V. Hagen, M. Younis, C. Fischer, and W. Wiesbeck, "Planar artificial magnetic conductors and patch antennas," IEEE Trans. Antennas Propag., vol. 51, no. 10, pt. 1, pp. 2704–2712, Oct. 2003, Special issue on metamaterials.

[9] A. Vallecchi and G. B. Gentili, “Microstrip-fed slot antennas backed by a very thin cavity,” Microwave Opt. Tech. Lett., vol. 49, no. 1, pp. 247–250, Jan. 2007.

[10] S. Dumanli, C. J. Railton, D. L. Paul, and G. S. Hilton, “Closely spaced array of cavity backed slot antennas with pin curtain walls,” IEEE Microwave Antennas Propag., vol. 5, no. 1, pp. 38–47, Jan. 2011.

[11] Sievenpiper, D., Lijun Zhang; Broas, R.F.J. Alexopolous, N.G., and Yablonovitch, E., “High-Impedance Electromagnetic Surfaces with a Forbidden Frequency Band”, IEEE Trans. Microwave Theory and Techniques, vol. 47, no. 11, pp.2059-2074, Nov. 1999.

[12] G. V. Eleftheriades, A. K. Iyer, and P. C. Kremer, “Planar negative refractive index media using periodically L-C loaded transmission lines,” IEEE Trans. Microwave Theory and Techniques., vol. 50, no. 12, pp. 2702–2712, Dec. 2002.

[13] M. Ermutlu, C. Simovski, M. Karkkainen, P. Ikonen, S. Tretyakov, and A. Sochava, “Miniaturization of patch antennas with new artificial magnetic layers,” in Proc. IEEE Int.Thesis workshop Antenna Technol.:Small Antennas Novel Metamaterials (IWAT), March 2005, pp. 87–90.

[14] F. Yang and Y. Rahmat-Samii, “Reflection phase characterization of an electromagnetic bandgap (EBG) surface,” in Proc. IEEE AP-S Int. Symp., Jun. 16–21, 2002, vol. 3, pp. 744–747.

[15] R. E. Collin and F. J. Zucker, Antenna Theory. Part 2. New York: McGraw-Hill, 1968.

[16] D. J. Hoppe and Y. Rahmat-Samii, Impedance Boundary Conditions In Electromagnetics. Boca Raton, FL: CRC, 1995.

[17] Al-Nuaimi, Mustafa K., Taher, Whittow, William G., “Low profile dipole antenna backed isotropic Artificial Magnetic Conductor reflector”, EuCAP 2010 Proceedings of the Fourth European Conference on, 12-16 April 2010, Barcelona, Spain.

[18] C. Caloz, C. C. Chang and T. Itoh, “A Novel Anisotropic Uniplanar Compact Photonic Band-Gap (UC-PBG) ground Plane’, the 31st European Microwave Conference, London 2001.

[19] M. Z. Azad and M. Ali, “Novel wideband directional dipole antenna on a mushroom like EBG structure,” IEEE Trans. Antennas Propag., vol. 56, no. 5, pp. 1242–1250, May 2008.

[20] Y. Zhang, M. Younis, C. Fischer, J.v. Hagen, and W. Wiesbeck, "Artificial Magnetic Conductors as Reflectors for Low Sidelobe Antenna Arrays", Microwave and Optical Technology Letters, vol. 35, no. 4, pp. 267-270, Feb. 2003.

[21] J. D. Shumpert, W. J. Chappell, and L. P. B. Katehi, “Parallel-plate mode reduction in conductor-backed slots using electromagnetic bandgap substrates,” IEEE Trans. Microwave Theory and Techniques., vol. 47, no. 11, pp. 2099–2104, Nov. 1999.

[22] H. Lentz, H. Braun, M. Younis, C. Fischer, W. Wiesbeck, and C. Mavrocordatos, “Concept and realization of an airborne SAR/interferometric radar altimeter system (ASIRAS),” presented at the Geoscience and Remote Sensing Symp., IGARSS’ 2002, Toronto, ON, Canada, June 2002.

[23] A. Perron, T. A. Denidni and A. R. Sebak, “High Gain Hybrid Dielectric Resonator Antenna for Millimeter-Wave Applications: Design and Implementation”, IEEE Trans. Antennas and Propag., vol. 57, no. 10, pp. 2882-2892, Oct. 2009.

[24] S. K. Yong, P. Xia, and A. V. Garcia, 60 GHz Technology for Gbps WLAN and WPAN: From Theory to Practice, 1st edition, Wiley, 2011.

[25] F. Elek, R. Abhari, and G. V. Eleftheriades, “A uni-directional ring-slot antenna achieved by using an electromagnetic band-gap surface,” IEEE Trans. Antennas Propag., vol. 53, no. 1, pp. 181–190, Jan. 2005.

[26] J. Joubert, J. C. Vardaxoglou, W. G. Whittow, and J. W. Odendaal, “CPW-fed cavity-backed slot radiator loaded with an AMC reflector, IEEE Trans Antennas Propag., vol. 60, no. 2, pp. 735–742, Feb. 2012.

[27] Y. Yoshimura, “A microstripline slot antenna,” IEEE Trans. Microwave Theory and Techniques, vol. MTT-20, pp. 760–762, Nov. 1972.

[28] M. Qiu, M. Simcoe, and G. V. Eleftheriades, “Radiation efficiency of printed slot antennas backed by a ground reflector,” inProc. 2000 IEEE AP-S Symp. Dig., pp. 1612–1615.

[29] D. Dawn, Y. Ohashi, and T. Shimura, “A novel electromagnetic bandgap metal plate for parallel plate mode suppression in shielded structures,” IEEE Microwave Wireless Compon. Lett., vol. 12, no. 5, pp. 166–168, May 2002.

[30] J. Y. Zhang, V. Hagen, M. Younis, C. Fischer, and W. Wiesbeck, “Planar artificial magnetic conductors and patch antennas,” IEEE Trans. Antennas Propag., vol. 51, no. 10, pt. 1, pp. 2704–2712, Oct. 2003, Special issue on metamaterials.

[31] A. Vallecchi and G. B. Gentili, “Microstrip-fed slot antennas backed by a very thin cavity,” Microwave Opt. Tech. Lett., vol. 49, no. 1, pp. 247–250, Jan. 2007.

[32] S. Dumanli, C. J. Railton, D. L. Paul, and G. S. Hilton, “Closely spaced array of cavity backed slot antennas with pin curtain walls,” IEEE Microwave Antennas Propag., vol. 5, no. 1, pp. 38–47, Jan. 2011.

[33] G. V. Eleftheriades, A. K. Iyer, and P. C. Kremer, “Planar negative refractive index media using periodically L-C loaded transmission lines,” IEEE Trans. Microwave Theory and Techniques., vol. 50, no. 12, pp. 2702–2712, Dec. 2002.

CHAPTER ONE: INTRODUCTION

This chapter starts by introducing the motivation of this thesis work. Afterwards, research problems and objectives are discussed. The thesis contributions are summarized and finally, an outline of the thesis is presented.

1.1 Motivations

Millimeter-wave (MMW) bands have drastically gained much focus and attracting researchers in the past few years. They have the potential to meet the demands of emerging communication systems and applications. Beside the high-speed, large bandwidth, high-capacity systems and applications, at the 60 GHz band, the integration of compact and high-efficiency antennas is easy. These attributes and others make the 60 GHz band a suitable choice for many short-range wireless applications [1].

In [2], four advantages of 60 GHz communications over UWB communications have been specified as follows:

- International coordination for the operating spectrums difficult for UWB, as opposed to 60 GHz communications.
- UWB systems may suffer from in-band interference from devices such as WLANs at 2.4 GHz and 5 GHz unlicensed bands, while 60 GHz bands are free of major interference sources.
- While UWB systems can provide data rates up to 480 Mbps, 60 GHz devices are capable of providing data rates on the order of several Gbps.
- Due to the path loss which depends tightly on the central frequency, the received signal strength may show considerably larger variations over the spectrum of UWB signals (where the spectrum may range between 3.1 GHz and 10.6 GHz), while the dynamic range of path loss over the spectrum range of 60 GHz systems is considerably lower.

However, some obstacles stand in the way of moving toward the MMW technology and deploying it commercially. The high conductor losses at MMW band deteriorate the radiation efficiency of the conventional metallic antennas. Another obstacle facing the MMW communication systems is the high attenuation characteristics. Since the wavelength at 60 GHz band is in the vicinity of 5 mm, one can expect high attenuation rate due to the path loss. Furthermore, at MMW band, attenuation due to oxygen molecule's absorption is significant.

Moving to antenna arrays, at MMW bands, and due to the compactness of the systems, mutual coupling between the radiating elements in arrays become severe, and has negative effects on the system's capacity and efficiency.

1.2 Research Problem and Objectives

Researchers have proposed several techniques to increase the antenna gain and re-direct the back radiation forward. One of these techniques is to use a perfect electric conductor (PEC) as backing reflector to reduce the back radiation and increase the gain in the forward direction [3-7]. Usually the PEC reflector is placed at a quarter of the guided wavelength from the antenna to obtain constructive radiation addition. In the existence of a slot layer in the antenna, the PEC reflector and the slot layer form a parallel-plate waveguide environment. This yields to parasitic radiation and energy leakage between the parallel plates, which distorts the radiation patterns and degrades the antenna efficiency [5-8]. Moreover, backing the antenna with closed metallic cavities [9], or inserting shorting pins around the aperture [10] are considered as other techniques to reduce the back radiation and increase the antenna gain. However, at MMW band, all these techniques add to the manufacturing complexity and reduce the bandwidth through spurious resonances that may occur [3].

To overcome some of these problems, research compass has recently moved to high-impedance surface (HIS) materials, firstly proposed by Sievenpiper et al. [11]. HISs are artificial composite materials that exhibit unique and novel characteristics, which are not

achievable from conventional materials. They are usually formed by periodic metallic patterns, like array of patches or strips, printed on dielectric substrates. Electromagnetic Band-Gap (EBG) materials are a subset of HIS materials. EBG materials are found to exhibit stopbands, where no electromagnetic-wave propagation is allowed [3]. This feature has made EBG materials suitable to be employed in designing antennas with improved efficiency, higher gain, lower back-lobe and sidelobe levels [12, 13]. EBGs are also found to have a frequency band where an incident plane wave is reflected with zero degrees reflection phase [8, 14-18]. This unique feature makes the EBGs mimic the behavior of a perfect magnetic conductor (PMC) over a limited frequency band [8]. PMCs, which don't exist in nature, have three interesting features. Firstly, the image currents are in-phase with the original ones, and hence; they can replace the PEC reflectors, and increase the antenna efficiency in the far-field [8]. Secondly, when used as reflectors, higher-order parallel-plate modes can be suppressed by choosing the proper distance between the antenna and the PMC, while keeping the dominant mode unaffected [8, 19-22]. Thirdly, PMCs suppress the surface-wave propagation and scattering by providing an equivalent high impedance surface, and hence, improving the antenna radiation and reducing edge scattering effects [8]. The physical realization of a PMC over a finite frequency band is known as artificial magnetic conductor (AMC) [20]. AMCs have recently gained enormous attention in the literature [18, 19, 23, 24].

Backing wire and simple antenna structures with HIS materials has been a research subject in the literature. In [19], a directional dipole antenna backed with an EBG surface has been proposed. The presented antenna shows wideband operation and improved radiation characteristics. An EBG-backed dipole antenna with improved bandwidth and radiation characteristics has been also investigated in [7]. In [4], a coplanar waveguide–fed slot radiator backed with an AMC has been presented. Results show that backing a ring-slot antenna with an EBG reflector, increases the gain, and improves the front-to-back-ratio. It has been also shown that the AMC reflector increases the antenna gain by 3 dBi. An EBG-backed ring-slot antenna with uni-directional pattern and gain improvement has been also proposed in [3]. In the previous studies, the main principle behind enhancing the antenna characteristics was using the periodic structures as ground

planes to improve the impedance matching and re-direct the back radiation forward. Moving to patch antennas, the radiation characteristics of a microstrip patch antenna over an EBG surface has been investigated in [25]. Probe-fed DRA array over a PMC surface has been introduced in [26], in which it has been shown that residing the DRA over a PMC reduces the mutual coupling and increases the directivity of the array. The above mentioned thesis work has been applied to simple and single layer antenna structures.

The aforementioned problems mainly apply to single element MMW antennas. However, for antenna arrays, at MMW bands, and due to the close proximity between the array elements, the problem of mutual coupling appears. Mutual coupling refers to the electromagnetic interactions between the elements of an antenna array. Mutual coupling appears when the antenna elements are closely spaced causing negative effect on signal integrity and channel capacity [27]. In [28, 29] it has been shown that the mutual coupling between antenna elements has a negative impact on the capacity of MIMO wireless channels. The level of mutual coupling depends on several parameters, to name a few: distance between elements, element radiation patterns, and array geometry. Several techniques have been reported on reducing the mutual coupling in antenna arrays. One of these techniques is to use Electromagnetic band-gap (EBG) structures [30, 31].

The objectives of this thesis work are to conduct a thorough investigation on using EBGs to improve the radiation characteristics of multilayer antenna structures at MMW bands. Up to now, Very few studies have reported on backing complicated and multilayer antenna structures by AMC surfaces. The first application of AMC surface as a reflector to multi-layer structure has been presented in [8], where a microstrip-fed aperture-coupled patches antenna array backed with AMC has been investigated in this thesis work. While the main focus of the work in [8] was to investigate the relation between the reflection properties of the AMC surface and the radiation pattern of the patches array, our objective mainly focuses on drastically increasing the gain and reducing the back-lobe level through backing it with a new stable AMC surface, while maintaining a wide bandwidth operation, an important concern at the MMW band.

While the first objective is based on the in-phase reflection property of the EBG, this thesis work aims also at using the EBG band-gap property, where no electromagnetic-wave propagation is allowed, to suppress surface-wave propagation in multilayer antennas at MMW bands. In [32, 33], a uniplanar compact EBG (UC-EBG) lattice has been placed around an aperture-coupled microstrip antenna. Results have shown no gain improvement, or even back-lobe level reduction. This is due to the fact that the UC-EBG can suppress only TE surface-waves, and since the TM_{00} is the dominant mode in surface-waves with zero cut off frequency, UC-EBG will never work with an antenna that excites both TM and TE surface waves [34]. However, in this thesis work, we will use new Mushroom like EBG, with shorting vias that can suppress surface-waves of both polarizations [11].

Mutual-coupling (MC) refers to the electromagnetic interactions between antenna array elements. It has an impact effect on antenna array performance through changing the input impedance of the radiating elements, gain, sidelobe level and radiation pattern shape . In multiple-input-multiple-output (MIMO) systems, for the signals to undergo different fading characteristics, and hence maximizing the channel capacity and improving the signal-to-noise ratio, the maximum interelement spacing in an array must be half of the wavelength. However, this condition yields strong mutual coupling. Moreover, in phased antenna arrays, to alleviate scan blindness, a high level of isolation between the array elements is required. Furthermore, in applications such as imaging radar systems, where the transmitting and receiving antennas operate at the same frequency band and are placed close to each other, the mutual coupling needs to be effectively reduced to achieve better system performance.

At millimeter-wave (MMW) bands, and due to the small absolute interelement spacing in an array, the manufacturing is more difficult and tolerances will be tighter. Therefore, the need of compact and easy-to-fabricate EBG structure becomes very challenging. In addition, the wide bandwidths associated with MMW bands require an EBG structure with wide frequency band-gap in order to efficiently suppress surface waves and improves the isolation over the whole bandwidth.

Consequently, our other objective is to design a new-shape, wide band-gap, compact MMW EBG structure to reduce the MC between closely-spaced antenna elements. .

Another main objective of this dissertation is to design a MMW antenna with reconfigurable radiation pattern by using EBGs. Pattern reconfigurability refers to the ability of the antenna to change/modify its basic pattern characteristics through electrical, mechanical, or other means. It can be achieved through several techniques: switching diodes, variable reactive loadings, MEMS, etc. It has the advantages of avoiding noisy environments, improving security and maneuver away from jamming, power saving, size and cost reduction, and increase diversity gain. Moreover, pattern reconfigurability helps with Wider scanning angles and grating nulls mitigation when incorporated in phased arrays. They also can maintain high quality communication systems in harsh and unpredictable conditions.

On the other hand, many challenges face antenna designer working on pattern reconfigurability:

- Obtaining the desired functionality of the mechanism that enables pattern reconfiguration (e.g. switching diodes).
- Integrating this functionality with the antenna in efficient and cost effective manners.
- Significant pattern direction change needs electrically large antenna structures.
- At MMW bands, incorporating active devices needs sophisticated design, tests and examinations: characterization, biasing circuit, matching circuit.
- Due to the close proximity between the switching circuit and the radiating element at MMW bands, the strong EM interactions drastically change the fundamental operational characteristics of both; active devices and radiating elements. Therefore, affecting the whole functionality of the communication systems.

Therefore, our objective is to Design a low-cost, electrically small, MMW Reconfigurable pattern antenna with wide radiation direction shifts and minimal number of active devices.

1.3 Thesis Contribution

Recently, communication systems and applications have been driven toward the MMW bands. In addition to the emerging demands of compact, high-speed, and large bandwidth systems, the crowd of RF bands, and the commercial availability of MMW components have made the MMW band a suitable choice for many short-range wireless applications. However, radiation characteristics and mutual coupling are still major concerns in this band. There is an increase demand on antennas with high gain and enhanced radiation properties to overcome the high attenuation characteristics associated with these bands. Moreover, mutual coupling at MMWs becomes severe, and drastically affects the systems capacity and efficiency.

This thesis work deals with using EBG properties to overcome the problems associated in the different MMW bands from antenna designers' point of view. The significance of this thesis work arises from the following points:

- Using EBGs with simple and single layer antenna structures have been reported in the literature. However, this thesis work is considered to be one of very few studies about using EBGs in multilayer antenna structures to increase the gain and enhance the radiation characteristics.

- This work deals with using EBGs to reduce mutual coupling between array elements at 60 GHz. This is considered to be challenging in the sense that at such high frequencies, the elements are in very close proximity. Therefore, designers need to design a compact EBG unit-cell that effectively reduces the mutual coupling. To the authors' knowledge, this idea has never been explored yet.

- Reconfigurable radiation pattern antennas have recently gained an increasing attention. Their ability to produce diversity in radiation pattern, polarization, and frequency made them very attractive to be used in wireless communication

systems and applications. Therefore, achieving reconfigurable pattern at MMW bands by using EBGs will be a very good contribution and will add to the significance of this thesis work.

1.4 Thesis Organization

This thesis work is organized in five chapters. The first chapter is an introduction of the thesis work. The motivation of the MMW is presented first. Then, the objectives of the thesis work are discussed. After that the contribution of this thesis work is summarized.

Chapter 2 presents a new MMW aperture-coupled dielectric resonator (ACDR) antenna backed with AMC surface with increased gain and improved radiation properties. Design methodology and experimental results are provided.

Chapter 3 presents another approach to increase the gain and enhance the radiation characteristics of ACDR antenna using EBGs. Again, design approach and experimental results are provided.

In **Chapter 4**, a new MMW, electromagnetic band-gap (EBG) structure is presented. The proposed EBG structure without the use of metallic vias or vertical components, is formed by etching two slots and adding two connecting bridges to a conventional uniplanar EBG unit-cell. Results show that the proposed EBG structure provides size compactness over other EBG structures reported in the literature. Its enhanced performance and applicability to reduce mutual coupling in antenna arrays are then investigated. Results show a drastic decrease in the mutual coupling level.

In **Chapter 5**, a new MMW hybrid isolator is presented to reduce the mutual-coupling (MC) between two closely-spaced dielectric resonator (DR) antennas. The proposed hybrid isolator comprises a new uni-planar compact electromagnetic band-gap (EBG) structure and MMW choke absorber.

Chapter 6 presents a new-concept MMW electromagnetic bandgap (EBG)-based dielectric resonator (DR) antenna with beam steering capability is presented. Six sectorized EBG patterns are placed symmetrically around the DR antenna to achieve beam steering in the azimuth plane. Results show flexible and effective beam steering capability in the azimuth plane using minimal number of diodes.

Chapter 7 gives the conclusion and discusses the ongoing research.

1.5 References

[1] A. Perron, T. A. Denidni and A. R. Sebak, "High Gain Hybrid Dielectric Resonator Antenna for Millimeter-Wave Applications: Design and Implementation", IEEE Trans. Antennas and Propag., vol. 57, no. 10, pp. 2882-2892, Oct. 2009.

[2] S. K. Yong, P. Xia, and A. V. Garcia, 60 GHz Technology for Gbps WLAN and WPAN: From Theory to Practice, 1st edition, Wiley, 2011.

[3] F. Elek, R. Abhari, and G. V. Eleftheriades, "A uni-directional ring-slot antenna achieved by using an electromagnetic band-gap surface," IEEE Trans. Antennas Propag., vol. 53, no. 1, pp. 181–190, Jan. 2005.

[4] J. Joubert, J. C. Vardaxoglou, W. G. Whittow, and J. W. Odendaal, "CPW-fed cavity-backed slot radiator loaded with an AMC reflector, IEEE Trans. Antennas Propag., vol. 60, no. 2, pp. 735–742, Feb. 2012.

[5] Y. Yoshimura, "A microstrip line slot antenna," IEEE Trans. Microwave Theory and Techniques., vol.20, issue 11, pp.760-762, Nov. 1972.

[6] M. Qiu, M. Simcoe, and G. V. Eleftheriades, "Radiation efficiency of printed slot antennas backed by a ground reflector," in Proc. 2000 IEEE AP-S Symp. Dig., pp. 1612–1615.

[7] D. Dawn, Y. Ohashi, and T. Shimura, "A novel electromagnetic bandgap metal plate for parallel plate mode suppression in shielded structures," IEEE Microwave Wireless Compon. Lett., vol. 12, no. 5, pp. 166–168, May 2002.

[8] J. Y. Zhang, V. Hagen, M. Younis, C. Fischer, and W. Wiesbeck, "Planar artificial magnetic conductors and patch antennas," IEEE Trans. Antennas Propag., vol. 51, no. 10, pt. 1, pp. 2704–2712, Oct. 2003, Special issue on metamaterials.

[9] A. Vallecchi and G. B. Gentili, "Microstrip-fed slot antennas backed by a very thin cavity," Microwave Opt. Tech. Lett., vol. 49, no. 1, pp. 247–250, Jan. 2007.

[10] S. Dumanli, C. J. Railton, D. L. Paul, and G. S. Hilton, "Closely spaced array of cavity backed slot antennas with pin curtain walls," IEEE Microwave Antennas Propag., vol. 5, no. 1, pp. 38–47, Jan. 2011.

[11] Sievenpiper, D., Lijun Zhang; Broas, R.F.J. Alexopolous, N.G., and Yablonovitch, E., "High-Impedance Electromagnetic Surfaces with a Forbidden Frequency Band", IEEE Trans. Microwave Theory and Techniques, vol. 47, no. 11, pp.2059-2074, Nov. 1999.

[12] G. V. Eleftheriades, A. K. Iyer, and P. C. Kremer, "Planar negative refractive index media using periodically L-C loaded transmission lines," IEEE Trans. Microwave Theory and Techniques., vol. 50, no. 12, pp. 2702–2712, Dec. 2002.

[13] M. Ermutlu, C. Simovski, M. Karkkainen, P. Ikonen, S. Tretyakov, and A. Sochava, "Miniaturization of patch antennas with new artificial magnetic layers," in Proc. IEEE Int.Thesis workshop Antenna Technol.:Small Antennas Novel Metamaterials (IWAT), March 2005, pp. 87–90.

[14] F. Yang and Y. Rahmat-Samii, "Reflection phase characterization of an electromagnetic bandgap (EBG) surface," in Proc. IEEE AP-S Int. Symp., Jun. 16–21, 2002, vol. 3, pp. 744–747.

[15] R. E. Collin and F. J. Zucker, Antenna Theory. Part 2. New York: McGraw-Hill, 1968.

[16] D. J. Hoppe and Y. Rahmat-Samii, Impedance Boundary Conditions In Electromagnetics. Boca Raton, FL: CRC, 1995.

[17] Al-Nuaimi, Mustafa K., Taher, Whittow, William G., "Low profile dipole antenna backed isotropic Artificial Magnetic Conductor reflector", EuCAP 2010 Proceedings of the Fourth European Conference on, 12-16 April 2010, Barcelona, Spain.

[18] C. Caloz, C. C. Chang and T. Itoh, “A Novel Anisotropic Uniplanar Compact Photonic Band-Gap (UC-PBG) ground Plane’, the 31st European Microwave Conference, London 2001.

[19] M. Z. Azad and M. Ali, “Novel wideband directional dipole antenna on a mushroom like EBG structure,” IEEE Trans. Antennas Propag., vol. 56, no. 5, pp. 1242–1250, May 2008.

[20] Y. Zhang, M. Younis, C. Fischer, J.v. Hagen, and W. Wiesbeck, "Artificial Magnetic Conductors as Reflectors for Low Sidelobe Antenna Arrays", Microwave and Optical Technology Letters, vol. 35, no. 4, pp. 267-270, Feb. 2003.

[21] J. D. Shumpert, W. J. Chappell, and L. P. B. Katehi, “Parallel-plate mode reduction in conductor-backed slots using electromagnetic bandgap substrates,” IEEE Trans. Microwave Theory and Techniques., vol. 47, no. 11, pp. 2099–2104, Nov. 1999.

[22] H. Lentz, H. Braun, M. Younis, C. Fischer, W. Wiesbeck, and C. Mavrocordatos, “Concept and realization of an airborne SAR/interferometric radar altimeter system (ASIRAS),” presented at the Geoscience and Remote Sensing Symp., IGARSS’ 2002, Toronto, ON, Canada, June 2002.

[23] A. Perron, T. A. Denidni and A. R. Sebak, “High Gain Hybrid Dielectric Resonator Antenna for Millimeter-Wave Applications: Design and Implementation”, IEEE Trans. Antennas and Propag., vol. 57, no. 10, pp. 2882-2892, Oct. 2009.

[24] S. K. Yong, P. Xia, and A. V. Garcia, 60 GHz Technology for Gbps WLAN and WPAN: From Theory to Practice, 1st edition, Wiley, 2011.

[25] F. Elek, R. Abhari, and G. V. Eleftheriades, “A uni-directional ring-slot antenna achieved by using an electromagnetic band-gap surface,” IEEE Trans. Antennas Propag., vol. 53, no. 1, pp. 181–190, Jan. 2005.

[26] J. Joubert, J. C. Vardaxoglou, W. G. Whittow, and J. W. Odendaal, “CPW-fed cavity-backed slot radiator loaded with an AMC reflector, IEEE Trans Antennas Propag., vol. 60, no. 2, pp. 735–742, Feb. 2012.

[27] Y. Yoshimura, “A microstripline slot antenna,” IEEE Trans. Microwave Theory and Techniques, vol. MTT-20, pp. 760–762, Nov. 1972.

[28] M. Qiu, M. Simcoe, and G. V. Eleftheriades, “Radiation efficiency of printed slot antennas backed by a ground reflector,” inProc. 2000 IEEE AP-S Symp. Dig., pp. 1612–1615.

[29] D. Dawn, Y. Ohashi, and T. Shimura, “A novel electromagnetic bandgap metal plate for parallel plate mode suppression in shielded structures,” IEEE Microwave Wireless Compon. Lett., vol. 12, no. 5, pp. 166–168, May 2002.

[30] J. Y. Zhang, V. Hagen, M. Younis, C. Fischer, and W. Wiesbeck, “Planar artificial magnetic conductors and patch antennas,” IEEE Trans. Antennas Propag., vol. 51, no. 10, pt. 1, pp. 2704–2712, Oct. 2003, Special issue on metamaterials.

[31] A. Vallecchi and G. B. Gentili, “Microstrip-fed slot antennas backed by a very thin cavity,” Microwave Opt. Tech. Lett., vol. 49, no. 1, pp. 247–250, Jan. 2007.

[32] S. Dumanli, C. J. Railton, D. L. Paul, and G. S. Hilton, “Closely spaced array of cavity backed slot antennas with pin curtain walls,” IEEE Microwave Antennas Propag., vol. 5, no. 1, pp. 38–47, Jan. 2011.

[33] G. V. Eleftheriades, A. K. Iyer, and P. C. Kremer, “Planar negative refractive index media using periodically L-C loaded transmission lines,” IEEE Trans. Microwave Theory and Techniques, vol. 50, no. 12, pp. 2702–2712, Dec. 2002.

CHAPTER TWO: MILLIMETER-WAVE APERTURE-COUPLED DIELECTRIC RESONATOR ANTENNA BACKED WITH ARTIFICIAL MAGNETIC CONDUCTOR SURFACE

2.1 Introduction

Millimeter-wave bands have drastically gained much focus and attracted researchers in the past few years. They have the potential to meet the demands of emerging communication systems and applications. Beside the high-speed, large bandwidth, high-capacity systems and applications, at the 60 GHz band, the integration of compact and high-efficiency antennas is easy. These attributes and others make the 60 GHz band a suitable choice for many short-range wireless applications [1].

However, the high attenuation characteristics associated with the 60 GHz band is a main obstacle in the way of moving toward the MMW technology and deploying it commercially. Therefore, researchers have proposed several techniques to increase the antenna gain and re-direct the back radiation forward. One of these techniques is to use high impedance surface (HIS) materials [2].

HISs are artificial composite materials that exhibit unique and novel characteristics, which are not achievable from conventional materials. They are usually formed by periodic metallic patterns, like array of patches or strips, printed on dielectric substrates.

Electromagnetic Band-Gap (EBG) materials are a subset of HIS materials. EBG materials are found to exhibit stopbands, where no electromagnetic-wave propagation is allowed [3]. This feature has made EBG materials suitable to be employed in designing antennas with improved efficiency, higher gain, lower back-lobe and sidelobe levels [4]. EBGs are also found to have a frequency band where an incident plane wave is reflected with zero degree reflection phase [5]. This unique feature makes the EBGs mimic the behavior of a perfect magnetic conductor (PMC) over a limited frequency band [6]. PMCs, which don't exist in nature, have three interesting features. Firstly, the image currents are in-phase with the original ones, and hence; they can replace the PEC reflectors, and increase the antenna efficiency in the far-field. Secondly, when used as

reflectors, higher-order parallel-plate modes can be suppressed by choosing the proper distance between the antenna and the PMC, while keeping the dominant mode unaffected. Thirdly, PMCs suppress the surface-wave propagation and scattering by providing an equivalent high impedance surface, and hence, improving the antenna radiation and reducing edge scattering effects. PMCs have recently gained enormous attention in the literature [7-9].

2.2 The proposed Artificial Magnetic Conductor Unit Cell

Square-patch artificial magnetic conductor (AMC), shown in Fig.2-1, has been analyzed using the dynamic model [10]. This model is based on calculating the equivalent input surface impedance Z_s. It is defined as the parallel connection of the grid impedance of an array of patches Z_g, and the surface impedance of a conductor-backed dielectric slab Z_d. The dynamic model is more accurate than the simple circuit model presented in [2] since it takes into account the field interactions between all the cells in the AMC. The final formulas will be provided here. Full demonstration is found in the [10, 11]

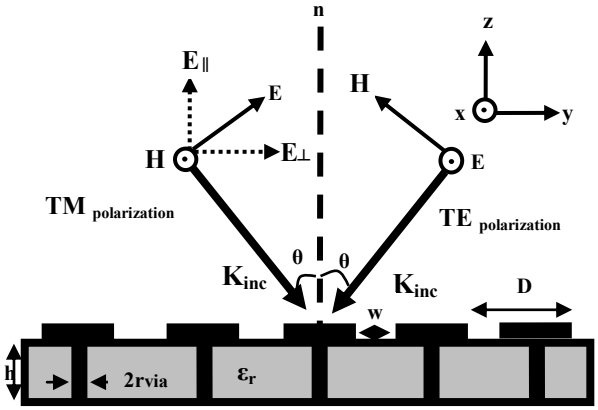

Fig.2-1. Geometry of the proposed AMC structure.

a) TE polarization

When a TE polarized plane-wave impinges on the AMC shown in Fig.2-1, the dielectric slab impedance Z_d^{TE} is given by:

$$Z_d^{TE} = j\frac{\eta}{\sqrt{\varepsilon_r}}\tan(k_{zd}h)\frac{1}{\sqrt{1-\frac{\sin^2\theta}{\varepsilon_r}}} \qquad (1\text{-}1)$$

$$k_{zd} = k\sqrt{\varepsilon_r}\sqrt{1-\frac{\sin^2\theta}{\varepsilon_r}} \tag{1-2}$$

where ε_r is the relative permittivity of the medium, h is the substrate thickness, θ is the angle of incidence, $\eta = \sqrt{\mu_o/\varepsilon_o}$ is the free space wave impedance, k is the free space wave number, and k_{zd} is the vertical component of the wave number of the refracted wave. The grid impedance Z_g^{TE} is given by:

$$Z_g^{TE} = -j\frac{\eta}{2}\frac{1}{\alpha}\frac{2}{(\varepsilon_r+1)}\frac{1}{(1-\frac{k^2}{k^2_{eff}}\frac{\sin^2\theta}{2})} \tag{1-3}$$

where $k_{eff} = k\sqrt{\varepsilon_{eff}}$ is the effective wave number and ε_{eff} is the effective permittivity of the medium.

$$\alpha = \frac{kD}{\pi}\ln\left(\frac{1}{\sin\frac{\pi w}{2D}}\right) \tag{1-4}$$

where α is defined as the grid parameter, D is the AMC period, and w is the gap width between the patches.

b) TM polarization

For the case of TM polarized plane-wave, the dielectric slab impedance Z_d^{TM} is given by:

$$Z_d^{TM} = j\frac{\eta}{\sqrt{\varepsilon_r}}\tan(k_{zd}h)\sqrt{1-\frac{\sin^2\theta}{\varepsilon_r}} \tag{1-5}$$

and the grid impedance Z_g^{TM} is given by:

$$Z_g^{TM} = -j\frac{\eta}{2\alpha}\frac{2}{(\varepsilon_r+1)} \tag{1-6}$$

Our proposed AMC consists of circular patches printed on conductor-backed, ROGERS 3006 (ε_r = 6.15 and tanδ = 0.002) substrate with 0.254 mm thickness. The patch diameter is 0.88 mm with a period of 1.05 mm. The centers of the circular patches are connected to the ground plane through vias with 0.16 mm diameter. The same formulas derived for the square–patch AMC surface will be applied to the proposed AMC by including the effects of the vias, and using proper modifications.

The effect of the vias is polarization dependent. Back to Fig.2-1, for a TE polarized plane-wave, the electric field is always perpendicular to the vias. If the radius of the vias, r_{via} is small, the electric field does not excite them. Therefore, the vias do not have any effect, and the medium between the patches and the ground plane still can be considered as an isotropic dielectric slab.

However, for a TM polarized plane-wave, Fig.2-1 shows that the electric field vector E has two components, $E_{\parallel}$(parallel to the vias) and $E_{\perp}$(perpendicular to the vias). The parallel component of the electric field vector, $E_{\parallel}$, excites the vias. Thus, the effect of the vias needs to be taken into account. Assuming that the vias are thin, and by applying the effective wire medium model, Z_d^{TM} is found to be:

$$z_d^{TM} = j\omega\mu \frac{\tan(\gamma_{TM} h)}{\gamma_{TM}} \frac{k_r^2 - \beta^2 - k_p^2}{k_r^2 - k_p^2} \tag{1-7}$$

$$\gamma_{TM}^2 = \varpi^2 \varepsilon_o \varepsilon_r \mu - \frac{\varepsilon_r}{\varepsilon_n} \beta^2 \tag{1-8}$$

$$\beta = k_d \sqrt{\frac{1}{\varepsilon_r} \sin^2 \theta} \tag{1-9}$$

$$k_p = \frac{1}{D\sqrt{\frac{1}{2\pi} \ln \frac{D^2}{4 r_{via}(D - r_{via})}}} \tag{1-10}$$

$$\varepsilon_n = \varepsilon_r \left(1 - \frac{k_p^2}{k^2 \varepsilon_r}\right) \tag{1-11}$$

where ε_n is the relative permittivity seen by the fields along the normal to the medium, r_{via} is the radius of the via, k_d is the wave vector of the refracted wave and k_r is the wave number in the medium

In [12], it has been shown that for a circular-patch-based AMC with a gap width w, an averaged equivalent rectangular gap width w_{rec} can be approximated and used in the dynamic model formulas for the square patches. It is based on the similarity between the electric field distribution along the edges of the square and circular patches. The two AMC structures must have the same period, same gap, and same dielectric slab properties. The averaged rectangular gap width is given by:

$$\overline{w}_{rect} \cong 0.91w + 0.09D \tag{1-12}$$

The reflection coefficient Γ is related to the equivalent input surface impedance, Z_s as:

$$\Gamma^{TE} = \frac{Z_s^{TE} - \eta\cos\theta}{Z_s^{TE} + \eta\cos\theta}, \Gamma^{TM} = \frac{Z_s^{TM} - \eta/\cos\theta}{Z_s^{TM} + \eta/\cos\theta} \tag{1-13}$$

Our proposed AMC consists of circular patches printed on conductor-backed, ROGERS 3006 (ε_r = 6.15 and tanδ = 0.002) substrate with 0.254 mm thickness. The patch diameter is 0.88 mm with a period of 1.05 mm. The centers of the circular patches are connected to the ground plane through vias with 0.16 mm diameter. The same formulas derived for the square–patch AMC surface will be applied to the proposed AMC by including the effects of the vias, and using proper modifications.

However, for a TM polarized plane-wave, Fig.2-1 shows that the electric field vector E has two components, $E_{\parallel}$(parallel to the vias) and $E_{\perp}$(perpendicular to the vias). The parallel component of the electric field vector, $E_{\parallel}$, excites the vias.

Fig.2- 2 shows a microscopic photo of the fabricated AMC. The plasma decomposition technique is used to fill the vias with copper.

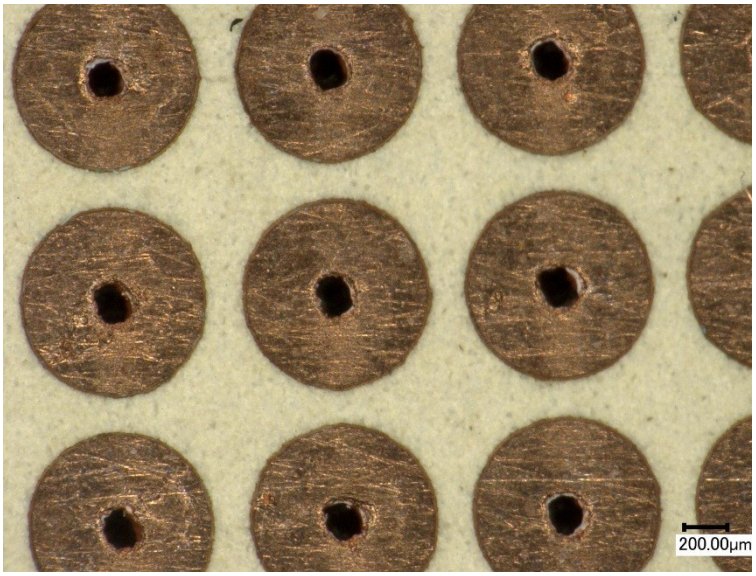

Fig 2-2. Photograph of the fabricated AMC.

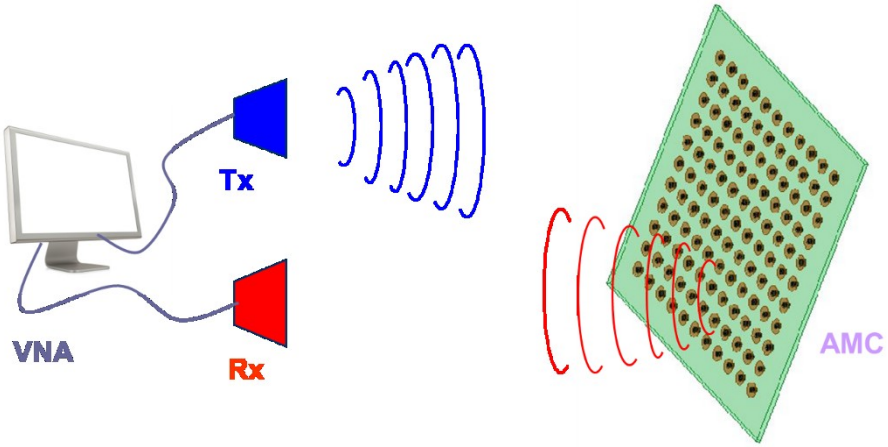

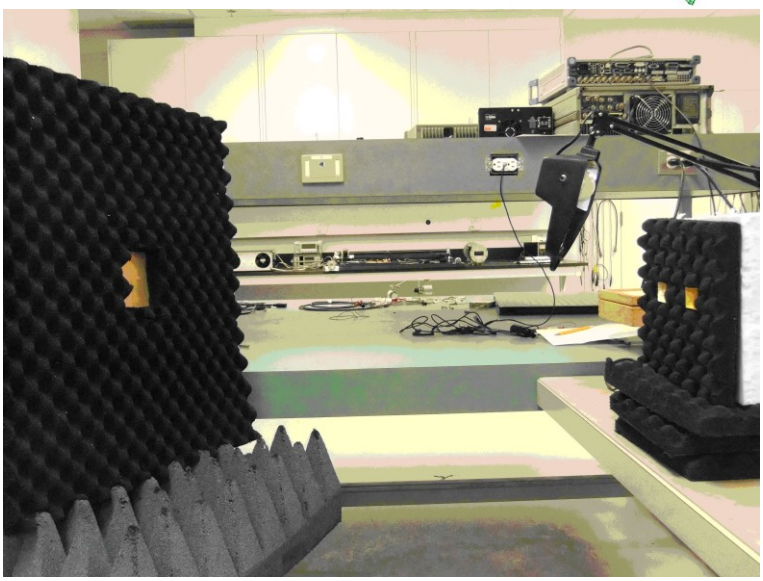

Fig.2-3. Reflection phase measurement set up.

2.3 Reflection Phase Characteristics of the Proposed AMC Surface

The measurement setup used to measure the reflection phase of the proposed AMC surface is shown in Fig. 2-3. The AMC is stacked to a foam board, and surrounded by absorption materials. Two broadband horn antennas operating at 60 GHz band are used as a transmitter and a receiver. In fact, the two horns are separated by an absorption material to reduce the coupling between them. To have a focused plane-wave and achieve accurate results, a large number of patches is fabricated (~ 9000 patches).

The reflection coefficient is measured for various angles of incidence and polarization. The distance between the AMC surface and the two horns is carefully chosen to ensure that the AMC surface is located in the far-field region, and hence; scattered fields in that region are captured. The reflection phase is then measured for various angles of incidence, for both TM and TE polarizations. Its worthy mentioning that when measuring oblique incidence plane-waves, the two horn antennas must be arranged according to the Snell's reflection law, and the two antennas are positioned in a circle according to the angle of incidence.

Since the observation plane (the plane of the horn apertures) and the AMC surface are in different locations, a reference plane must be defined to obtain the reflection phase exactly at the AMC surface. Therefore, a PEC sheet with the same AMC dimensions is placed at the same distance from the observation plane. The reflection phase from the PEC is then measured and used as a reference to the AMC. The AMC reflection phase is calculated by:

$$\phi = \phi^{AMC} - \phi^{PEC} + 180^{o} \tag{1-14}$$

In fact, the 180^{o} takes into account the PEC reflection phase. The reflection phase is measured in the frequency band between 55 and 65 GHz, since the VNA used in the measurements only goes up to 65 GHz.

Fig. 2.4 to Fig. 2.8 show the reflection phase of the proposed AMC obtained from the dynamic model, HFSS full-wave simulator [13], and measurements for various incident angles, for both TM and TE polarizations. The measured reflection phase of this AMC closely matches the theoretical calculation and full-wave simulation results. Tables 2-1

and 2-2 list the stability of the proposed AMC in terms of its active band. The active band is defined as the bandwidth, in which the reflection phase is within ±45^{o} [14]. Table 2-1 summarizes the results for a TM polarized plane-wave. The proposed AMC unit cell has a stable reflection phase for various angles of incidence around 60 GHz band.

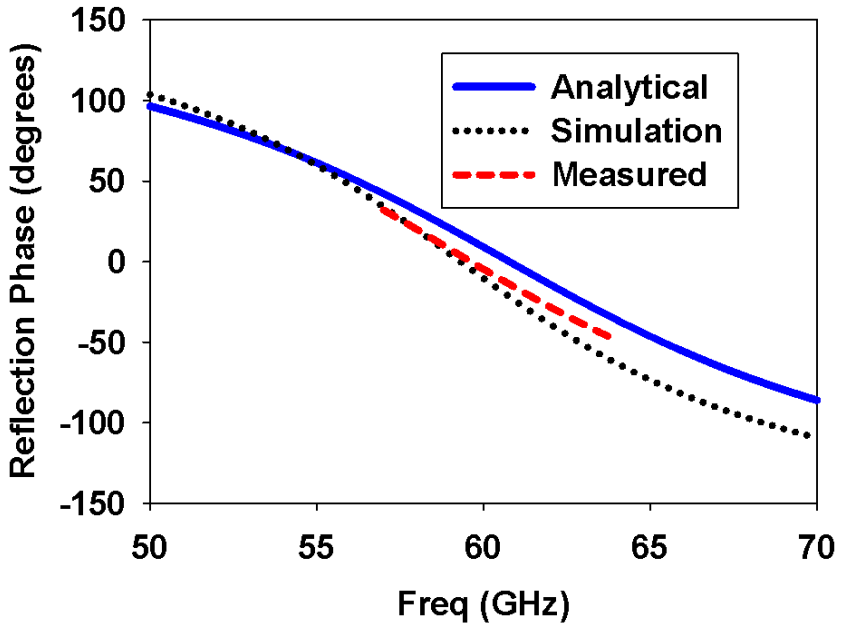

Fig.2-4. Proposed AMC reflection phase of normal incidence.

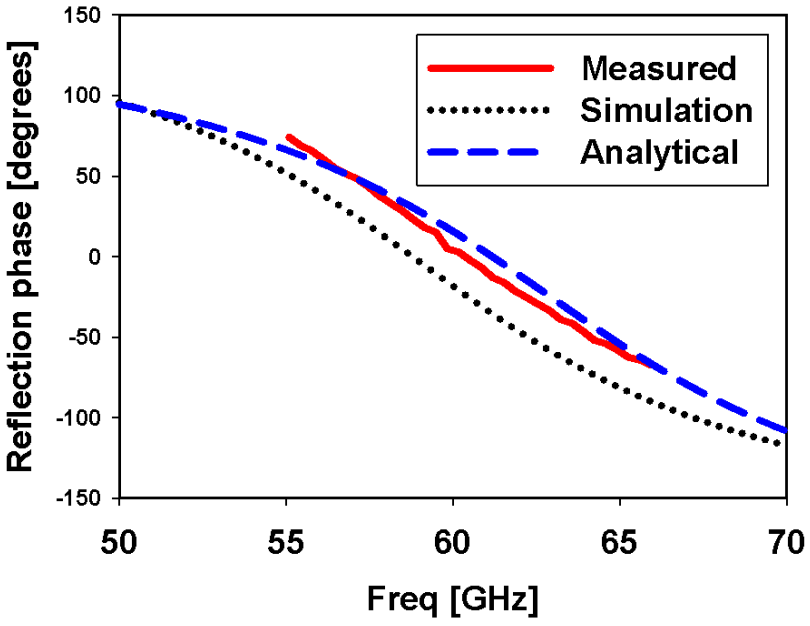

Fig.2-5. Proposed AMC reflection phase of TM polarized plane wave with 30o angle of incidence.

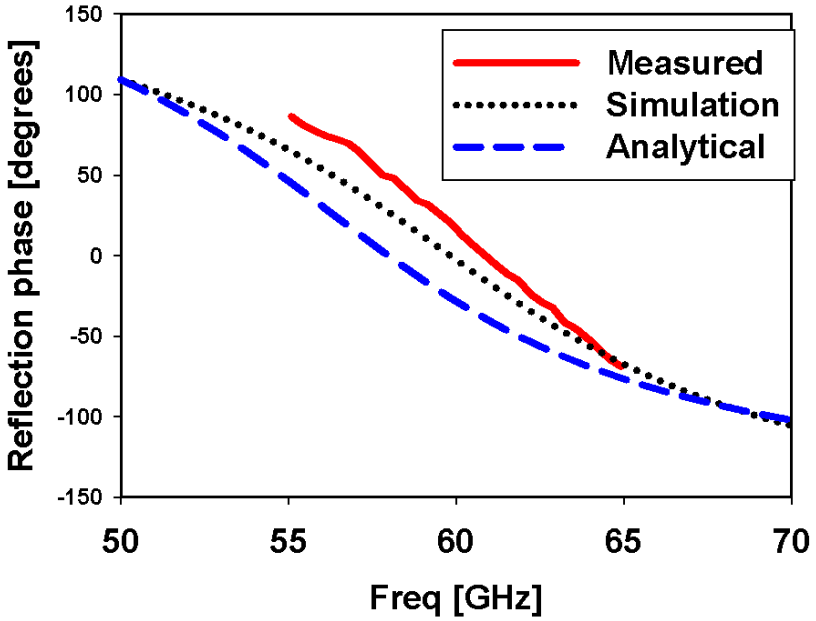

Fig. 2-6. Proposed AMC reflection phase of TM polarized plane wave with 60o angle of incidence.

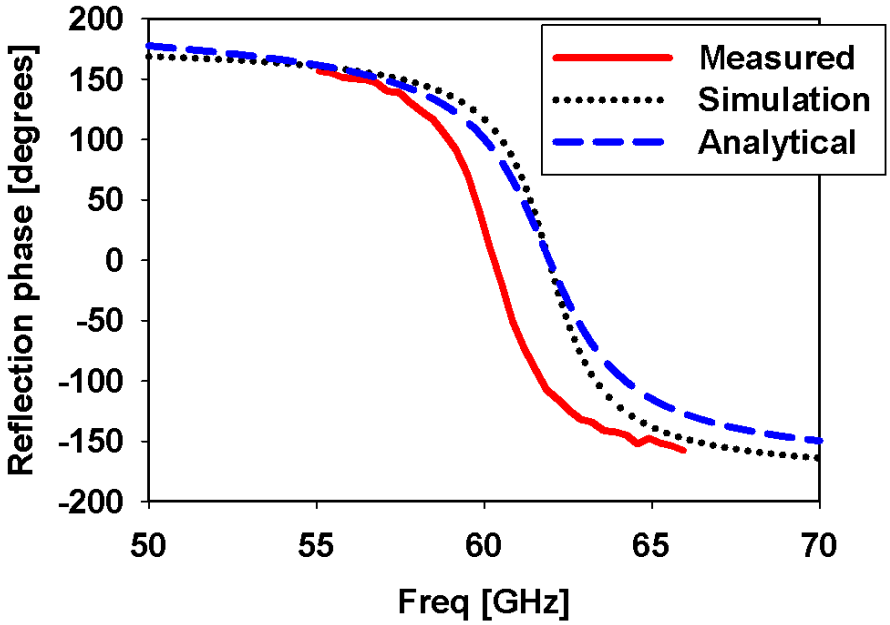

Fig. 2-7. Proposed AMC reflection phase of TE polarized plane wave with 30o angle of incidence.

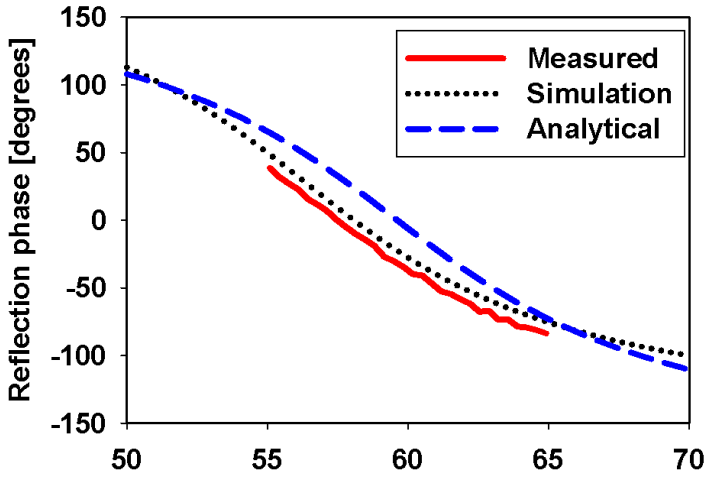

Fig.2-8. Proposed AMC reflection phase of TE polarized plane wave with 60o angle of incidence.

Table 2-1 AMC reflection phase of a TM polarized plane-wave.

Incident Angle (degrees)	± 45° bandwidth (GHz)		
	Analytical	Simulation	Measurement
0	56.2-65	55.7-62.6	56.8-63.1
30	57-64.3	55-62	57.2-63.6
60	56-63.8	56.8-63.3	58.3-63.2

Table 2-2 AMC reflection phase of a TE polarized plane-wave.

Incident Angle (degrees)	± 45° bandwidth (GHz)		
	Analytical	Simulation	Measurement
0	56.2-65	55.7-62.6	56.8-63.1
30	61.2-62.7	61.6-62.4	59.8-60.9
60	56.4-62.9	55.5-61.5	55.4-61.2

Results for a TE polarized plane- wave are summarized in Table 2-2. The proposed AMC unit cell has also a stable reflection phase. However, for 30° incident angle, the active band becomes very narrow (59.8-60.9 GHz). The stability of this AMC makes it attractive to be used as a reflector to increase the gain and reduce the back-lobe level. A practical application is presented in the next.

2.4 Antenna Geometry

The geometry of the proposed antenna is shown in Fig.2-9. A 1.27 mm high cylindrical DRA with 1.08 mm diameter made from ROGERS RT/duriod 6010.2LM (ε_r = 10.2 and tanδ = 0.0023) material is placed on the top of ROGERS RT/duroid 6006.2LM (ε_r = 6.15 and tanδ = 0.0027) substrate with 0.254 mm thickness. The cylindrical DRA is slot-fed by a 50 Ω microstrip line of 0.572 mm width, printed on a 0.381 mm thick ROGERS RT/duroid 6006.2LM substrate. The AMC surface, presented in the previous section, is then used as a reflector. The AMC surface and the microstrip feed line are separated by a Rohacell foam spacer.

Placing the slot at the center of the DRA yields to the excitation of the fundamental mode $HEM_{11\delta}$. The resonance frequency, according to the magnetic wall model, is given by [1]:

$$f^{HEM}{}_{11\delta} = \frac{6.324}{\sqrt{\varepsilon_r + 2}}\left(0.27 + 0.36\frac{r}{2h} + 0.02\left(\frac{r}{2h}\right)^2\right).\frac{4.7713}{r} \quad (1\text{-}15)$$

where r is the radius, h is the height, and ε_r is the relative permittivity of the DRA.

However, the cylindrical DRA in [1] was directly put on an infinite ground plane, which is quite different from the present case in which the DRA is put on the dielectric substrate. The calculated resonance frequency from (15) is 55.8 GHz. However, by taking the combination "resistance peak/reactance zero" as a reference, it was found from the simulation that the resonance frequency of the DRA is 57.3 GHz when its put on the dielectric substrate. The slight increase in the resonance frequency is believed to be due to the reduction of the effective permittivity caused by the substrate.

To achieve wide impedance bandwidth, the slot is set to resonate around the 60 GHz band. The slot resonates at slightly less a half of the guided wavelength. For this purpose the length of the slot is chosen in the vicinity of $\lambda_g/2$, where λ_g is the guided wavelength in the feed substrate. However, the resonance frequency of the slot is also affected by the substrate above the ground plane. Thus, further parametric studies were

carried out to optimize the antenna performance. Final slot length and width are found to be 0.85 mm and 0.18 mm, respectively.

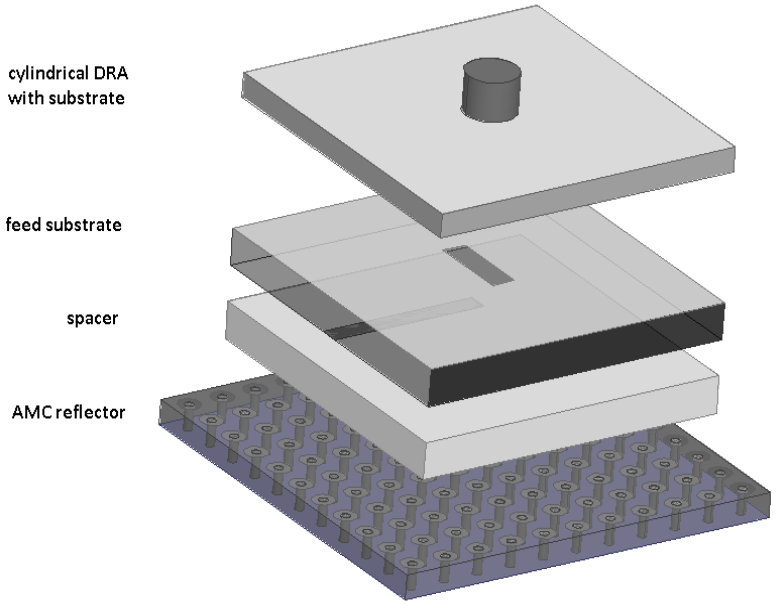

Fig.2-9. Exploded view of the proposed antenna.

Its worthy mentioning here that the slot can be replaced by an equivalent horizontal magnetic dipole, and the cylindrical DRA can also be replaced by an equivalent horizontal magnetic dipole when excited in its $HEM_{11\delta}$ mode. Thus, the radiation pattern for both modes is the one of a horizontal magnetic dipole; broadband in the H-plane and almost omnidirectional in the E-plane.

PEC-backed ACDR Antenna

To study the effect of backing the reference antenna by a PEC surface on the radiation characteristics and impedance bandwidth, simulations were carried out using the HFSS full wave simulator.

From the image theory, placing the slot and the cylindrical DRA above a PEC layer at a distance s, where s represents the distance between the PEC backing layer and the slot layer, creates a 180^{o} out of phase image current at the same distance under the PEC layer, as illustrated in Fig.2-10.

In order to add the two currents constructively in the far-field, the distance s should be around a quarter of the guided wavelength of the medium between the two layers. To

calculate the guided wavelength, the effective permittivity of the medium between the two layers should be calculated first.

The effective dielectric permittivity of two different mediums is given by:

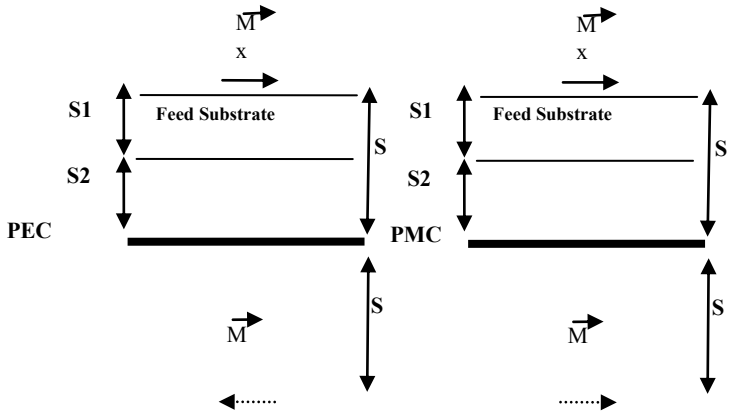

Fig.2-10. Equivalent image of a horizontal magnetic current above a PEC surface (left) and PMC surface (right).

$$\varepsilon_{eff} = \frac{s\varepsilon_1\varepsilon_2}{s2\varepsilon_1 + s1\varepsilon_2} \tag{1-16}$$

where s, s1, s2 are total and individual lengths of the two mediums, as shown in Fig.2-10.

The simulated H-plane power patterns at 60 GHz of the PEC-backed antenna for three different values of s are shown in Fig.2-11. At 60 GHz, s=1.2 mm corresponds to a quarter of the guided wavelength, s=1.8 mm corresponds to a third of the guided wavelength, and s=2.4 mm corresponds to a half of the guided wavelength. The maximum radiation, 7.8 dBi in the broadside direction, occurs, at s=1.2 mm. This is due to the constructive interference of the fields of the two magnetic currents. However, for s=2.4 mm, a destructive interference occurs, values are between -10 dBi and 2 dBi in the broadside direction.

Even when placing the slot layer at a quarter of the guided wavelength from the PEC backing layer, the gain improvement, when compared to the reference antenna, is around 2.5 dB, and this degradation is due to the parallel-plates modes.

To understand the effect of the parallel-plate modes clearly, the structure consists of the upper PEC (slot layer), the feed substrate, the spacer and the lower PEC (backing layer) must be considered. These two PEC layers form a traditional parallel plate waveguide, with a zero cutoff frequency, and parallel-plate modes being propagating along the layers. These parallel-plate modes cause parasitic radiations and energy leakage.

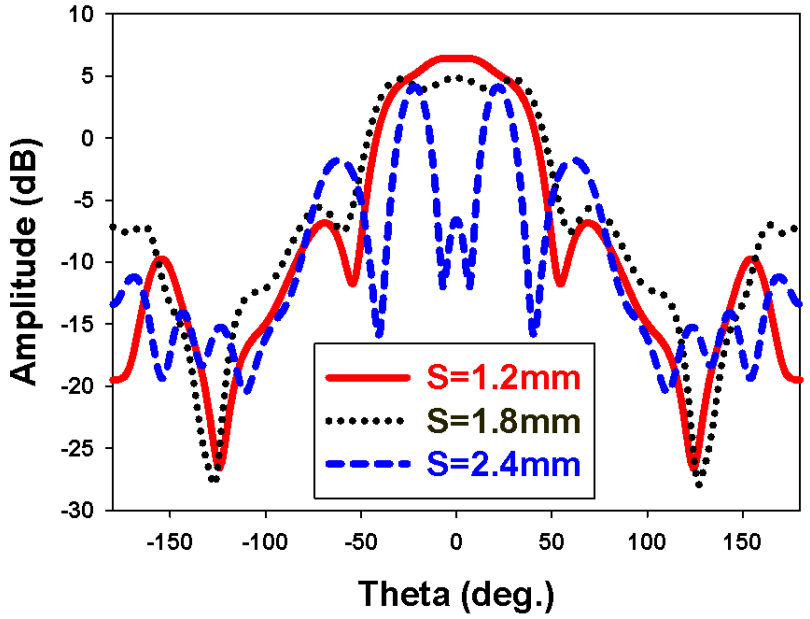

Fig.2-11. Simulated H-plane power patterns at 60 GHz of the PEC-backed antenna for different values of s.

AMC-backed ACDR Antenna

The AMC surface presented in the previous section is placed underneath the reference antenna. The effect of the distance between the slot layer and the AMC surface on the antenna characteristics was studied. Fig.2-12. shows the simulated H-plane power patterns of the AMC-backed antenna at 60 GHz for three different values of s, where s represents the distance between the AMC surface and the slot layer,

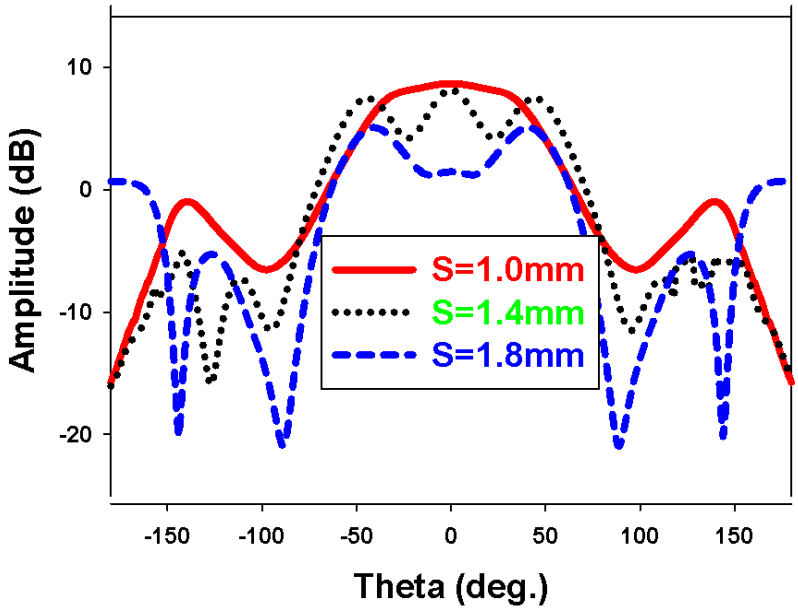

Fig.2-12. Simulated H-plane power patterns at 60 GHz of the proposed antenna for different values of s.

A drastic increase in the gain is obtained when backing the reference antenna by our proposed AMC structure. When waves impinge on the AMC surface with different angles of incidence and polarizations, they are reflected back in-phase, and this yields to a constructive interference with the overall radiation pattern. The gain improvement depends on the value of s, for s=1.0mm, the gain is 10.1 dBi in the broadside direction, 9.4 dBi for s=1.4 mm, and 4.2 dBi for s=1.8mm.

The justification of this drastic gain improvement associated with the insertion of the AMC surface is twofold. First, around 3 dBi increase is anticipated by the existence of the ground-plane with in-phase reflection characteristics. Second, the mushroom-based AMC operates based on the resonant system. Therefore, at resonance, the AMC surface itself contributes to the radiation through the large currents induced into it. Above resonance, the AMC surface blocks both TM and TE-polarized surface waves, and further shapes the radiation pattern. In addition, it reduces the back radiation resulting from edge diffraction. Below resonance, the AMC surface has a small effect on the radiation characteristics.

Theoretically, the distance between the antenna and the AMC must be zero, which is electrically not possible. Thus, the distance between the antenna and the AMC reflector

should be chosen properly for a total suppression of parallel-plate modes.

For the structure consists of the upper PEC (slot layer), the feed substrate, the spacer, and AMC surface, the PMC reflector changes the boundary conditions of the traditional parallel plate environment, resulting in reducing the parallel-plate modes by creating a non-zero cut off frequency medium. Therefore, if the operating frequency of the antenna is chosen to be below the cut off frequency, no parallel-plate modes will propagate. The cut off frequencies of both the dominant TE and the dominant TM modes are the same and are given by:

$$f_c = \frac{0.5}{2s\sqrt{\mu\varepsilon}} \tag{1-17}$$

where μ and ε are the permeability and permittivity of the medium between the slot layer and the AMC surface.

And for an operating frequency f_o, the distance between the antenna and the AMC must satisfy [8]:

$$s \leq \frac{1}{4f_o\sqrt{\mu\varepsilon}} \tag{1-18}$$

The calculated cut off frequencies from (5) are 62 GHz, 47.6 GHz and 36.8 GHz for s=1.0mm, 1.4mm and 1.8 mm respectively. Thus a total suppression of parallel-plates modes occurs only for s=1mm. For s= 1.4 mm, we still suffer from parallel-plate modes, and for s=1.8 mm, these mode become more severe (more ripples and lower efficiency). Its clear that the proposed antenna outperforms the PEC-backed antenna by 2.4 dBi, and the reference antenna by 4.4 dBi.

Since the AMC surface has a high impedance value in its active band, then by making it very close to the antenna, the input impedance of the antenna changes and the matching is lost. Therefore, a tradeoff between the radiation characteristics and the impedance matching must be considered.

2.5 Experimental Results

To validate the proposed designs, three antenna prototypes were fabricated and tested. From Fig.2-11, the optimum foam thickness to be inserted between the microstrip feed line and the PEC surface for the PEC-backed antenna is 0.8 mm (corresponds to s=1.2mm). From Fig.2-12, the optimum foam thickness to be inserted between the microstrip feed line and the AMC surface for the proposed antenna is found to be 0.6 mm (corresponds to s=1.0 mm). However, the minimum available foam thickness we could obtain from Rohacell® was 1 mm. Therefore, we used 1.4 mm thick foam for the PEC-backed antenna (corresponds to s=1.8 mm), and 1 mm thick foam for the proposed antenna (corresponds to s=1.4 mm). The dimensions of the AMC reflector were chosen to be slightly larger than the ground plane of the antenna to reflect back the waves scattered from the edges of the substrates. Fig.2-13 shows photos of the fabricated reference antenna, the proposed antenna (with AMC backing) and the PEC-backed antenna.

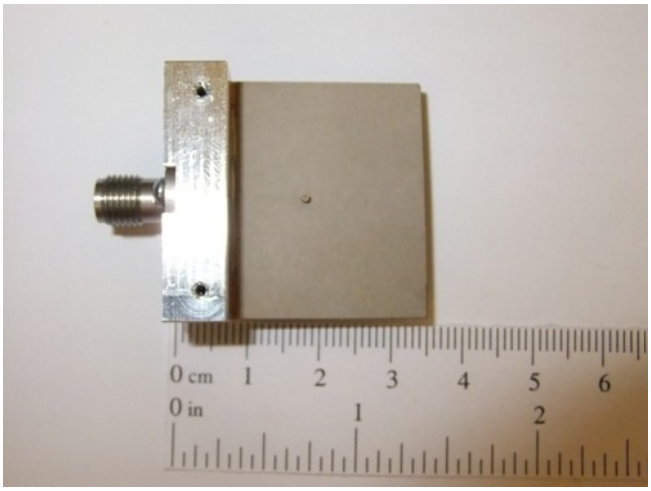

(a)

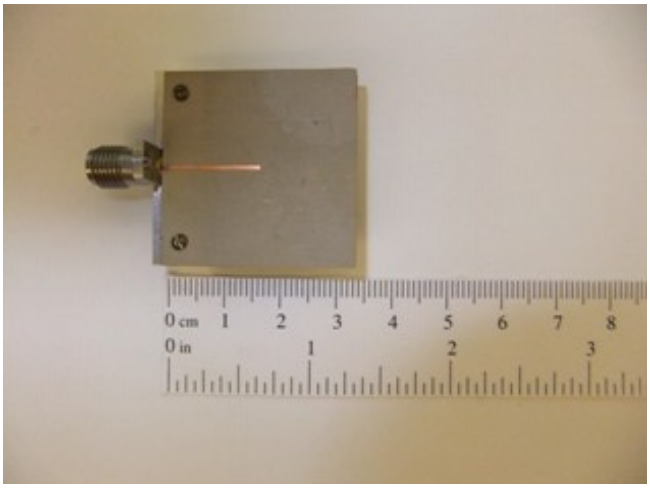

(b)

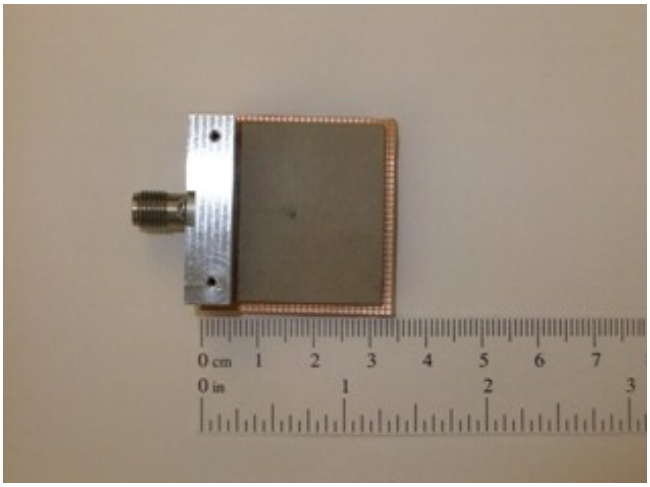

(c)

(d)

Fig. 2-13. Photos of the fabricated antenna prototypes. (a) Reference antenna (top view) (b) Reference antenna (bottom view) (c) Proposed antenna (top view) (d) PEC-backed antenna (top view).

S-Parameter

The simulated and measured reflection coefficients of the proposed, PEC-backed and reference antennas are shown in Fig.2-14. Simulated and measured results show good correlation. The impedance bandwidth of the proposed antenna is 19 % centered at 60.45 GHz, while it is 24 % centered at 60.2 GHz for the reference antenna

It is important to mention that the overall bandwidth of the proposed antenna is limited to the active band of the AMC surface [4]. Our proposed antenna has only 5 % bandwidth reduction compared to the reference one. Thanks to our stable and wide-band AMC surface. The AMC negatively affects the reflection coefficient through changing the input impedance of the antenna. When the AMC surface is used a reflector, and due to its close proximity from the antenna, a strong mutual coupling occurs between the equivalent magnetic current and its image current, and the input impedance of the antenna is changed. Therefore, the antenna cannot directly match well to a 50 Ω transmission line, and this worsens the efficiency from the reference antenna. However, a proper impedance transformation can be used. Moreover, some higher-order floquet modes (evancent modes) are excited, and affect the antenna performance.

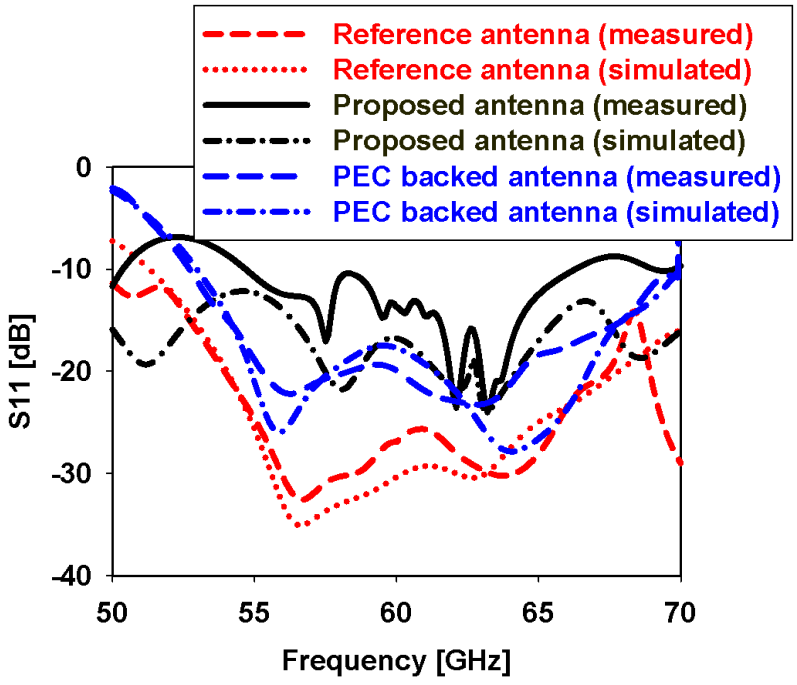

Fig.2-14. Simulated and measured reflection coefficients of the reference, PEC-backed, and proposed antennas.

Radiation Patterns

Radiation patterns were measured in an anechoic chamber. To reduce amplitude and phase ripples, a reflector with serrated edges has been used. Yet, a large ripple is observed when measuring the patterns, and especially in the E-plane.

After the measurements, simulations using the HFSS were carried out including the v-connector and its metallic base shown in Fig.2-13, and identical ripple, but slightly shifted, is seen in the patterns. The connectors' base is 8 mm in height (~1.6λ at 60 GHz), and extends along the whole edge of the ground plane. The distance between the cylindrical DRA and the connectors' base is 9.2 mm (~1.8λ at 60 GHz). Therefore, this metallic base will create some multiple reflections and diffractions that will interfere destructively in some directions, and constructively in others. Moreover, at some angles, this base will block waves from the standard testing antenna from propagating, causing some spoils in the pattern. In addition, for the thickness of the foam used in the proposed antenna, the cut off frequency was calculated from the previous section to be 47.6 GHz, i.e., a total parallel-plate suppression is not achieved, and hence, parasitic radiation and energy leakage caused by the parallel-plate modes will yield to pattern disturbance.

The fact that ripples are stronger in the E-plane than the H-plane can be understood by considering the fields of the excited mode. The $HEM_{11\delta}$ mode has a stronger lateral radiation (radiation along the ground plane) in the E-plane (almost omnidirectional) than in the H-plane (broadband), and hence, corrupting the overall pattern due to diffraction from the edges. These ripples are mainly due to the need to modify the test prototypes for measurements, and can be avoided in the final application with a careful design.

For the sake of clarity, we will plot the simulated and measured power patterns of the proposed and PEC-backed antennas on two separate graphs, each compared with the measured power pattern from the reference antenna in each plane.

Normalized H- and E-plane power patterns of the proposed and reference antennas at 60 GHz are shown in Figs. 2-15 and 2-16, respectively. Simulated and measured patterns show a good agreement. As it can be observed from these figures, the power pattern is improved when the ACDR antenna is backed with AMC. The front-to-back ratio is 21 dB and 9.5 dB for the proposed and reference antennas, respectively. An improvement of 11.5 dB is achieved when backing the reference antenna with the AMC. The cross

polarization level was below -18 dB in both planes.

Figs. 2-17 and 2-18 show the normalized H- and E-plane power patterns of the PEC-backed and reference antennas at 60 GHz, respectively. Again, the simulated and measured patterns agree well with each other. The front-to-back ratio of the PEC-backed antenna is 14 dB. An improvement of 4.5 dB is achieved when backing the reference antenna with the PEC surface.

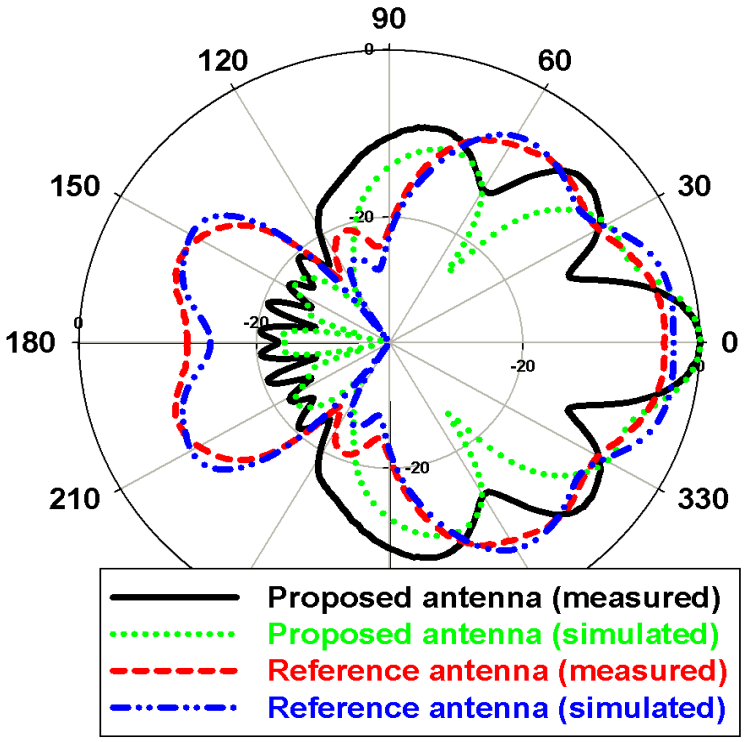

Fig.2-15. Simulated and measured normalized H-plane power patterns at 60 GHz of the reference and proposed antennas.

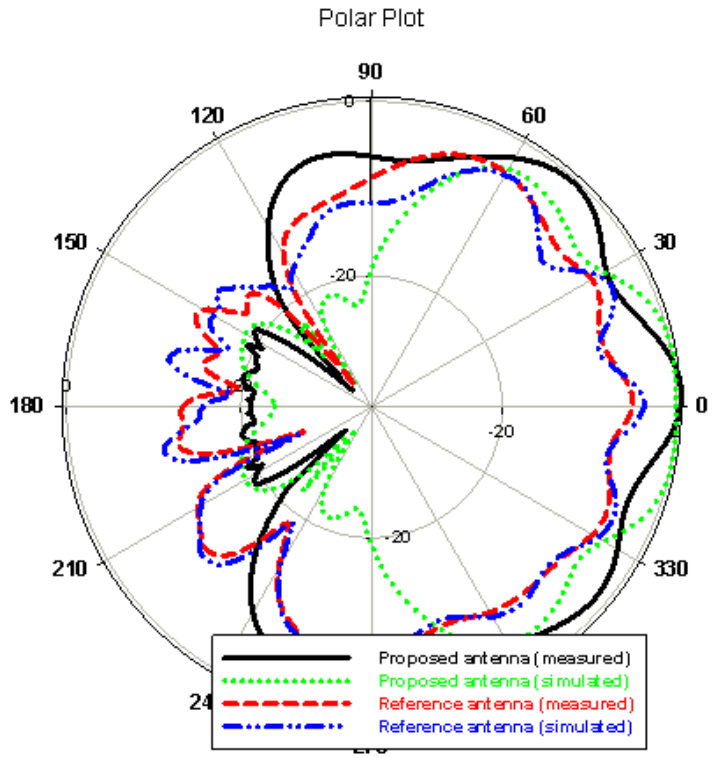

Fig. 2-16. Simulated and measured normalized E-plane power patterns at 60 GHz of the reference and proposed antenna.

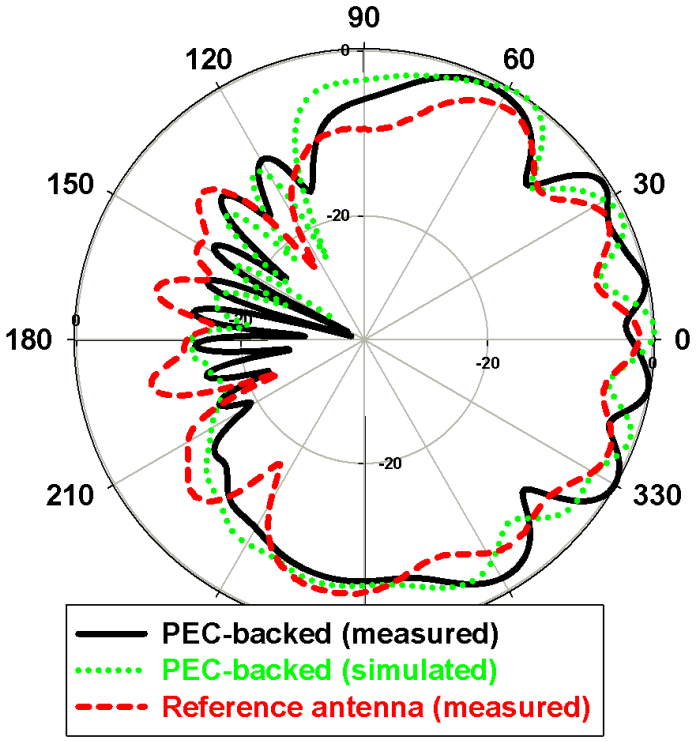

Fig.2-17. Simulated and measured normalized H-plane power patterns at 60 GHz of the reference and PEC-backed antenna.

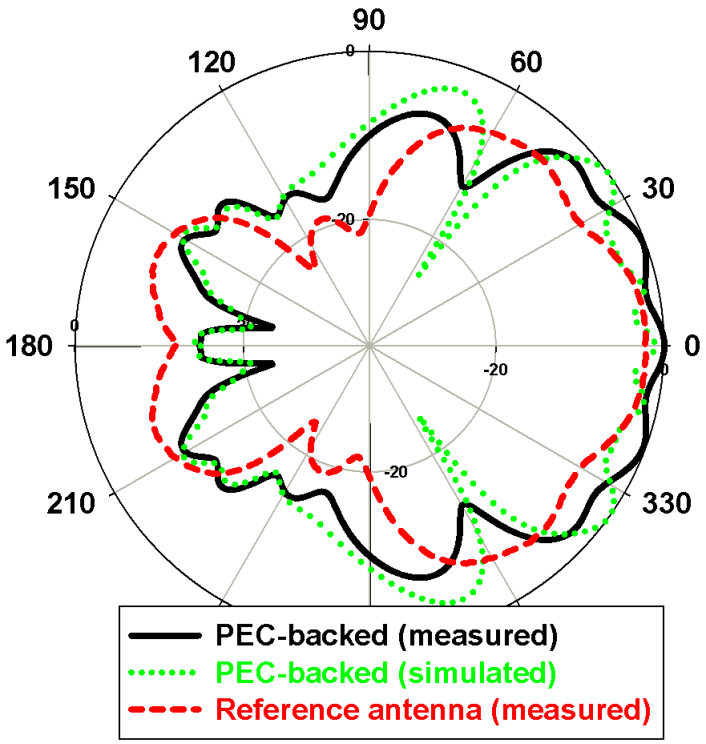

Fig.2-18. Simulated and measured normalized E-plane power patterns at 60 GHz of the reference and PEC-backed antennas.

Gains

The most appealing feature of this antenna is its high gain. The gain of the proposed, PEC-backed and reference antennas was simulated and measured. Fig. 2-19 summarizes the results. The measured gain of the proposed antenna varies between 6.6 dBi and 7.9 dBi within the 57-64 GHz band, and between 5.9 dBi and 6.6 dBi for the PEC-backed antenna over the same frequency span. For the reference antenna, it varies between 4.90 dBi and 5.25 dBi within the same band. Again, simulated and measured results show good agreement.

For PEC-backing, a traditional parallel-plate environment is created between the slot layer (the ground plane that contains the aperture) and the PEC layer with a zero cut-off frequency. Therefore, ripples are observed in the radiation patterns of the PEC-backed antenna because of the parallel modes and energy leakage between the plates. However, in EBG backing, the slot layer and the EBG layer forms a non-traditional parallel-plate environment with a non-zero cut-off frequency by changing the boundary conditions on

the two plates. Thus, if the operating frequency of the antenna is chosen to be below the cut off frequency, no parallel-plate modes will propagate.

The justification of this drastic gain improvement associated with the insertion of the proposed EBG structure is threefold: First, the existence of the EBG reflector with in-phase reflection characteristics. Moreover, parallel-plate modes are suppressed when using EBG structure as a ground plane [6]. Second, the mushroom EBG structure operates based on the resonant system. Therefore, at resonance, the EBG structure itself contributes to the radiation through the large currents induced into it. Third, the EBG structure has a surface-wave suppression band gap around the 60 GHz band. Therefore, it blocks surface waves with from propagating, and further shapes the radiation pattern. In addition, it reduces the back radiation resulting from edge diffraction.

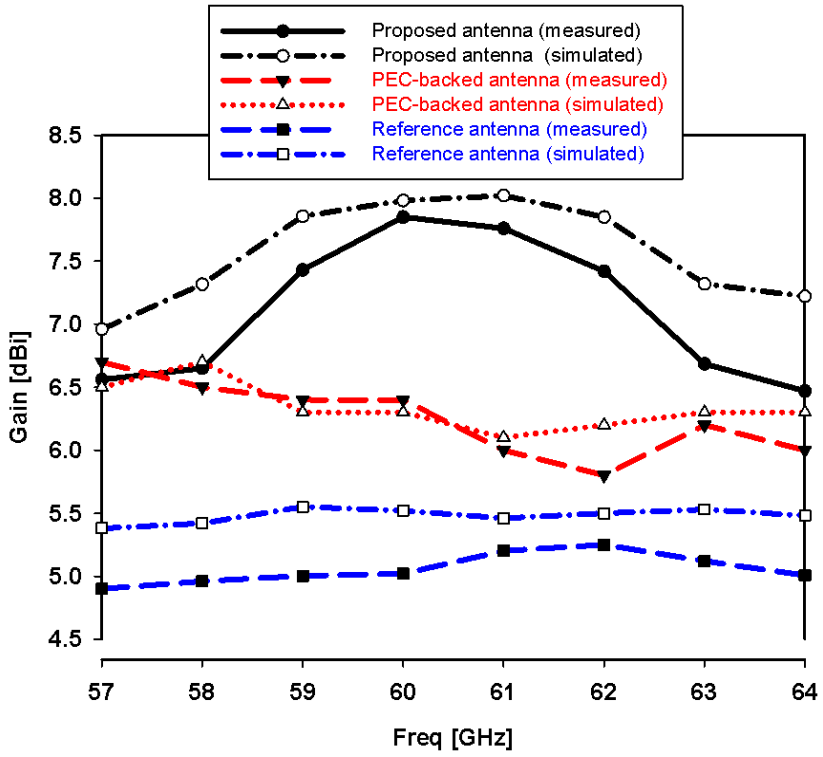

Fig.2- 19. Simulated and measured gain as function of frequency of the reference, proposed, and PEC-backed antennas

2.6 References

[1] A. Perron, T. A. Denidni and A. R. Sebak, "High Gain Hybrid Dielectric Resonator Antenna for Millimeter-Wave Applications: Design and Implementation", IEEE Trans. Antennas and Propag., vol. 57, no. 10, pp. 2882-2892, Oct. 2009.

[2] Sievenpiper, D., Lijun Zhang; Broas, R.F.J. Alexopolous, N.G., and Yablonovitch, E., "High-Impedance Electromagnetic Surfaces with a Forbidden Frequency Band", IEEE Trans. Microwave Theory and Techniques, vol. 47, no. 11, pp.2059-2074, Nov. 1999.

[3] F. Elek, R. Abhari, and G. V. Eleftheriades, "A uni-directional ring-slot antenna achieved by using an electromagnetic band-gap surface," IEEE Trans. Antennas Propag., vol. 53, no. 1, pp. 181–190, Jan. 2005.

[4] M. Ermutlu, C. Simovski, M. Karkkainen, P. Ikonen, S. Tretyakov, and A. Sochava, "Miniaturization of patch antennas with new artificial magnetic layers," in Proc. IEEE Int.Workshop Antenna Technol.:Small Antennas Novel Metamaterials (IWAT), pp. 87–90, March 2005.

[5] F. Yang and Y. Rahmat-Samii, "Reflection phase characterization of an electromagnetic bandgap (EBG) surface," in Proc. IEEE AP-S Int. Symp., Jun. 16–21, 2002, vol. 3, pp. 744–747.

[6] J. Y. Zhang, V. Hagen, M. Younis, C. Fischer, and W. Wiesbeck, "Planar artificial magnetic conductors and patch antennas," IEEE Trans. Antennas Propag., vol. 51, no. 10, pt. 1, pp. 2704–2712, Oct. 2003, Special issue on metamaterials.

[7] M. Z. Azad and M. Ali, "Novel wideband directional dipole antenna on a mushroom like EBG structure," IEEE Trans. Antennas Propag., vol. 56, no. 5, pp. 1242–1250, May 2008.

[8] Y. Sun, Z. Chen ; Y. Zhang ; H. Chen and T. See "Subwavelength substrate-integrated Fabry-Perot cavity antennas using artificial magnetic conductor," IEEE Trans. Antennas Propag., vol. 60, no. 1, pp. 30-35, Jan. 2012.

[9] A. Feresidis, G. Goussetis, S.Wang, and J. C. Vardaxoglou, “Artificial magnetic conductor surfaces and their application to low-profile high gain planar antennas,” IEEE Trans. Antennas Propag., vol. 53, no. 1, pp. 209–215, Jan. 2005.

[10] S. A. Tretyakov and C. R. Simovski, “Dynamic model of artificial impedance surfaces,” J. Electromagn. W. Applic., vol. 17, no. 2, pp. 193–240, 2003.

[11] O. Luukkonen, C. Simovski, A. V. Räisänen, and S. A. Tretyakov, “An efficient and simple analytical model for analysis of propagation properties in impedance waveguides,” IEEE Trans. Microwave Theory and Techniques, Vol. 56, No. 7, pp. 1624-1632, July 2008.

[12] D. Ramaccia, A. Toscano, F. Bilotti, "A new accurate model of high-impedance surfaces consisting of circular patches," Progress in Electromagnnetics Research (PIER-M), vol. 21, pp. 1-17, 2011.

[13] HFSS software of Ansoft Inc. (www.ansoft.com).

[14] M. Samani, A. Borji, and R. Safian, “Relation between Reflection Phase and Surface-Wave Bandgap in Artificial Magnetic Conductors,” IEEE Trans. Microwave Theory and Techniques, vol. 59, no. 8, pp. 1901-1908, August 2011

CHAPTER THREE: MMW EBG-BASED APERTURE COUPLED DIELECTRIC RESONATOR ANTENNA

3.1 Introduction

Recently, communication systems and wireless applications have been driven toward the millimeter-wave band (MMW). In addition to the emerging demands of compact, high-speed and large bandwidth systems, the crowd of RF bands and the commercial availability of MMW components have made the MMW band a suitable choice for many short-range wireless applications.

Dielectric resonator antennas (DRAs) [1] have received an increasing attention due to several striking characteristics. In fact, their zero conductor losses, wide impedance bandwidth, different excitation techniques and high radiation efficiency have made them suitable candidates to wireless communications at MMW band [2].

High attenuation characteristics are main concerns at MMW band. Therefore, researchers have proposed several techniques to improve the radiation characteristics of MMW antennas. In [3], higher order modes are excited in a DRA to enhance the gain. While the most appealing feature of this technique is its simplicity, it requires taller DRA, which makes fitting it in ever smaller packages at high frequencies difficult. Moreover, the proposed technique yields a narrow bandwidth operation, and has no means for surface wave suppression to minimize the near field coupling to the environment.

Electromagnetic band-gap (EBG) structures [4] are artificial materials that exhibit unique electromagnetic properties, which are not achievable from conventional materials. EBG materials are found to have stopbands where electromagnetic-wave propagation is prohibited. This feature has attracted the researchers to use EBG structures in antenna design to block surface-wave from propagating, and hence, to improve the radiation characteristics of the antenna. Using an EBG structure as a ground-plane to enhance different performance characteristics of low profile antennas has been explored by many researchers [5-9]. It is based on the ability of the EBG structure to mimic an artificial magnetic conductor surface over a limited frequency span [10]. Applying this technique to complex antenna structures is quite complicated. For multilayer antenna structures

that contain a ground-plane, adding an EBG surface will distort the radiation characteristics by causing multiple reflections and creating a parallel-plate environment [10]. Moreover, it will add to the antenna design complexity. Very few studies have been reported on using the EBG bandgap property to suppress surface-wave propagation in multilayer MMW antennas. In [11,12], a uniplanar compact EBG (UC-EBG) lattice has been placed around an aperture-coupled microstrip antenna. In [13], 60 GHz DRA surrounded by UC-EBG has been also reported. Results have shown no significant gain improvement, or backlobe level reduction. This is due to the fact that the UC-EBG can suppress only TE surface-waves. Since the TM_{00} is the dominant mode in surface-waves with zero cut off frequency, UC-EBG lattice may not work with an antenna that excites both TM and TE surface waves [14]. However, Mushroom like EBG lattice, with shorting vias, can suppress surface-waves of both TM and TE polarizations [3].

3.2 Circular patch (CP)-EBG Design and Characteristics

EBG-unit cell

Our proposed CP-EBG structure consists of circular patches printed on conductor-backed with 0.254 mm thick ROGERS 3006 (ε_r = 6.15 and tanδ = 0.002) substrate. The patch diameter is 1.28 mm with a period D = 1.45 mm. As shown in Fig.3-1, the centers of the circular patches are connected to the ground plane through vias with 0.16 mm diameter.

The procedure started by designing an square patch mushroom EBG unit cell with bandgap around the 60 GHz. After that the square patch shape was approximated to an average equivalent circular patch shape based on the similarity between the electric field distribution along the edges of the square and circular patches. The averaged circular gap width between the EBG unit cells is given by [15]:

$$w_{circular} = 1.1 w_{square} - 0.1D \qquad (2\text{-}1)$$

where w is the gap width between the EBG unit cells.

The circular shape has the advantage over the square shape of being a body of revolution. Therefore, it will be symmetric to the electromagnetic waves with different wave vectors and directions, and hence, ensuring a complete wide-bandgap over the frequency band of interest. Further parametric studies were carried out to optimize the EBG characteristics.

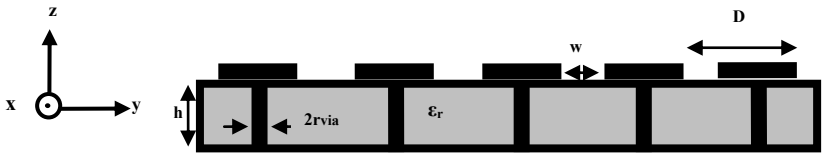

(a)

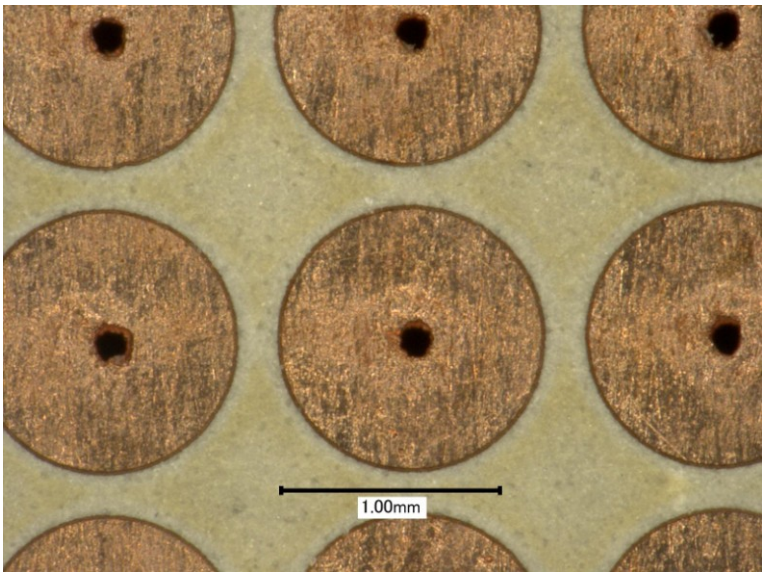

(b)

Fig.3-1. The proposed EBG structure. (a) Geometry of the structure. (b) Microscopic photo of the proposed EBG unit cell.

The dispersion diagram of the first three propagating modes of the proposed CP-EBG is shown in Fig.3-2. It has a complete band-gap over the irreducible Brillioun zone, Γ-X, X-M, and M-Γ, shown in the inset of Fig.3-2. The band gap extends from 57.2 GHz to 72.3 GHz, with 23.32% gap to mid-gap ratio ($\Delta\omega/\omega_o$). Over this frequency span, no wave propagation is allowed. Therefore, this structure can be used in antenna design, as demonstrated in section III, to suppress surface-waves, and hence improving the radiation properties.

To further evaluate the properties of the CP-EBG structure, an experiment concerning its transmission properties has been carried out using the asymmetrically placed microstrip method [16]. A 16 x 25 CP-EBG array is inserted between two equal open-ended microstrip lines, as shown in Fig.3-3.

Surface waves are launched along the substrate by the first microstrip line. The second microstrip line is employed to detect the electromagnetic fields, and the transmission coefficient is measured. Making the two microstrip lines nonaligned (asymmetric configuration), ensures detecting electromagnetic fields with different wave vectors and directions. Thus, this method is considered to give the most accurate results, compared to the bandgap obtained from the dispersion diagram, among other methods. Moreover, this method is considered to be a strongly coupling technique, which reduces the influence of other parasitic propagation modes. Fig.3-4 shows both the measured and simulated transmission coefficients S_{21}. The measured and simulated results show a good agreement. The measured transmission coefficient is restricted to 65 GHz since the VNA used in the measurement only goes up to 65 GHz. An average of about 15 dB reduction of the transmission coefficient is observed. Simulated and measured results show good correlation. Clearly, there is a good agreement between the measured transmission coefficient and the calculated bandgap from the dispersion diagram.

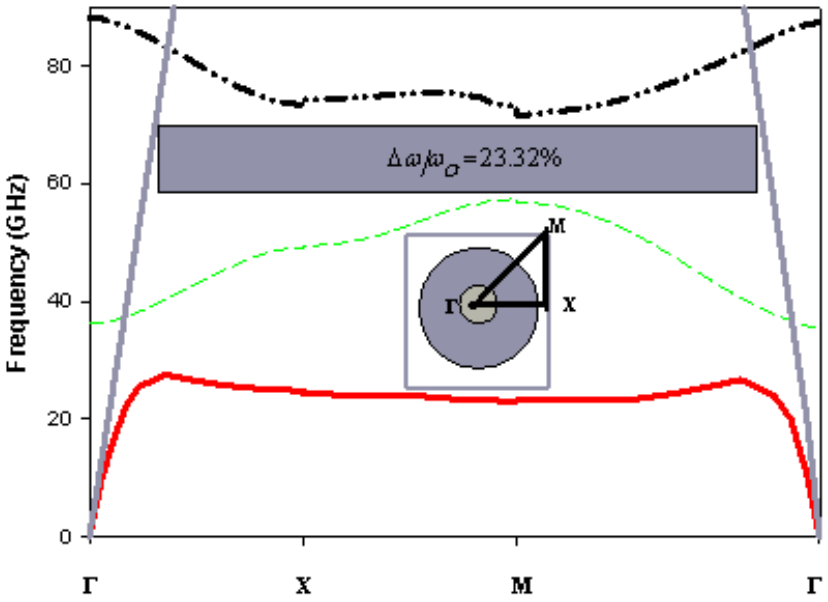

Fig.3-2. Dispersion diagram of the proposed CP-EBG.

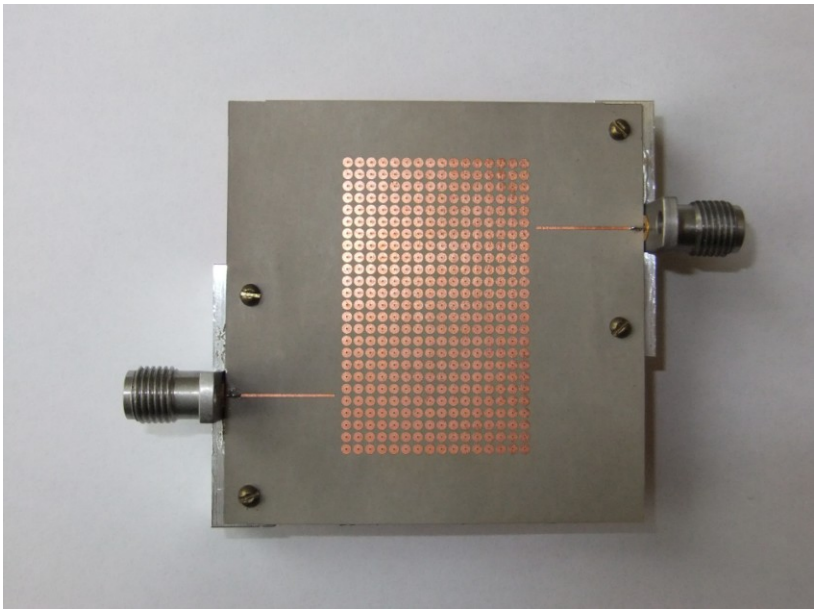

Fig.3-3. Photo of the measured asymmetric microstrip line structure.

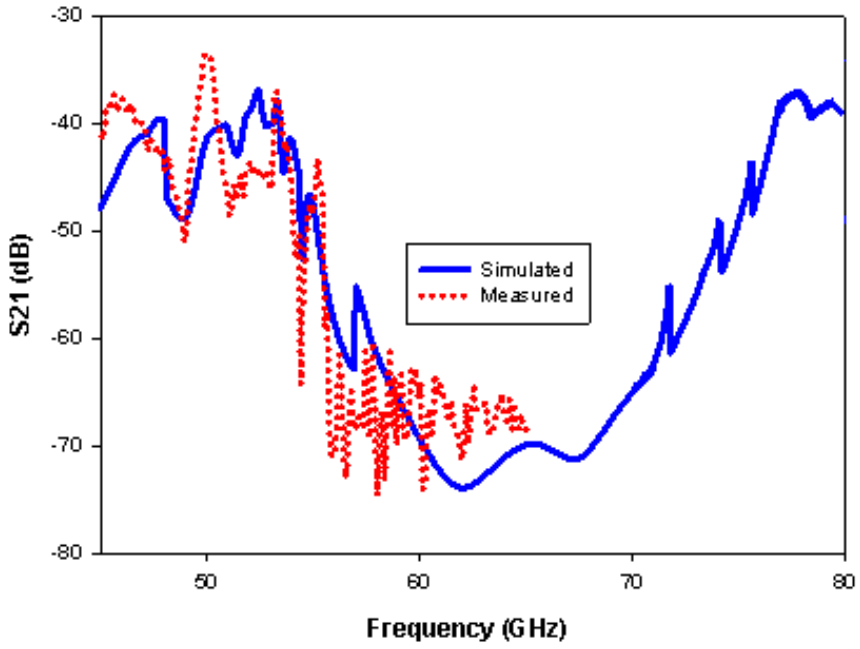

Fig.3- 4. Simulated and measured transmission coefficients of the asymmetric microstrip line structure shown in Fig.3-3.

3.3 MMW EBG-Based Aperture Coupled Dielectric Resonator Antenna

Antenna Geometry

A 1.27 mm high cylindrical DRA with 1.06 mm diameter made from ROGERS RT/duriod 6010.2LM (ε_r = 10.2 and tanδ = 0.0023) material is placed on the top of ROGERS RT/duroid 6006.2LM (ε_r = 6.15 and tanδ = 0.0027) substrate with 0.254 mm thickness. The cylindrical DRA is slot-fed by a 50 Ω microstrip line of 0.572 mm width, printed on a 0.381 mm thick ROGERS RT/duroid 6006.2LM substrate.

In aperture coupling technique, the energy is coupled from the microstrip feedline to the DRA through an aperture in the ground plane. It has the advantages of polarization purity and isolating the microstrip feedline from the radiating element (DRA), a common problem encountered at MMW band.

Placing the slot at the center of the DR antenna yields to the excitation of the fundamental $HEM_{11\delta}$ mode. Its resonance frequency, according to the magnetic wall model, is given by [17]:

$$f^{HEM}{}_{11\delta} = \frac{6.324}{\sqrt{\varepsilon_r + 2}}\left(0.27 + 0.36\frac{r}{2h} + 0.02\left(\frac{r}{2h}\right)^2\right).\frac{4.7713}{r} \qquad (2\text{-}2)$$

where r is the radius, h is the height, and ε_r is the relative permittivity of the DR antenna. However, the cylindrical DR antenna in [15] was directly put on an infinite ground plane, which is quite different from the present case in which the DR antenna is put on the dielectric substrate. The calculated resonance frequency from (2) is 56.3 GHz. However, by taking the combination "resistance peak/reactance zero" as a reference, it was found from the simulation that the resonance frequency of the DR antenna is 57.4 GHz when its put on the dielectric substrate. The slight increase in the resonance frequency is believed to be due to the reduction of the effective permittivity caused by the substrate

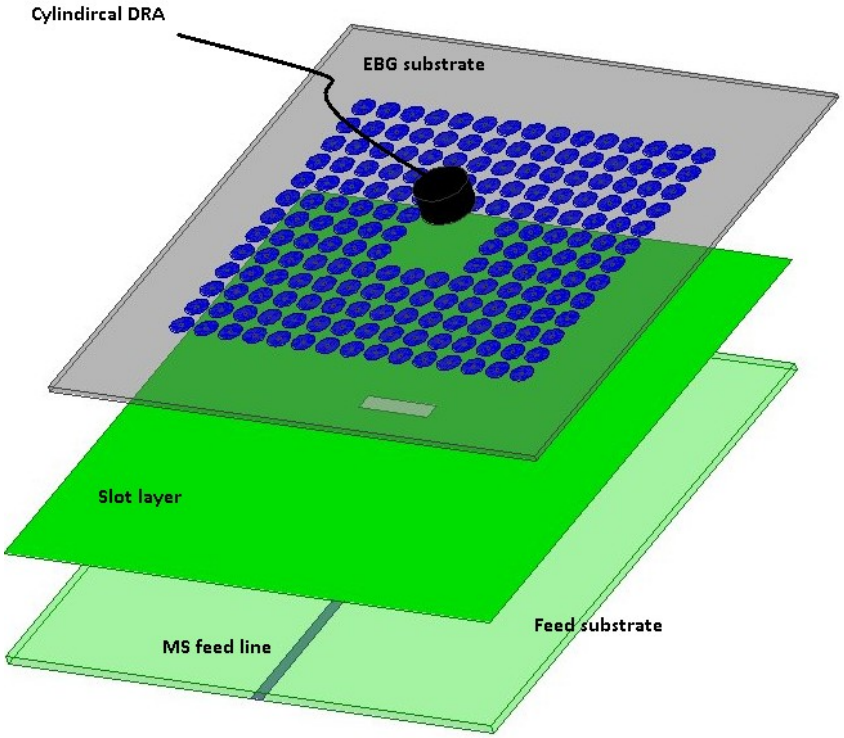

Fig.3-5. Exploded view of the proposed antenna.

To achieve a wide impedance bandwidth, the slot is set to resonate around the 60 GHz band. The slot resonates at slightly less a half of the guided wavelength. For this purpose, the length of the slot is chosen in the vicinity of $\lambda_g/2$, where λ_g is the guided wavelength in the feed substrate. However, the resonance frequency of the slot is also affected by the substrate above the ground plane. Thus, further parametric studies were carried out to optimize the antenna performance. Final slot length and width are found to be 0.85 mm and 0.18 mm, respectively.

Five periods of the CP-EBG structure presented in the previous section were placed symmetrically around the cylindrical DRA. The distance *S* between the DRA and the CP-EBG lattice is crucial in terms of impedance matching and radiation characteristics (shape of radiation pattern and gain) of the antenna. Fig.3-6 shows the antenna's reflection coefficients for different values of *S*. If *S* is small, the near field interaction between the DRA and the EBG lattice is large and the antenna cannot be tuned. Increasing the distance *S* will decrease the coupling between the DRA and the EBG

lattice and improve the matching. Simulated maximum gain at 60 GHz for four different values of *S* is shown in the inset of Fig.3-6. Its apparent that increasing the distance *S* yields decrease the effect of the EBG on the radiation characteristics of the antenna. This is due to the lower level of surface-wave suppression, and the less contribution of the radiation from the EBG structure. The optimum value of *S* that yields maximum gain while maintaining good matching is 2.6 mm.

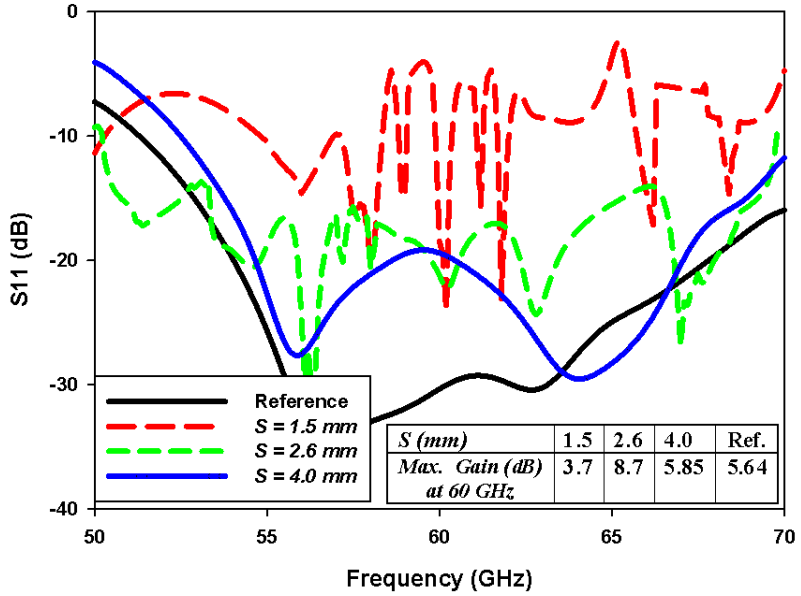

Fig.3-6 Simulated reflection coefficientsand maximum gain for different values of *S*

3.4 Experimental Results

To validate the proposed antenna design, two prototypes were fabricated and tested. Fig.3-7 shows photos of the fabricated reference antenna (without CP-EBG), and the proposed antenna (with CP-EBG).

a) S-Parameters

The reflection coefficient of the proposed antenna is simulated using HFSS software. Fig.3-8 shows simulated and measured return losses. Results for the reference antenna are also presented for comparison. Simulated and measured results show a good correlation. The small dips in the reflection coefficient of the proposed antenna are

expected by considering the operational principle of the mushroom EBG, which is based on the resonant system [11]. The EBG structure negatively affects the reflection coefficient through changing the input impedance of the antenna due to its close proximity to the antenna. However, the antenna is still matched over the suggested bandwidth with high radiation efficiency.

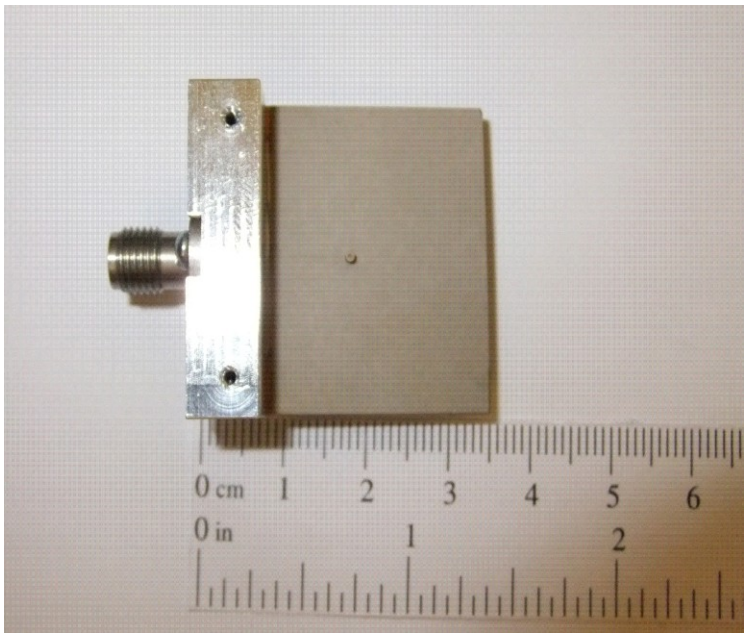

(a)

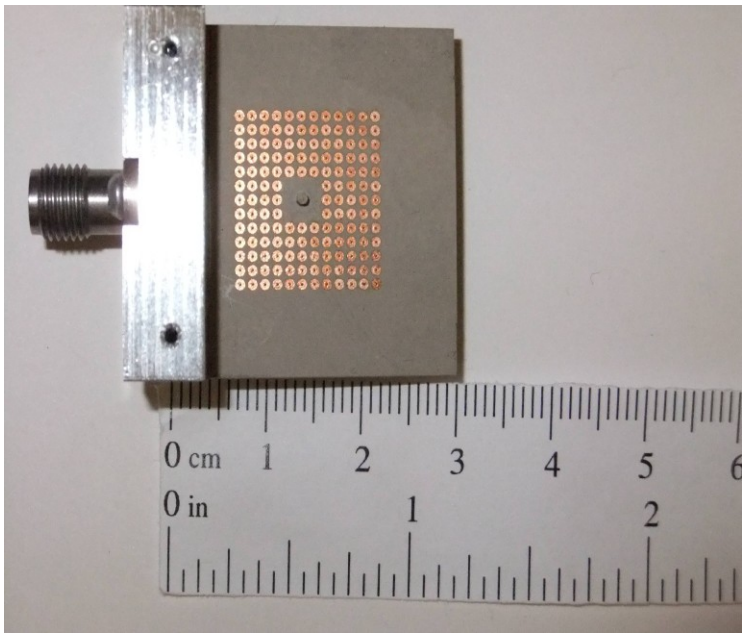

(b)

Fig. 3-7. Photos of the fabricated antenna prototypes. (a) Reference antenna (b) Proposed antenna

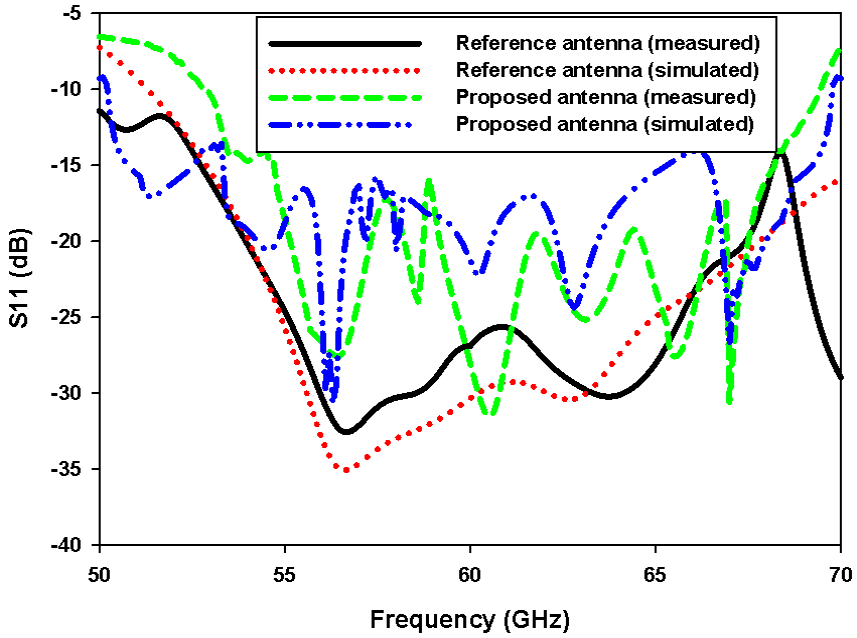

Fig.3-8. Simulated and measured reflection coefficients of the reference, and proposed antennas.

b) Radiation Patterns and Antenna Gain

Simulated and measured normalized H and E-plane power patterns of the proposed and reference antennas at 60 GHz are shown in Fig. 3-9 and Fig. 3-10, respectively. Simulated and measured patterns agree well with each other. Surrounding the DRA by the CP-EBG lattice drastically improves the radiation characteristics of the antenna. The front-to-back ratio is 21 dB and 12 dB for the proposed and reference antennas, respectively. Moreover, the radiation toward substrate edges (90 and -90) is decreased by about 10 dB. Fig.3-11 shows the simulated power patterns at two other frequency points, 57 GHz, and 63 GHz. Its apparent that the proposed antenna has a consistent radiation pattern over the suggested bandwidth. Large ripples are observed in the E-plane pattern. This can be understood by considering the fact that the $HEM_{11\delta}$ mode has a stronger lateral radiation in the E-plane (almost omnidirectional) than in the H-plane (broadband), and hence, corrupting the overall pattern due to the strong diffraction from the edges. The measured cross polarization levels were less than -16 dB and -13 dB in both planes for the proposed and reference antennas, respectively. The small discrepancies between simulated and measured results are believed to be due to the fabrication tolerances.

The maximum gain of the proposed and reference antennas were measured. Fig.3-12 summarizes the results. The proposed antenna gain varies between 7.2 dBi and 8.6 dBi over the suggested frequency bandwidth, and between 4.9 dBi and 5.2 dBi for the reference antenna over the same frequency span.

To further understand the functionality of the proposed EBG structure, Fig.3-13 shows the simulated electric field distribution in the surface of the EBG plane. The proposed CP-EBG the CP-EBG surface has high equivalent input surface impedance in its bandgap, therefore it blocks surface waves from propagating, which, in turns, reduces the energy leakage and further shapes the radiation pattern. In addition, it reduces the back radiation resulting from edge diffraction. Moreover, it contributes to the radiation through the large currents induced into it. The wide-bandgap associated with our CP-EBG structure (57.2 GHz to 72.3 GHz) has yielded gain improvement with ± 0.7 dB flatness over the suggested bandwidth compared to ± 0.15 dB flatness for the reference antenna over the same band.

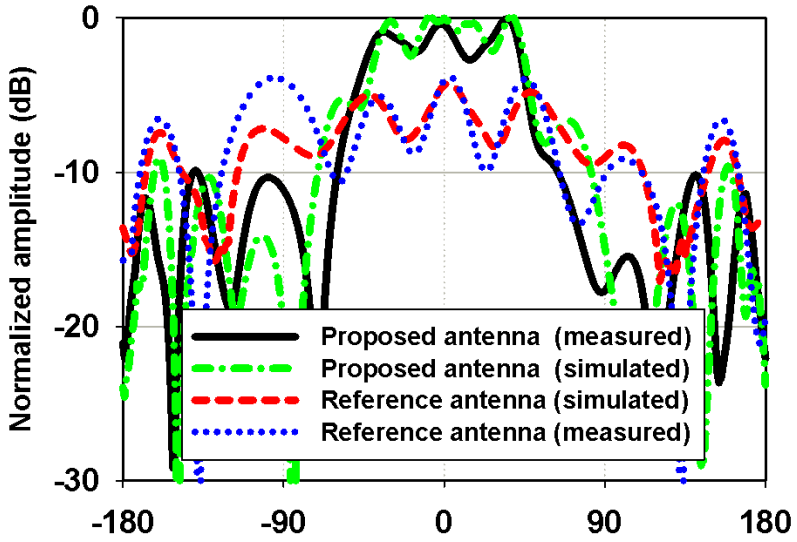

Fig.3-9. Simulated and measured normalized H-plane power patterns at 60 GHz of the reference and proposed antennas.

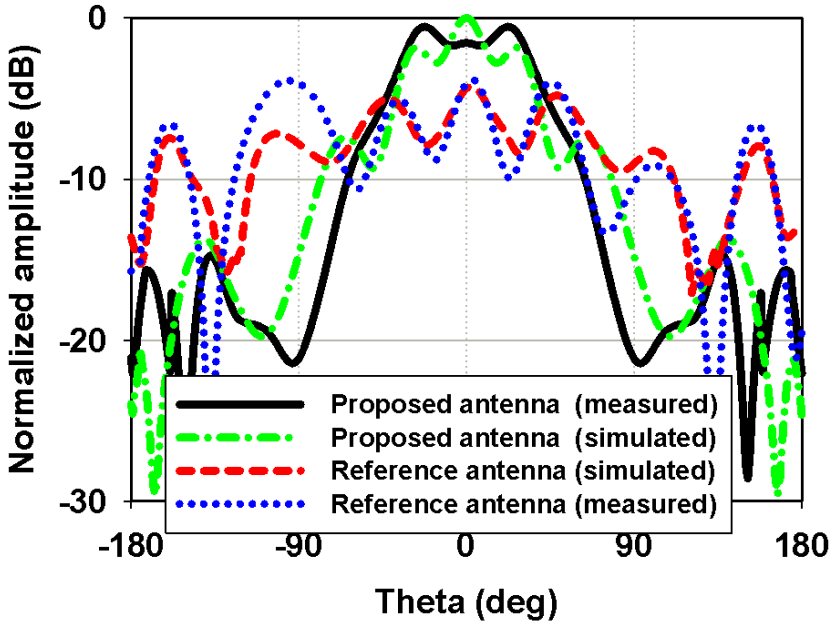

Fig.3-10. Simulated and measured normalized E--plane power patterns at 60 GHz of the reference and proposed antennas

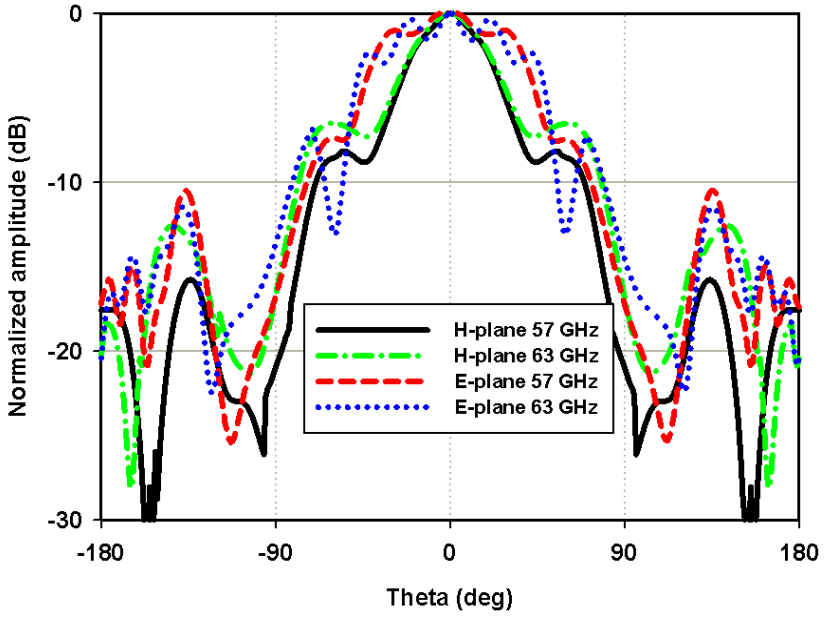

Fig.3-11. Simulated normalized H- and E--plane power patterns at 57 GHz and 63 GHz of the proposed antenna.

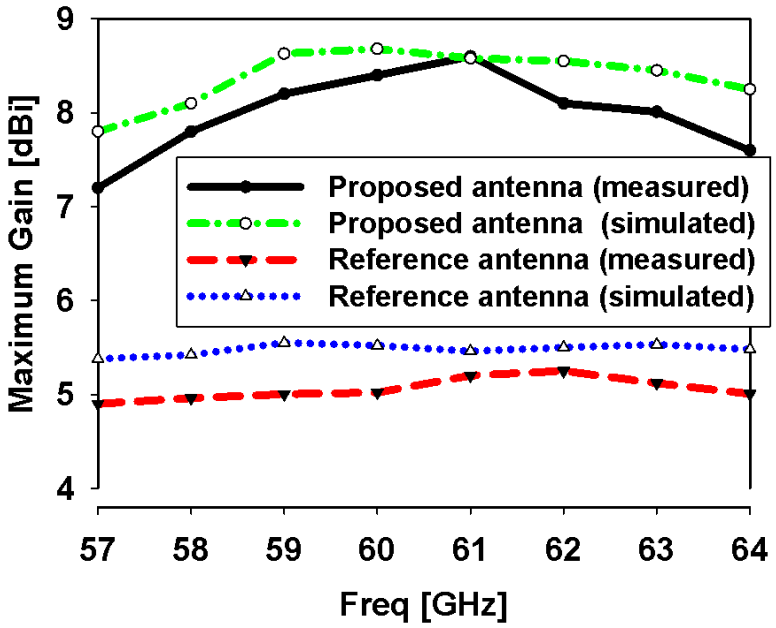

Fig.3-12. Simulated and measured maximum gain as function of frequency of the reference and proposed antennas.

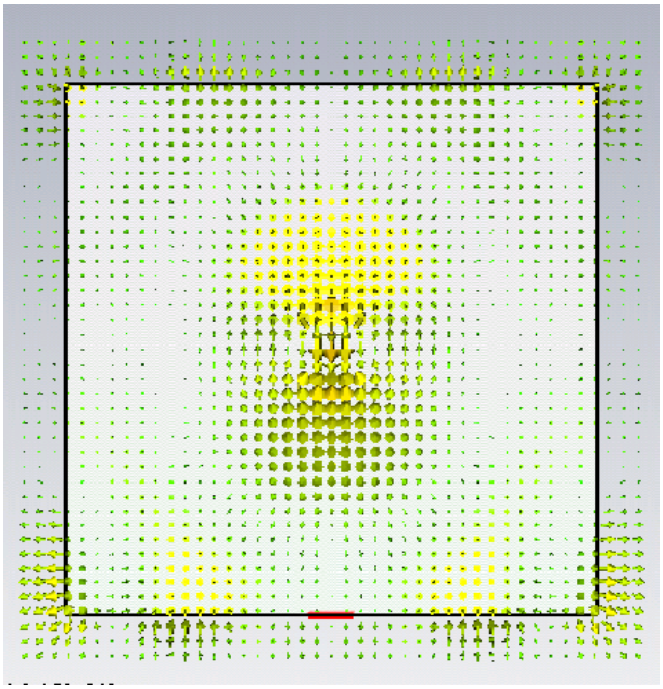

(a)

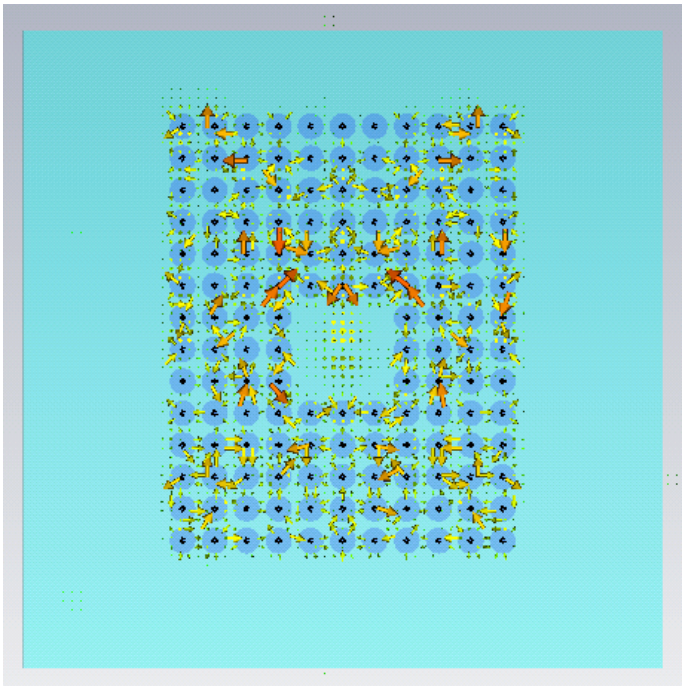

(b)

Fig.3-13. Simulated electric field distribution in the surface of the EBG plane, (a) without EBG, (b) with EBG (right).

3.5 References

[1] S. A. Long, M.W. McAllister, and L. C. Shen, "The resonant cylindrical dielectric cavity antenna," IEEE Trans. Antennas Propag., vol. AP-31, no. 5, pp. 406–612, May 1983.

[2] M. N. Jazi and T. A. Denidni, "Design and implementation of an ultrawideband hybrid skirt monopole dielectric resonator antenna," IEEE Antennas Wireless Propag. Lett., vol. 7, pp. 493–496, Dec. 2008.

[3] A. Petosa and S. Thirakoune, "Rectangular dielectric resonator antennas with enhanced gain," IEEE Trans. Antennas Propag., vol. 59, no. 4, pp. 1385–1389, April 2011.

[4] Sievenpiper, D., Lijun Zhang; Broas, R.F.J. Alexopolous, N.G., and Yablonovitch, E., "High-Impedance Electromagnetic Surfaces with a Forbidden Frequency Band",

IEEE Trans. Microwave Theory and Techniques, Vol. 47, no. 11, pp.2059-2074, Nov. 1999.

[5] M. Z. Azad and M. Ali, "Novel wideband directional dipole antenna on a mushroom like EBG structure," IEEE Trans. Antennas Propag., vol. 56, no. 5, pp. 1242–1250, May 2008.

[6] D. Dawn, Y. Ohashi, and T. Shimura, "A novel electromagnetic bandgap metal plate for parallel plate mode suppression in shielded structures," IEEE Microwave Wireless Compon. Lett., vol. 12, no. 5, pp. 166–168, May 2002.

[7] J. Joubert, J. C. Vardaxoglou, W. G. Whittow, and J. W. Odendaal, "CPW-fed cavity-backed slot radiator loaded with an AMC reflector, IEEE Trans Antennas Propag., vol. 60, no. 2, pp. 735–742, Feb. 2012.

[8] F. Elek, R. Abhari, and G. V. Eleftheriades, "A uni-directional ring-slot antenna achieved by using an electromagnetic band-gap surface," IEEE Trans. Antennas Propag., vol. 53, no. 1, pp. 181–190, Jan. 2005.

[9] J. Liang and H. Y. D. Yang, "Radiation characteristics of a microstrippatch over an electromagnetic band-gap surface," IIEEE Trans. Antennas Propag., vol. 55, no. 6, pp. 1691–1697, Jun. 2007.

[10] J. Y. Zhang, V. Hagen, M. Younis, C. Fischer, and W. Wiesbeck, "Planar artificial magnetic conductors and patch antennas," IEEE Trans. Antennas Propag., vol. 51, no. 10, pt. 1, pp. 2704–2712, Oct. 2003, Special issue on metamaterials.

[11] A. E. I. Lamminen, A. R. Vimpari, and J. Saily, "UC-EBG on LTCC for 60-GHz frequency band antenna applications," IEEE Trans. Antennas Propag., vol. 57, no. 10, pp. 2904–2912, Oct. 2009.

[12] R. Coccioli, F. R. Yang, K. P. Ma, and T. Itoh, "Aperture-coupled patch antenna on UC-PBG substrate," IEEE Trans. Microwave Theory and Techniques,vol. 47, no. 11, pp. 2123–2130, Nov. 1999.

[13] P. Kovacs, T. Urbanec,"EBG structures: practical tips and advice for antenna engineers, " Radio engineering, vol. 21, no. 1, April, 2012.

[14] M. J. Al-Hasan, T. A. Denidni, and A. Sebak, “A New UC-EBG Based dielectric Resonator Antenna for Millimeter-wave Applications,” 2011 IEEE International Symposium on Antennas and Propagation (APSURSI), pp. 1274-1276, 2011.

[15] D. Ramaccia, A. Toscano, and F. Bilotti, "A new accurate model of high-impedance surfaces consisting of circular patches," Progress in Electromagnnetics Research (PIER-M), vol. 21, pp. 1-17, 2011.

[16] S. Assimonis, T. Yioultsis, and C. Antonopoulus, “Design and optimization of uniplanar EBG structures for low profile antenna applications and mutual coupling reduction,” IEEE Trans. Antennas Propag., vol. 60, no. 10, pp 4944-4949, Oct. 2012.

[17] A. Perron, T. A. Denidni and A. R. Sebak, “Computer-Aided Design and Analysis of Dielectric Resonator Antennas,” International Journal of RF and Microwave Aided Engineering, vol. 20, no. 1, pp. 42-50, January 2010.

CHAPTER FOUR: MUTUAL COUPLING REDUCTION IN MILLIMETER-WAVE DIELECTRIC RESONATOR ANTENNA ARRAYS USING NEW COMPACT ELECTROMAGNETIC BAND-GAP STRUCTURE

4.1 Introduction

Mutual-coupling (MC) refers to the electromagnetic interactions between antenna array elements. It has an impact effect on antenna array performance through changing the input impedance of the radiating elements, gain, sidelobe level and radiation pattern shape [1]. In MIMO systems [2], for the signals to undergo different fading characteristics, and hence maximizing the channel capacity and improving the signal-to-noise ratio, the maximum interelement spacing in an array must be half of the wavelength. However, this condition yields strong mutual coupling. Moreover, in phased antenna arrays, to alleviate scan blindness, a high level of isolation between the array elements is required [3]. Furthermore, in applications such as imaging radar systems [4], where the transmitting and receiving antennas operate at the same frequency band and are placed close to each other, the mutual coupling needs to be effectively reduced to achieve better system performance [4]. Therefore, several techniques have been proposed to reduce mutual coupling including defected ground structures (DGS) [5], parasitic element slots [6], slotted ground plane [7], and electromagnetic band-gap (EBG) structures [8]. Among these techniques, EBG structures are found to have the best performance in terms of wideband operation and radiation pattern preservation.

EBGs [9] are periodic structures which have a frequency band-gap, in which no surface-wave propagation is allowed. Therefore, by the proper design of the EBG structure, it can reduce the mutual coupling between array elements by blocking surface-waves propagation. At millimeter-wave (MMW) bands, and due to the small absolute interelement spacing in an array, the manufacturing is more difficult and tolerances will be tighter. Therefore, the need of compact and easy-to-fabricate EBG structure becomes very challenging. In addition, the wide bandwidths associated with MMW bands require an EBG structure with wide frequency band-gap in order to efficiently suppress surface

waves and improves the isolation over the whole bandwidth.

To meet the above mentioned requirements, the authors present a new-shape, wide band-gap, compact EBG structure operating at the 60 GHz band. Two aperture-coupled dielectric resonator (DR) antennas [10] separated by a half of the wavelength incorporating the developed EBG structure are also presented. It is worthy mentioning that the design process of the proposed EBG unit cell is systematic and has a tunable frequency bandgap. Therefore, optimization and frequency conversion can be applied on the unit cell.

4.2 EBG Unit Cell Design

An EBG structure can be described by an equivalent capacitance *C,* introduced by the gaps between the conductor edges of adjacent cells, and equivalent inductance *L*, introduced by the strips connecting the adjacent cells. The center frequency of the bandgap is given by [9]:

$$f_c = 1/2\pi\sqrt{LC} \tag{4-1}$$

The design procedure started by a conventional uniplanar EBG cell [11], Fig.4-1. It consists of one central square patch and four narrow connecting bridges. Additional inductances are formed by adding two connecting bridges (b). Then, the inductance value was increased by prolonging the connecting bridges (c). Therefore, by creating such bridges, the resonance frequency of the proposed EBG unit-cell is significantly reduced from that of the conventional EBG unit-cell while keeping the same dimensions. Finally, the EBG cell dimensions are tuned to have a bandgap over the desired frequency band.

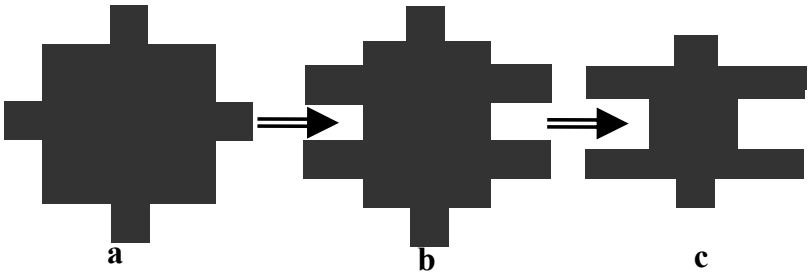

Fig.4-1. Design procedure of the proposed EBG unit-cell.

The proposed EBG structure is shown in Fig.4-2. Each EBG unit-cell has a shunt capacitance Cp, and is coupled to other unit-cells by one series inductor (Lsh) in parallel with two series capacitances (Csh) in the horizontal direction, and two one series inductors (Lsv) in the vertical direction.. The EBG is printed on 0.5-mm-thick conductor-backed ROGERS 3006 substrate. The dimensions of the proposed EBG cell are shown in Table 3-1. It has periodicities of 0.98 mm and 0.23 mm in the vertical and horizontal directions, respectively. The dimensions of the conventional uniplanar EBG unit-cell [11] which yields similar transmission characteristics to the proposed EBG unit-cell, are shown in Table 3-2. The asymmetry of the proposed EBG yields different transmission characteristics in each direction. This work focuses on the bandgap characteristics in the horizontal direction.

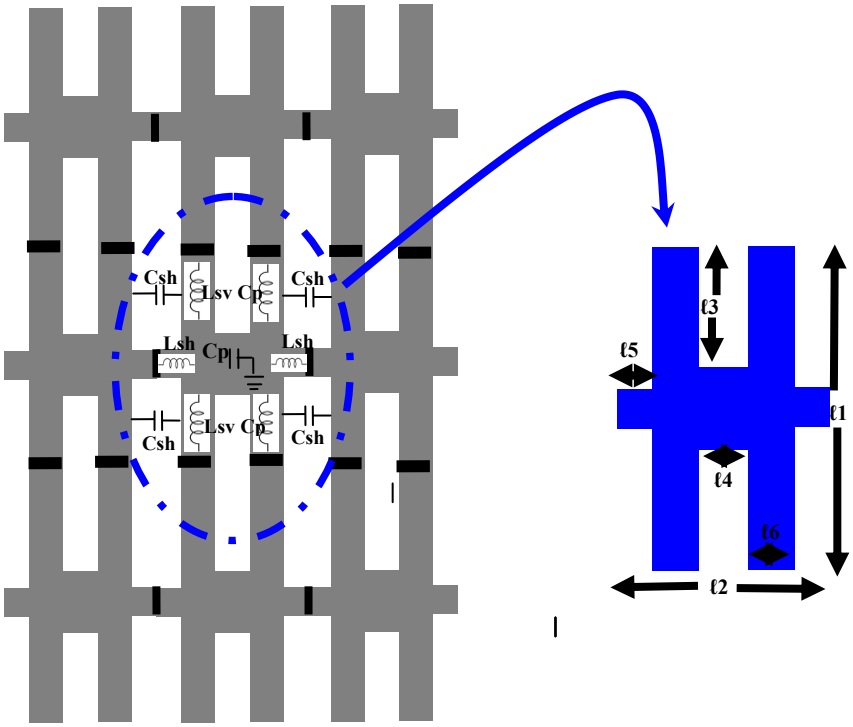

Fig.4-2. Geometry of the proposed EBG unit-cell.

Table 4-1 Proposed EBG Unit-cell dimensions

Parameter	ℓ1	ℓ2	ℓ3	ℓ4	ℓ5	ℓ6
Length (mm)	0.98	0.23	0.39	0.05	0.04	0.05

Table 4-2 Dimensions of the proposed and conventional EBG unit-cells

EBG Unit-cell	Periodicity in horizontal direction (mm)	Periodicity in vertical direction (mm)
Conventional	1.1	**1.1**
Proposed	**0.23**	**0.98**

Fig.4-3 shows the dispersion diagram of the proposed EBG unit-cell in the *OX* direction. It shows the bandgap between the first two propagating modes for different wave vectors directions in the *OX* direction, and in the region above the light line. Simulations where carried out using the CST simulator [12]. The solid blue and the dashed black lines represent the light line and the line for the dielectric material, respectively. Along this direction, the proposed EBG has a band-gap from 58.8 GHz to 65.1GHz, with a gap to mid-gap ratio (the ratio of the bandgap width to the center frequency of the bandgap) of 9.8%, where electromagnetic waves with different phases are prohibited from propagating.

The symmetric microstrip line technique [13] has been used to further investigate and verify the transmission characteristics of the proposed EBG structure along the same direction. It is considered to be a strongly coupling technique, and reduces the influence of parasitic modes. In this technique, a lattice of the proposed EBG is inserted between two open ended, symmetric microstrip lines, as shown in Fig.4-4 (a). Electromagnetic waves are launched by the first microstrip line, and detected by the second line. Then the transmission coefficient is measured and compared to the transmission coefficient from the reference structure. The reference structure is shown in Fig.4-4 (b). It is identical two-open ended microstrip lines without EBG in the middle. In this case, the attenuation due to losses will be the same in both structures. Therefore, any difference in the transmission characteristics will solely be due to the EBG structure.

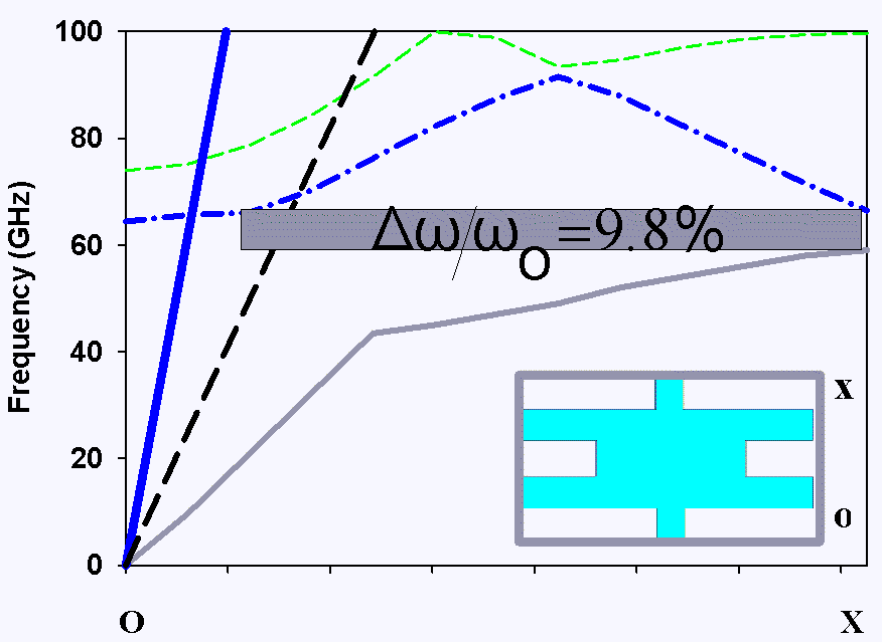

Fig.4-3. Dispersion diagram of the proposed EBG in the *OX* direction.

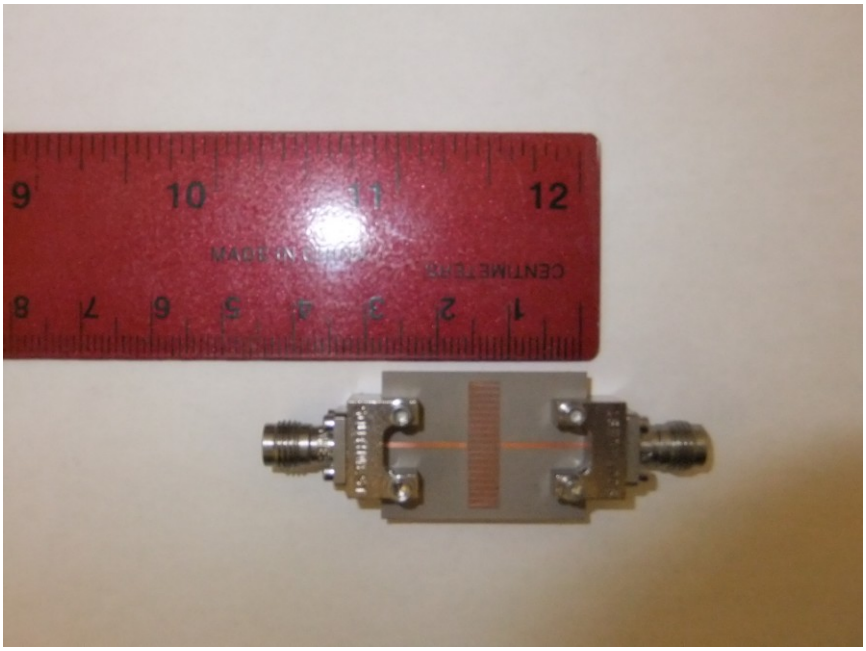

(a)

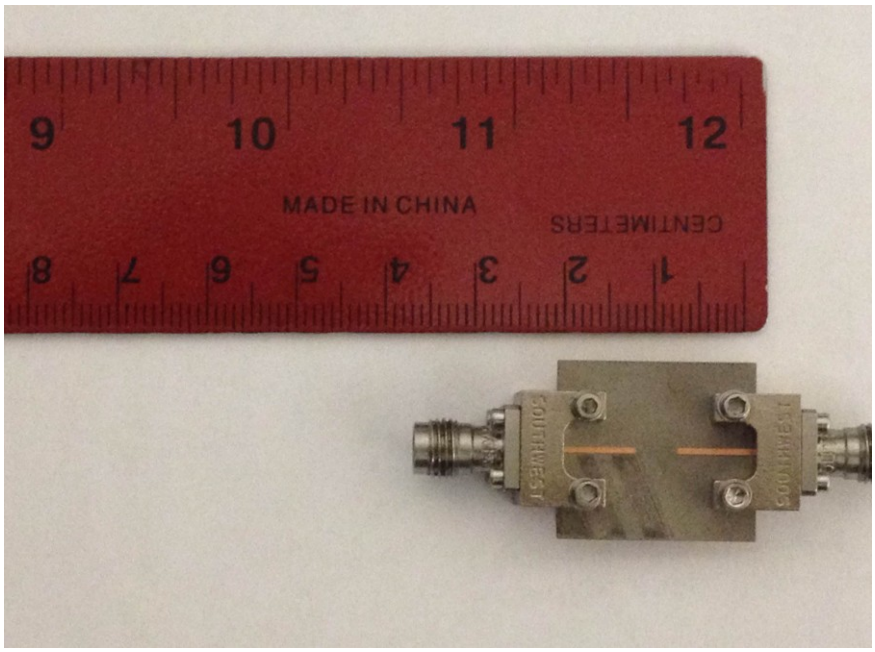

(b)

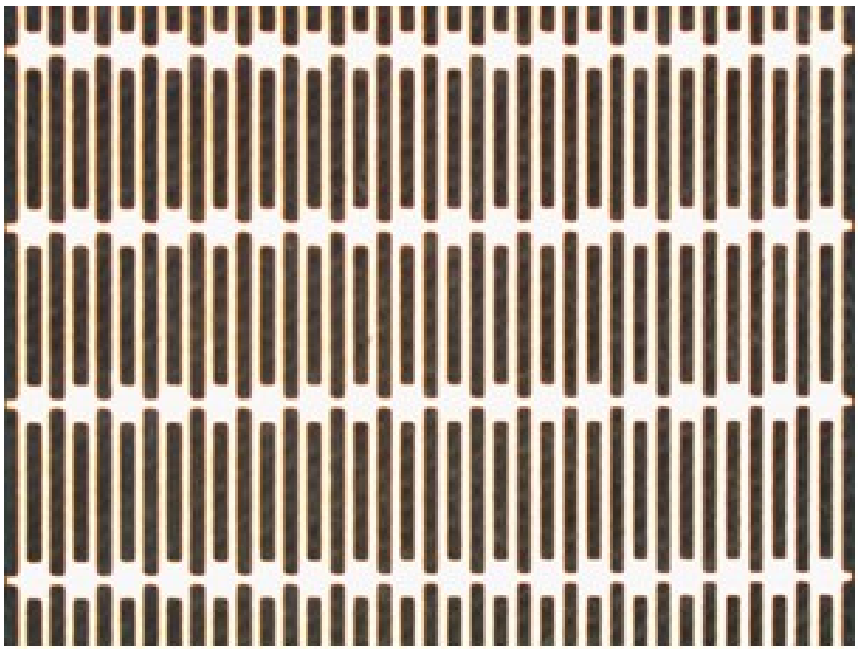

(c)

Fig.4-4. (a)The fabricated symmetric microstrip line structure. (b) Reference structure. (c) Zoomed view of the proposed EBG structure.

The simulated and measured transmission coefficients of the proposed EBG structure in the horizontal direction are shown in Fig.4-5.

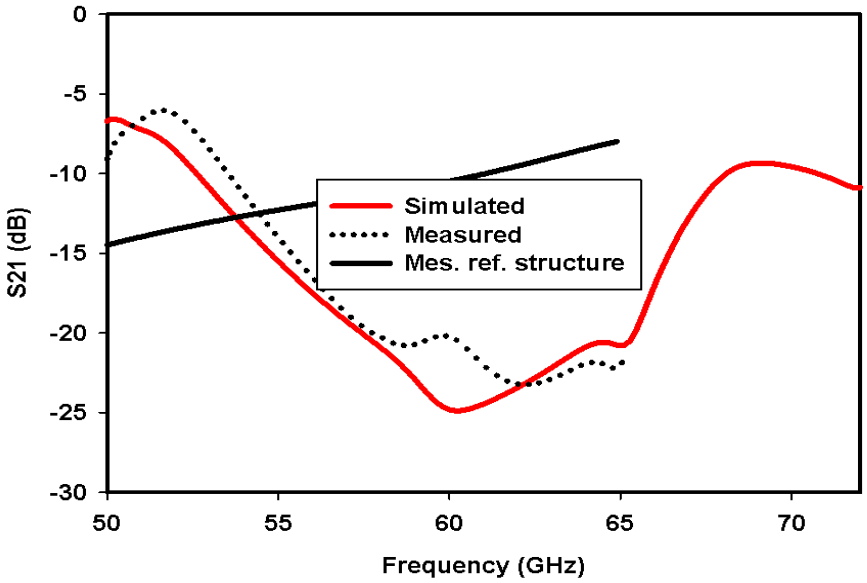

Fig.4-5. Simulated and measured transmission coefficients of proposed EBG structure.

An average of about 13 dB reduction in the transmission coefficient is observed over the 57-64 GHz bandwidth. The VNA used in the measurement goes up to 65 GHz only. Clearly, there is a good agreement between measured and simulated results.

In [14], a uniplanar-compact EBG (UC-EBG) operating at the 60 GHz band was used to reduce the mutual coupling between two patch antennas at 60 GHz. It is considered to be the only work reported in the literature about using planar EBG to reduce mutual coupling at 60 GHz. Comparing this with our work, we find that the proposed EBG unit-cell is 72% less in area. Moreover, in [14], the LTCC technology was used to fabricate the EBG structure. However, in our work the simple and cheap PCB technology was used. Furthermore, in [14], the interelement spacing between the array elements is 5.8 mm (1.16 λ), compared to 2.5 mm (0.5λ) in our work. Finally, an average of 8 dB reduction of mutual coupling was obtained in [14], compared to 13 dB reduction level in our work.

The size occupied by the proposed EBG unit cell is 78% less than that of an equivalent conventional uniplanar EBG unit cell operating at the same frequency band. Besides, there have been many different planar EBG structures reported in the literature that provide a size reduction compared to the uniplanar EBG [11]. For example, in [15], 60 % size reduction was obtained using a spiral EBG. Moreover, in [16], 39 % size

reduction was achieved. In terms of periodicity, in [17], the periodicity of the proposed rabbit spiral EBG is 0.055λ, and 0.1 λ for the uniplanar-compact EBG in [18]. Furthermore, a planar EBG was introduced in [19] with 0.08 λ periodicity. This compares to only 0.046λ periodicity in the horizontal direction of the proposed EBG unit cell. Indeed, and despite the fabrication limitations at 60 GHz, the proposed EBG unit cell provides at least 12 % more size reduction than any other planar EBG structure.

With these characteristics, the proposed EBG structure can be used to reduce the mutual coupling between closely-spaced array elements operating around the suggested bandwidth. A practical application is presented in the next section.

4.3 MMW EBG-based Dielectric Resonator Antenna Array

Antenna Array Design

The geometry of the proposed antenna array is shown in Fig.4-6. Two identical 1.27 mm high cylindrical DR antennas with 1.06 mm diameter made from ROGERS RT/duriod 6010.2LM material are placed on the top of ROGERS 3006 substrate (first substrate) with 0.254 mm thickness. Two identical 50 Ω microstrip lines of 0.375 mm width were printed on the bottom of another 0.254 mm thick ROGERS 3006 substrate (second substrate), the energy is coupled to the DR antennas through two narrow slots etched in a partially-removed ground plane on the top of the second substrate. The two cylindrical DR antennas are spaced by 2.5 mm center-to-center distance (half of the free space wavelength at 60 GHz). Partially-removed ground plane yields reducing creeping waves (waves propagating along the conductor-dielectric interface).

Six periods of the proposed EBG structure were placed between the two radiating DR antennas. The EBG ground plane is printed on the bottom of the second substrate.

Placing the slot at the center of the DR antenna yields the excitation of the fundamental mode $HEM_{11\delta}$. Its resonance frequency, according to the magnetic wall model, is given by [20]:

$$f^{HEM}{}_{11\delta} = \frac{6.324}{\sqrt{\varepsilon_r + 2}}\left(0.27 + 0.36\frac{r}{2h} + 0.02\left(\frac{r}{2h}\right)^2\right).\frac{4.7713}{r} \qquad (4\text{-}2)$$

where r is the radius, h is the height, and ε_r is the relative permittivity of the DR antenna.

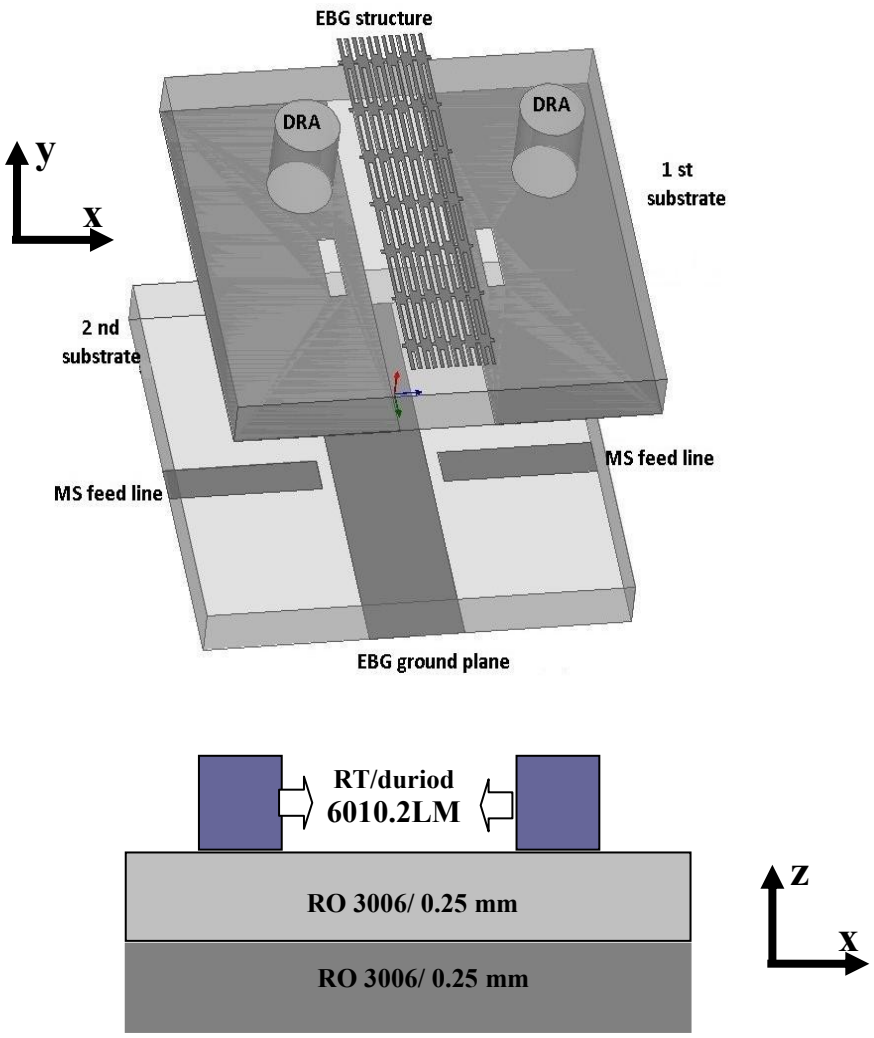

Fig.4-6. The proposed antenna array: exploded view (top), side view (bottom).

To achieve wide impedance bandwidth, the slot is set to resonate around the 60 GHz band. The slot resonates at slightly less a half of the guided wavelength. For this purpose, the length of the slot is chosen in the vicinity of $\lambda g/2$, where λg is the guided wavelength in the feed substrate. However, the resonance frequency of the slot is also affected by the substrate above the ground plane. Thus, further parametric studies were carried out to optimize the antenna performance. The final slot length and width are found to be 0.87 mm and 0.18 mm, respectively.

It is worthy mentioning here that the slot can be replaced by an equivalent horizontal

magnetic dipole, and the cylindrical DR antenna can also be replaced by an equivalent horizontal magnetic dipole when excited in its $HEM_{11\delta}$ mode. Thus, the radiation pattern for both modes is the one of a horizontal magnetic dipole, broadband in the H-plane and almost omnidirectional in the E-plane.

4.4 Experimental Results

The proposed antenna array design incorporating the developed EBG structure was fabricated and tested. For comparison, an antenna array without the EBG structure (reference array) was also fabricated and tested as well. Fig.4-7 shows photos of the proposed and reference antenna arrays.

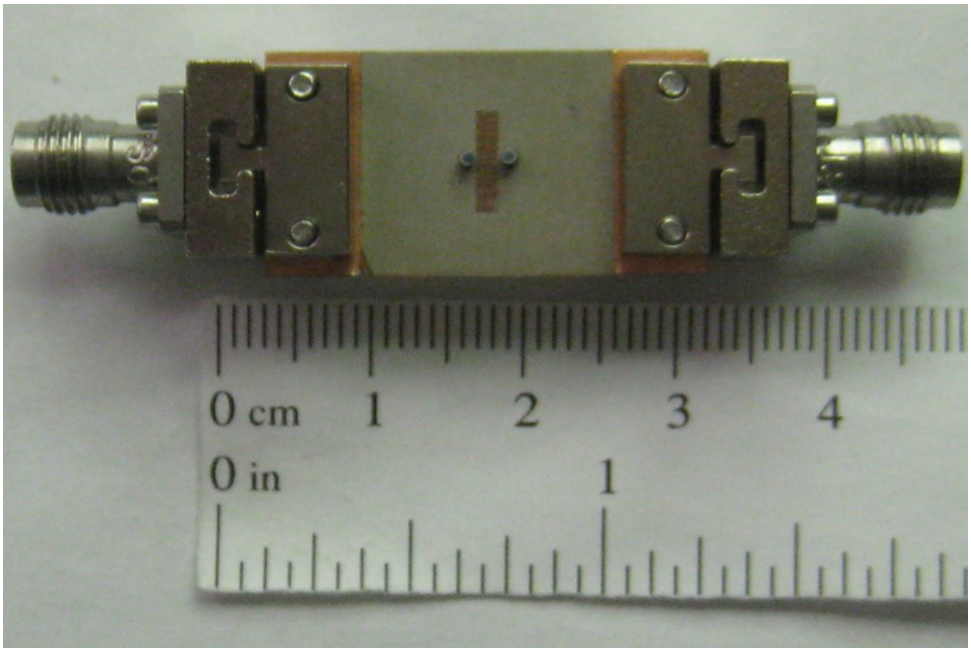

(a)

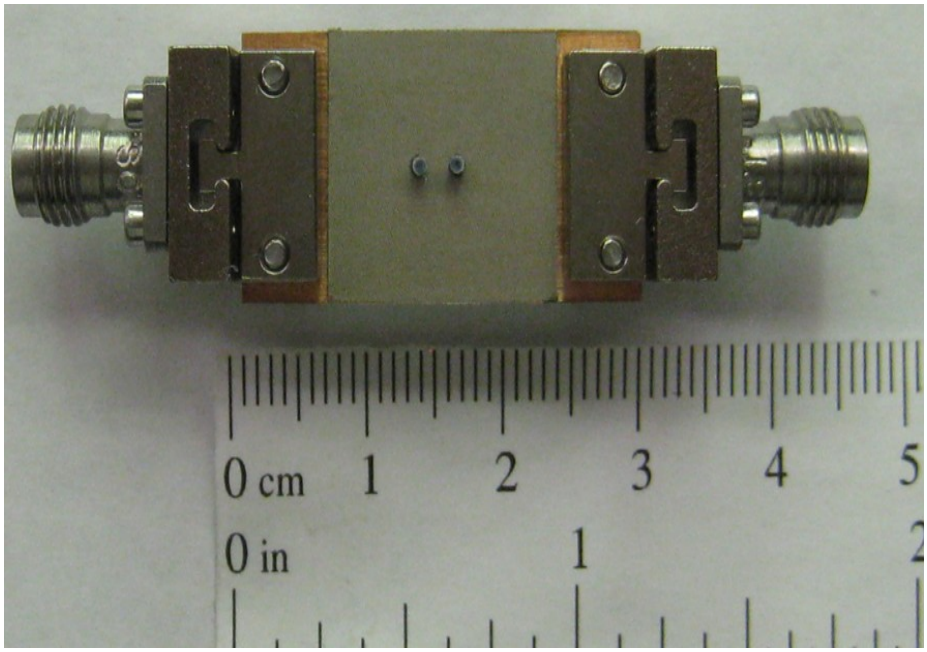

(b)

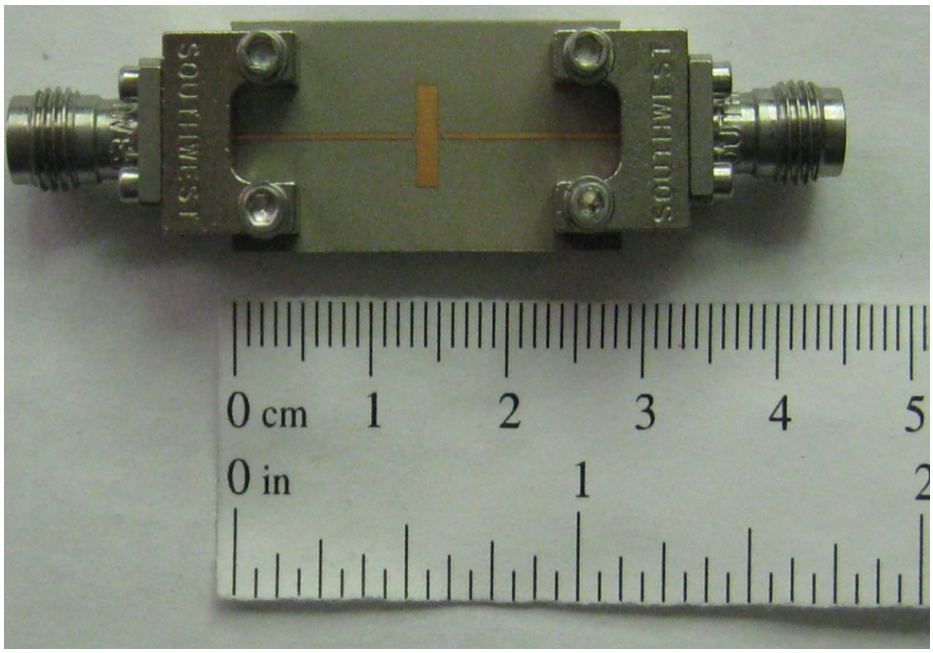

(C)

Fig.4-7. Photos of the fabricated antenna array prototypes: (a) proposed array, (b) reference array, and (c) bottom view of the proposed/ reference array.

S-parameters

The measured and simulated transmission and reflection coefficients of the proposed antenna array are shown in Fig. 4-8 and Fig. 4-9, respectively. For comparison, results from the reference array are also presented. Simulated and measured results show a good agreement. Again, the measured results are limited to the maximum frequency of the VNA used during the measurements. Inserting the proposed EBG between the two DRAs efficiently improves the isolation level. An average of 13 dB mutual coupling reduction is obtained over the suggested bandwidth compared to the reference array. To further verify the functionality of the proposed EBG structure, the simulated transmission coefficient of the DRA array with single row of conventional uniplanar EBG is also shown. A little isolation improvement around 4 dB is obtained when using the conventional EBG. It is because only one row of the conventional EBG can be inserted between the two DR antenna elements. This compares to six rows of the proposed EBG structure. Thanks to our compact EBG unit cell.

The conductor backed dielectric slab on which the two DR antennas are mounted generates surface waves propagating along the surface. The proposed EBG structure suppresses these surface waves within its bandgap, resulting in mutual coupling reduction. Efficient surface-wave suppression over the whole suggested bandwidth is due to the wide bandgap of the proposed EBG structure, and the relatively-large number of rows inserted between the radiating elements. The close proximity between the DR antennas and the EBG structure yields near field interactions and changing the input impedance of the radiating elements, resulting in affecting the matching level of the antenna. However, the proposed antenna array is still matched over the suggested bandwidth.

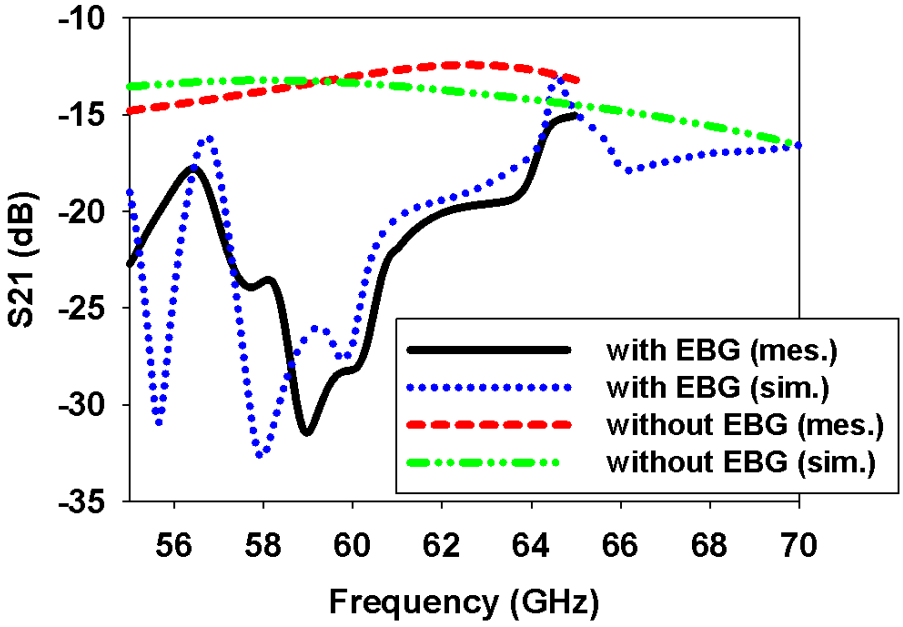

Fig.4-8. Simulated and measured transmission coefficients of the proposed and reference antenna arrays.

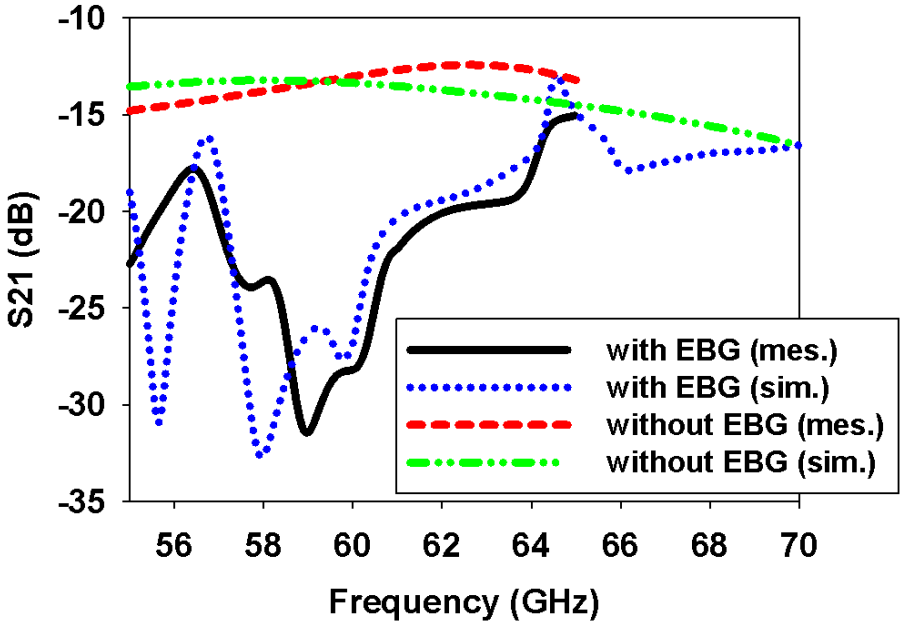

Fig.4-9. Simulated and measured reflection coefficients of the proposed and reference antenna arrays.

To further understand the operational principle of the EBG structure, the simulated volume and surface current distributions at 60 GHz for the proposed and reference antenna array are shown in Fig.4-10. It shows the effectiveness of the EBG structure in

reducing mutual coupling between the two DR antennas. The EBG structure effectively traps and confines the EM-fields, resulting in significant reduction in the near field interactions between the two DR antennas (less energy is coupled to the matched DR antenna from the excited one). Therefore, improving the isolation between the two antennas.

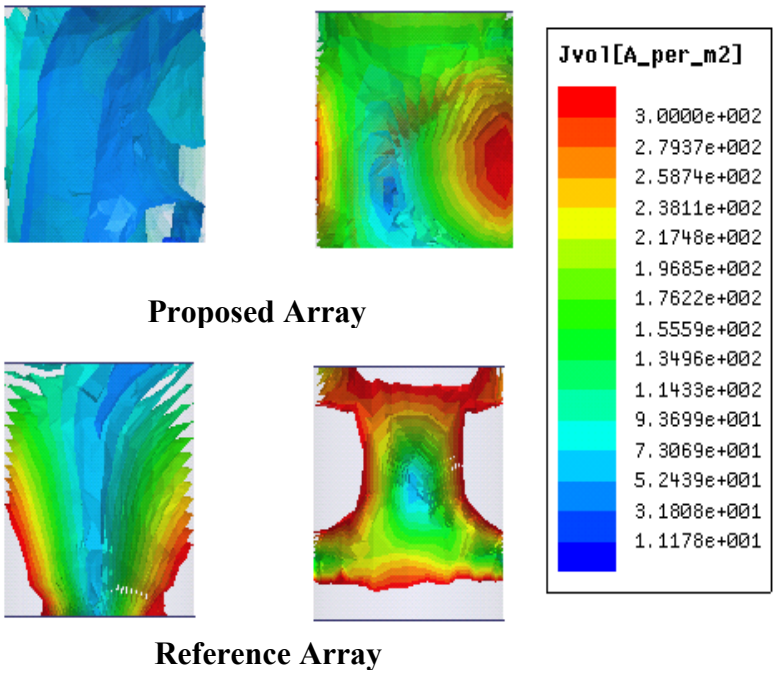

(a)

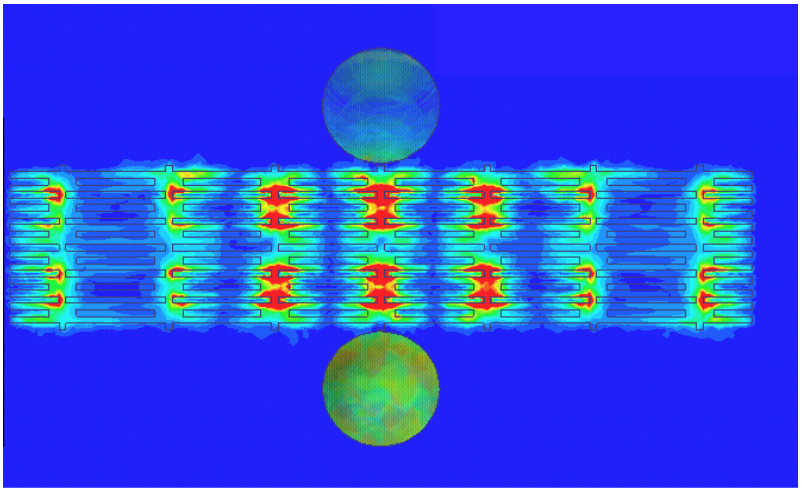

(b)

Fig.4-10. (a): Volume current distribution inside the two DR antennas at 60 GHz (*XZ* plane). (b) Surface current distribution on the EBG structure at 60 GHz (*XY* plane).

Radiation Patterns and Gain

Fig.4-11 shows the normalized measured E- and H-plane power patterns at 60 GHz of a single-fed DR antenna, while the other element was matched. The front-to-back ratio is 20 dB and 17 dB for the proposed and reference antenna, respectively. The pattern in the E-plane is slightly tilted because of the asymmetry in this plane. It is apparent that surface-wave suppression not only yields mutual coupling reduction, but also it improves the back radiation by reducing edge scattering waves.

The maximum gain of one DR antenna element while the other element was matched was measured over the suggested bandwidth. Fig.4-12 summarizes the results. The gain varies between 3.9dBi and 4.8 dBi over the suggested bandwidth. The maximum gain of the proposed antenna array was calculated from the measured gain of a single element DR antenna by using the antenna array theory.

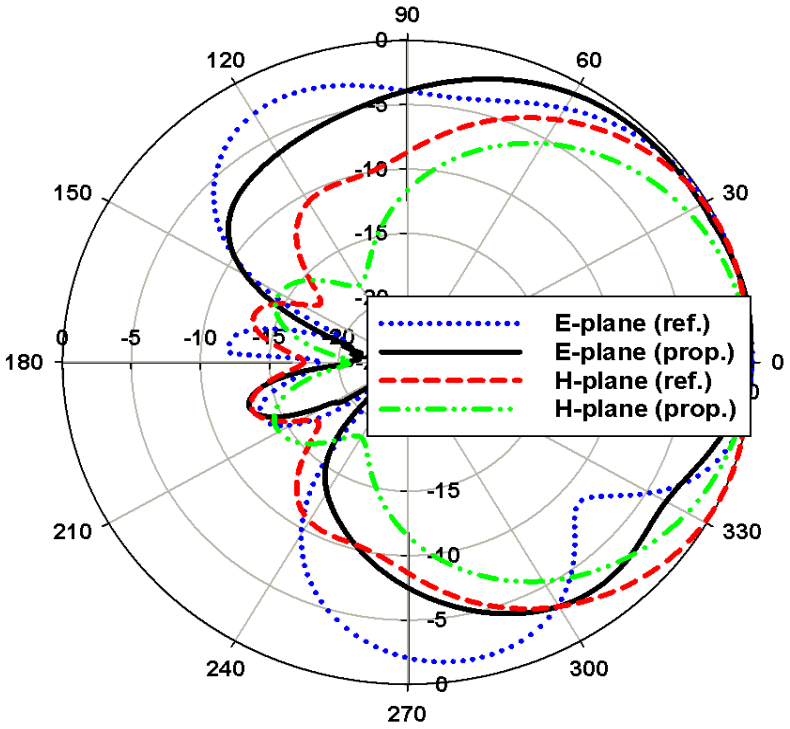

Fig.4-11. Measured normalized E- and H-plane power patterns at 60 GHz of the proposed and reference antenna arrays.

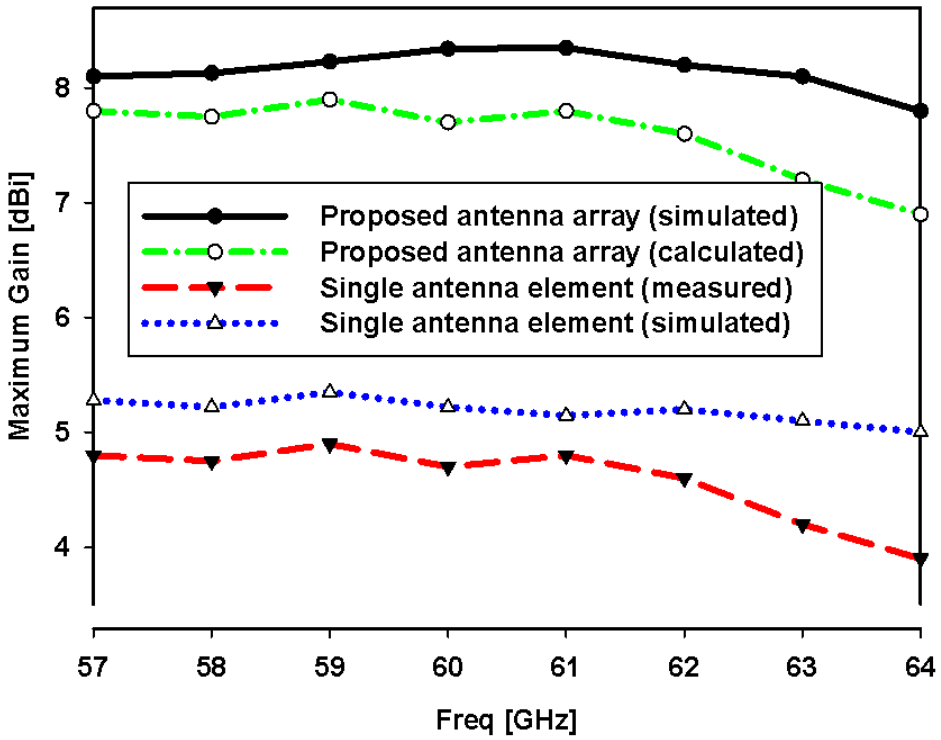

Fig.4-12. Measured and calculated maximum gain of the proposed antenna array.

4.5 References

[1] H. Farahani, M. Veysi, M. Kamyab, and A. Tadjalli, "Mutual coupling reduction in patch antenna arrays using a UC-EBG superstrate," IEEE Antennas Wireless Propag. Lett., vol. 9, pp. 57–59, Jan. 2010.

[2] J. Wallace and M. Jensen, "Mutual coupling in MIMO wireless systems a rigorous network theory analysis," IEEE Trans on Wireless Communications, vol. 3 no. 4, pp. 1317–1325, July 2004.

[3] R. J. Mailloux, Phased Array Antenna Handbook. Dedham, MA: Artech House, 1993.

[4] Q. Lei, Z. Fei, X. Ke, C. Shun-Lian and M. Jun-Jie, "Transmit and receive isolation improvement of antenna arrays by using EBG structures," IEEE Antennas Wireless Propag. Lett., vol. 11, p.p. 93- 96, Jan. 2012.

[5] M. M. Bait-Suwailam, O. F. Siddiqui, and O. M. Ramahi, "Mutual coupling reduction between microstrip patch antennas using slotted-complementary split-ring resonators," IEEE Antennas Wireless Propag. Lett., vol. 9, pp. 876–878, Sept. 2010.

[6] L. Minz and R. Garg, "Reduction of mutual coupling between closely spaced PIFAs," Electron. Lett., vol. 46, no. 6, pp. 392–394, March 2010.

[7] J. Ou Yang, F. Yang, and Z. M. Wang, "Reducing mutual coupling of closely spaced microstrip MIMO antennas for WLAN application," IEEE Antennas Wireless Propag. Lett., vol. 10, pp. 310–312, 2011.

[8] Z. Iluz, R. Shavit, and R. Bauer, "Microstrip antenna phased array with electromagnetic bandgap substrate," IEEE Trans. Antennas Propag., vol. 52, no. 6, pp. 1446–1453, Jun. 2004.

[9] Sievenpiper, D., Lijun Zhang; Broas, R.F.J. Alexopolous, and N.G. Yablonovitch, E., "High-Impedance Electromagnetic Surfaces with a Forbidden Frequency Band", IEEE Trans. Microwave Theory and Techniques, vol. 47, no. 11, pp.2059-2074, Nov. 1999.

[10] M. J. Al-Hasan, T. A. Denidni, and A. Sebak, "A New UC-EBG Based dielectric Resonator Antenna for Millimeter-wave Applications," 2011 IEEE International Symposium on Antennas and Propagation (APSURSI), pp. 1274-1276, 2011.

[11] S. K. Sharma and L. Shafai, "Enhanced performance of an aperture coupled rectangular microstrip antenna on a simplified unipolar compact photonic bandgap (UC-PBG) structure," in IEEE Antennas and Propagation Soc. Int. Symp., Jul. 2001, vol. 2, pp. 498–501.

[12] Microwave Studio. (www.cst.com) .

[13] M. J. Al-Hasan, T. A. Denidni, and A. Sebak, "Millimeter-wave EBG-Based Aperture-Coupled Dielectric Resonator Antenna ," IEEE Trans. Ant. and Propag., vol. 61, no. 8, pp. 4354-4357, August 2013.

[14] A.E. I.Lamminen, A. R. Vimpari, and J. Saily, "UC-EBG on LTCC for 60 GHz frequency band antenna applications," IEEE Trans. AntennasPropag., vol. 57, no. 10, pp. 2904–2912, Oct. 2009.

[15] Q. R. Zheng,Y.Q. Fu, and N. C.Yuan, "Anovel compact spiral electromagnetic band-gap (EBG) structure," IEEE Trans. Antennas Propag, vol. 56, no. 6, pp. 1656–1660, Jun. 2008.

[16] M. T. Islam and M. S. Alam, “Compact EBG structure for alleviating mutual coupling between patch antenna array elements,” Progress in Electromagnetic Research, vol. 137, pp. 425–438, 2013.

[17] Y. Yao, X. Wang, and Z. Feng, “A novel dual-band Compact Electromagnetic Bandgap (EBG) structure and its application in multi-antennas1,” in Proceedings of the IEEE Antennas and Propagation Society International Symposium (APS' 06), pp. 1943–1946, Albuquerque, NM, USA, July 2006.

[18] F. R. Yang, K. P. Ma, M. Y. Qian, and T. Itoh, “A uniplanar compact photonic-bandgap (UC-PBG) structure and its applications for microwave circuits,” IEEE Trans on Microwave Theory and Techniques, vol. 47, no. 8, pp. 1509–1514, August 1999.

[19] A novel compact EBG structures with relative wide band-gap,” in Proceedings of the Asia-Pacific Microwave Conference (APMC' 07), pp. 1–3, Bangkok, Thailand, December 2007.

[20] A. Perron, T. A. Denidni and A. R. Sebak, “Computer-Aided Design and Analysis of Dielectric Resonator Antennas,” International Journal of RF and Microwave Aided Engineering, vol. 20, no. 1, pp. 42-50, January 2010.

CHAPTER FIVE: NEW MILLIMETER-WAVE HYBRID ISOLATOR FOR MUTUAL-COUPLING REDUCTION IN ANTENNA ARRAYS

5.1 Introduction

The demand of size reduction in modern communication industry has become an intense research topic. Therefore, size reduction in antenna arrays has drawn antenna designers' attention. However, the undesirable mutual coupling (MC) effects arise [1-3]. It is detrimental to antenna performance including array radiation pattern, manifold, sidelobe level, gain and impedance matching of the radiating elements [4]. In some applications, it is strictly required to have an isolation level of as low as -30 dB. In multiple-input-multiple-output (MIMO) systems [5, 6], for instance, to obtain de-correlated channels, and hence enhancing the system capacity and improving the bit-error-rate, the radiating elements need to be spaced at a maximum of half of the free-space wavelength. Additionally, in phased antenna array systems [7], a high isolation level is required to alleviate scan blindness. Furthermore, in imaging radar systems [8], the transmission and receiving antenna arrays are operating at the same frequency band and are closely spaced. Accordingly, a very high isolation level is required in order to reduce the interference between the transmitted and received signals.

Several approaches have been reported to reduce the MC effects and improve the isolation between radiating elements [9-14]. Electromagnetic band-gap (EBG) structures are among the most practical and easier to fabricate.

EBGs, when interposed in antenna arrays, suppress surface waves by introducing frequency band-gaps where EM propagation is not allowed. However, since EBGs fail to suppress other main sources of MC, their contribution to the isolation level is usually limited. Consequently, hybrid techniques were introduced in order to further improve the isolation level through controlling the other sources of MC. Nonetheless, these techniques have an impact effect on the radiation characteristics of the radiating elements.

Besides, a paucity of practical investigations on MC reduction at MMWs still exists. This is mainly due to two main reasons: First, the manufacturing complexity and tolerance caused by the small physical interelement spacing between the radiating elements. Consequently, the need of a compact and easy-to-fabricate EBG structure to fit within becomes very challenging. Second, the wide bandwidths associated with MMW bands require isolators that work effectively over wide frequency bandwidths.

In this perspective, a simple, yet efficient, hybrid isolator is proposed and demonstrated. The proposed hybrid isolator comprises two isolation techniques: a compact uni-planar EBG structure and choke absorber. The proposed EBG unit-cell is designed and miniaturized based on the stepped-impedance resonator (SIR) technique [15]. The EBG miniaturization process is systematic and tunable to different frequency bands. Henceforth, by incorporating the proposed hybrid structure in antenna arrays, the main sources of MC can be controlled without considerably affecting the radiation characteristics.

5.2 Proposed Hybrid structure

Main Sources of Mutual-Coupling

In antenna arrays, the MC level depends on several parameters: the spacing between the radiating elements, the geometry of the array, and physical parameters of the antennas. In planar antenna arrays with common ground plane, the main sources of MC are space waves, creeping waves propagating along the ground plane, and surface waves propagating along the dielectric/air interface.

In typical antenna arrays, the radiating elements have a common ground plane. Consequently, creeping waves cannot be controlled. However, both surface waves and space waves can be deliberately controlled to keep the MC under the desired level.

Proposed Hybrid Structure

a) Proposed EBG Unit-Cell

The design approach treats the EBG as a stepped impedance resonator (SIR) structure [15], which offers impedance discontinuity to the EM wave propagation, and hence providing stop bands.

The design procedure starts by a conventional uni-planar EBG unit-cell [16] as shown in Fig.5-1. The proposed EBG unit-cell consists of three rectangular patches connected through narrow metallic branches in the vertical direction. Two connecting bridges are added to connect the central patches in adjacent EBG unit-cells in the horizontal direction. Both the conventional and proposed EBG structures were printed on the top of a 0.25 mm thick ROGERS RO3006 substrate.

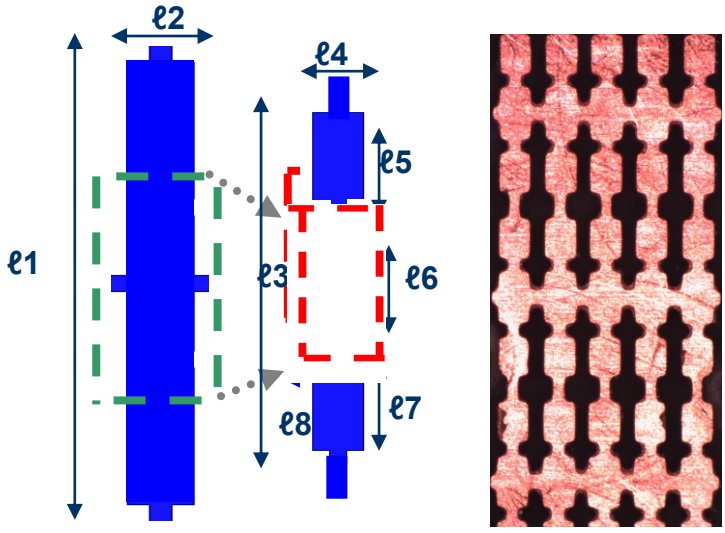

Fig.5-1. Geometry of the conventional (left) and proposed (middle) EBG unit-cells, macroscopic photo of the fabricated EBG structure (right).

Table 5-1 Proposed EBG Unit-cell dimensions

Parameter	ℓ1	ℓ2	ℓ3	ℓ4	ℓ5
Length (mm)	1.2	0.16	0.31	0.4	0.31

The transmission coefficient of the proposed EBG unit-cell was measured using the symmetric microstrip line technique [14], as shown in Fig.5-2. In this technique, the EBG structure is interposed between two identical open-ended microstrip lines. When the first microstrip line is excited, the EM coupling at the second microstrip line is considerably reduced in the frequency range where the EBG is designed to have a bandgap as shown in Fig.5-3. Clearly, both unit-cells have similar transmission coefficients over the suggested frequency.

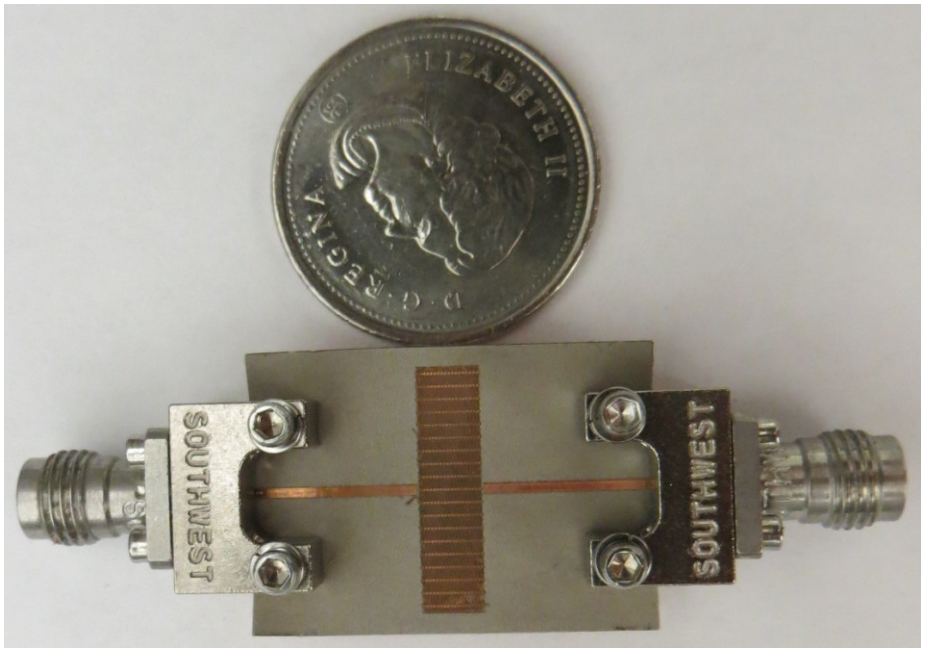

Fig.5-2. The fabricated symmetric microstrip line structure.

Fig.5-4 shows the dispersion diagram of the proposed EBG structure along the *OX* direction and in the region above the light line. Simulations were carried out using the CST simulator [17]. The proposed EBG has a bandgap from 56.8 GHz to 66.6 GHz, with a gap to mid-gap ratio of 14.8%. This agrees well with the results previously shown in Fig.5-3.

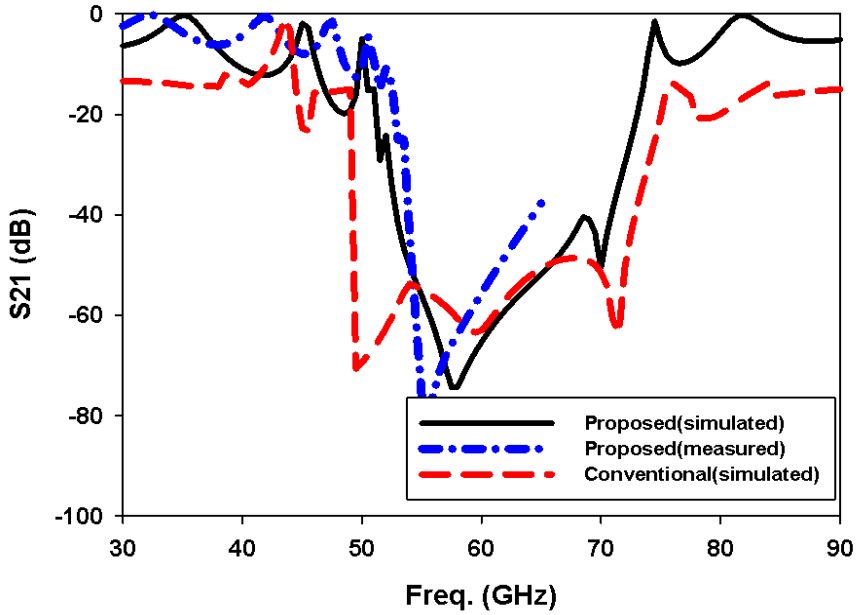

Fig.5-3. Transmission coefficients of the proposed and conventional EBG structures.

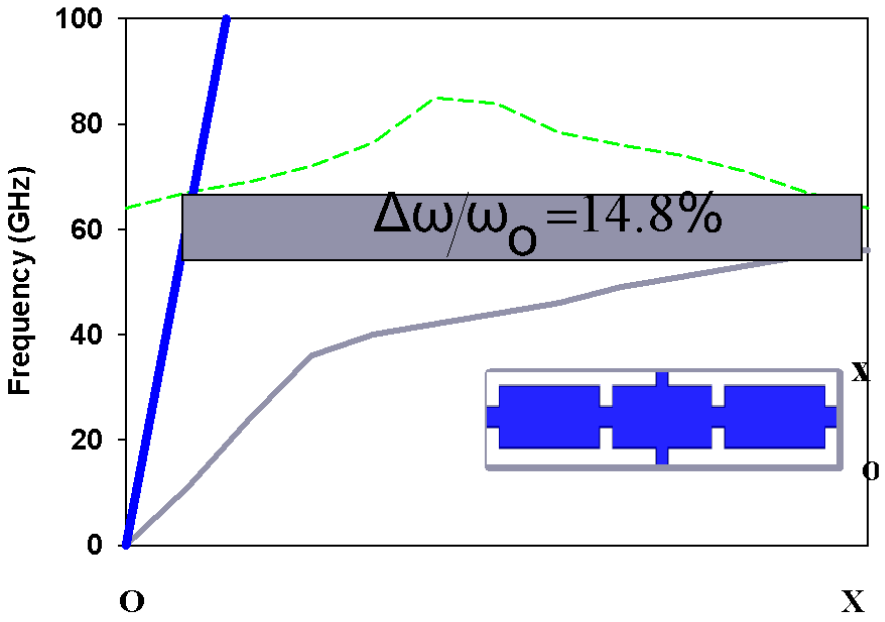

Fig.5-4. Dispersion diagram of the proposed EBG in the *OX* direction.

The proposed EBG unit-cell can be considered as a three-segment SIR structure, where each patch and its two branches represent a SIR segment. Considering the segment contoured by the green line in the conventional EBG unit-cell and its SIR equivalent

contoured by the red box in the proposed EBG unit-cell as shown in Fig.5-1. By choosing the appropriate dimensions for the different lengths of the SIR configuration, both configurations can have similar transmission characteristics, and accordingly identical ABCD matrices. Moreover, the physical dimensions of the SIR configuration are smaller than that of the conventional one.

According to the analysis in [18], the calculated miniaturization factor for the proposed EBG unit-cell is 0.79. On the other hand, the physical areas of the conventional and proposed EBG unit-cells are 2.64 mm^2 and 1.92 mm^2, respectively, with a miniaturization factor of 0.73. Both miniaturization factors are well matched with each other.

b) MMW Choke Absorber

The 0.75 mm thick MS-600N from Epoch Microelectronics [19] was used in the hybrid structure. Fig.5-5 shows the absorption performance obtained from the manufacturer data sheet.

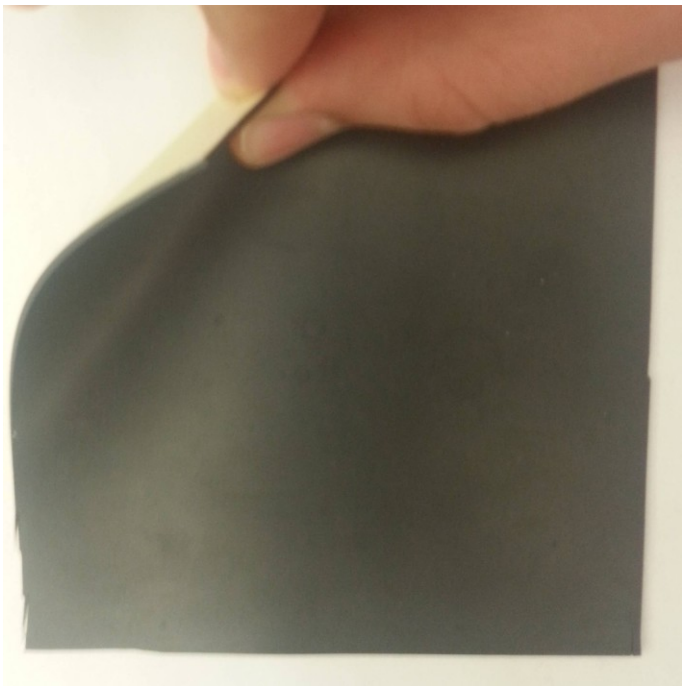

(a)

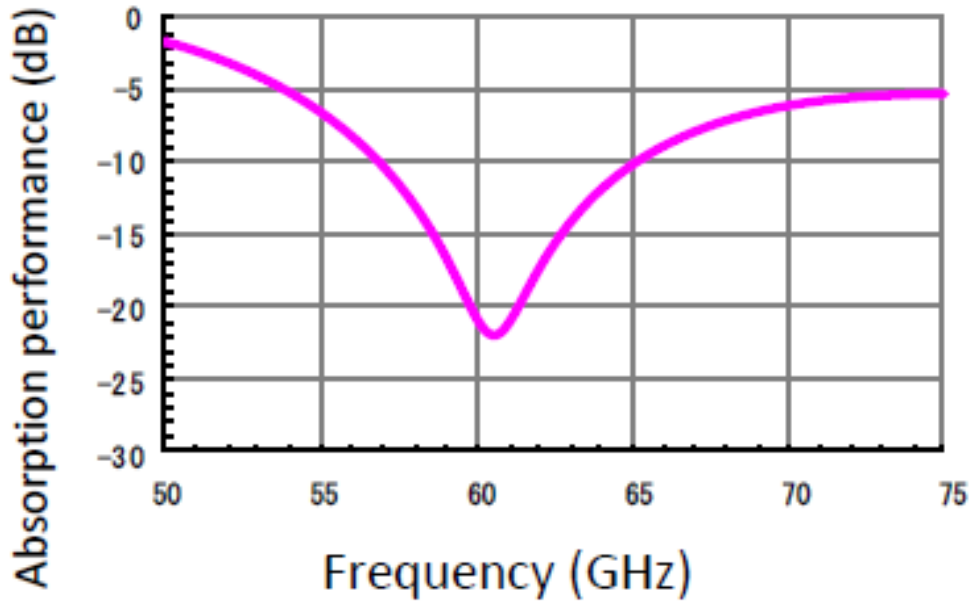

(b)

Fig.5-5. (a) The MS-600N absorber , and (b) the absorption performance from the data sheet.

5.3 Validation and experimental results

Antenna Array Design

The geometry of the proposed array is shown in Fig.5-6. It consists of two aperture-coupled DR antennas mounted on the top of 0.25 mm thick ROGERS 3006 substrate. The radiating elements are spaced by half of the free space wavelength at 60 GHz (corresponds to 2.5 mm). The DR antennas are fed by two microstrip lines printed on the bottom of another 0.25 mm thick ROGERS 3006 substrate. The energy is coupled to the DR antennas through two narrow slots etched in the ground plane.

Five periods of the proposed EBG structure were interposed between the two radiating elements. Finally, 0.9mm~1.0 mm high 0.75 mm thick choke absorber was vertically mounted between the two radiating elements

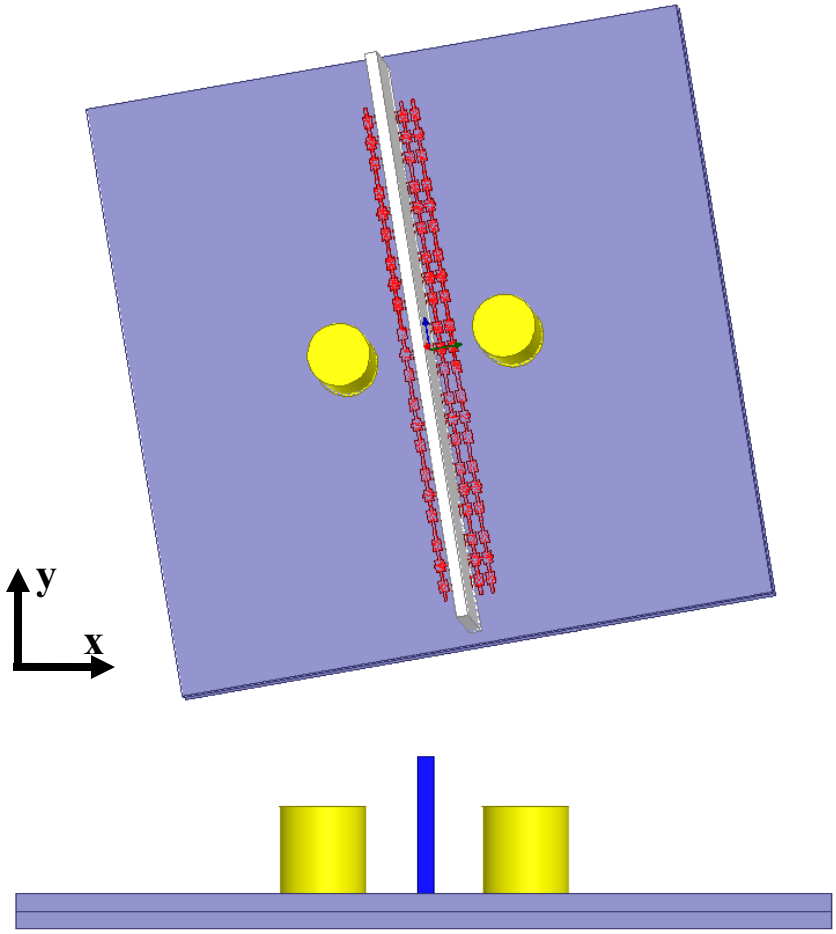

Fig.5-6. Geometry of the proposed antenna array; perspective view (top), and side view (bottom).

Experimental Results

To verify the effectiveness of the proposed hybrid structure, three antenna array prototypes were fabricated and tested as shown in Fig.5-7. The choke absorber was rubbed against a piece of sand paper to elaborate the required height and thickness.

The measured reflection and transmission characteristics of the three antenna array prototypes are shown in Figs. 5-8 and 5-9, respectively. For the sake of comparison, simulated results of the hybrid isolator presented in [20] comprising the proposed EBG and a metallic choke are also presented.

The absorber choke is basically designed to alleviate the EM interactions caused by the space waves. On the other hand, the EBG structure is introduced to enhance the isolation

level through controlling surface-waves propagation. Therefore, by deliberately combining the two isolation techniques, sources of MC can be controlled.

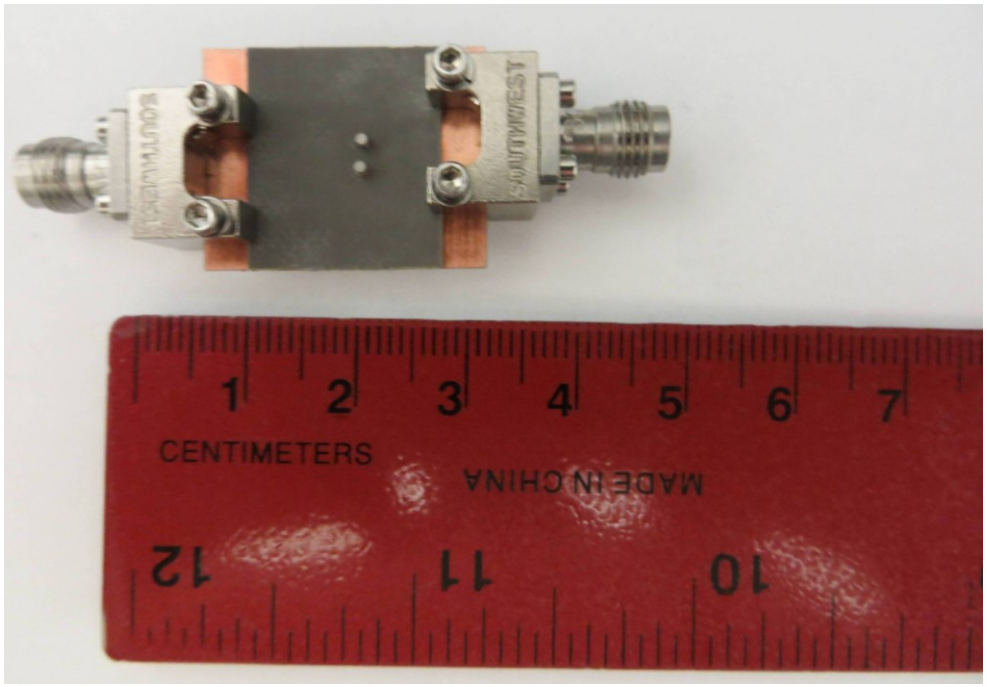

(a)

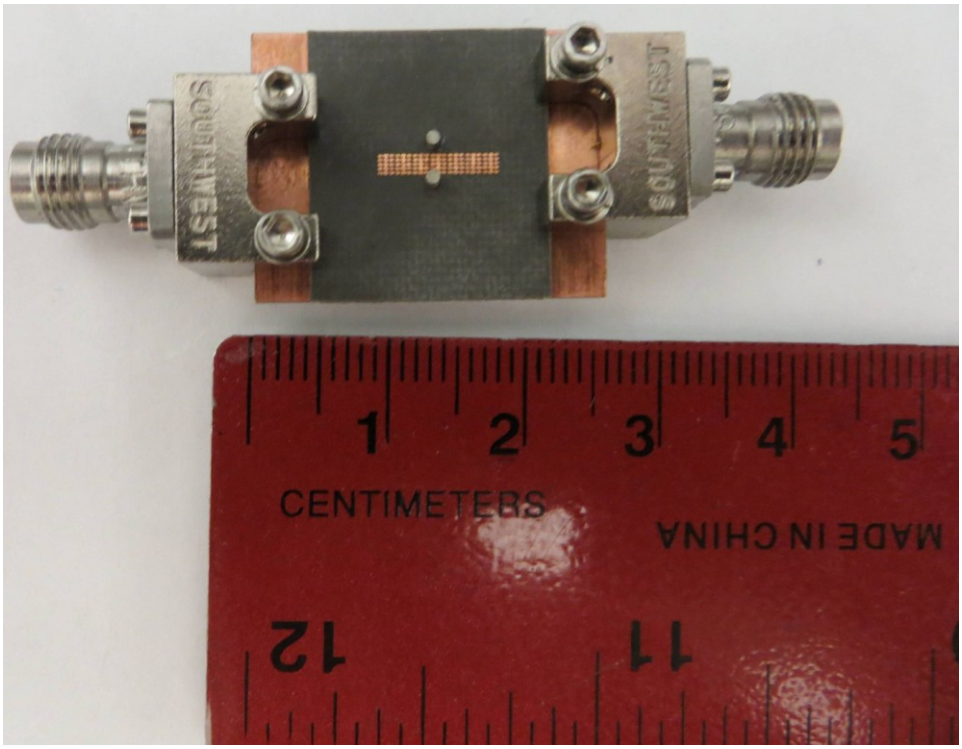

(b)

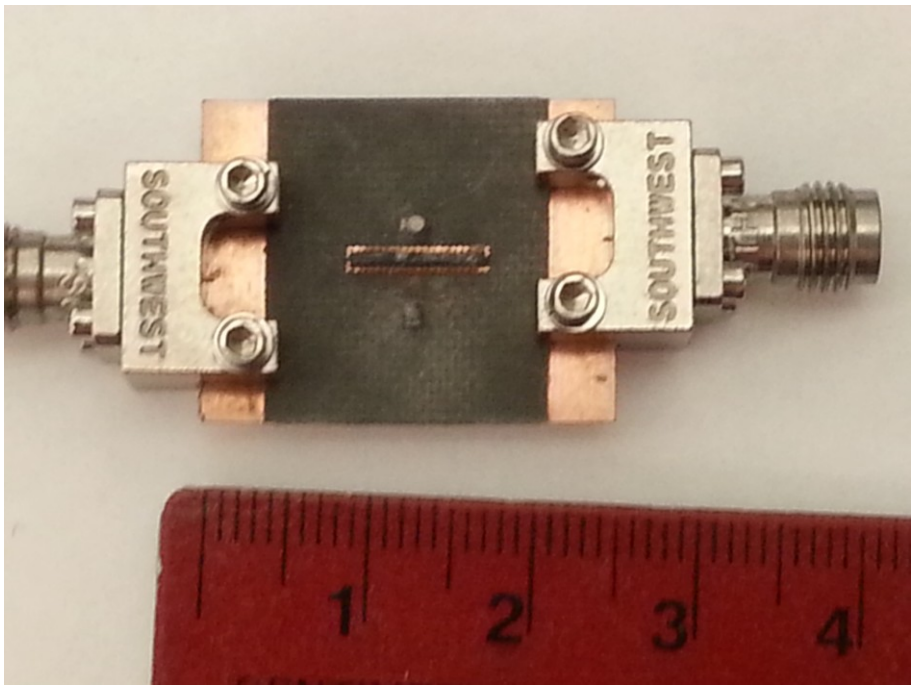

(c)

Fig.5-7. Photographs of the fabricated antenna array prototypes: (a) reference array, (b) array with EBG isolator, and (c) array with the proposed hybrid isolator.

As it can be observed from the results in Fig.5-9, when the choke absorber is used as an isolator between the two DR antennas, the coupling level is reduced by 14-17 dB. On the other hand, when the EBG isolator is used, the isolation level is improved by 6-8 dB at the desired operating frequency around 60 GHz. However, by applying the proposed hybrid isolator, the isolation level is significantly improved by at least 22 dB.

For the case of the hybrid isolator presented in [20], consisting from the proposed EBG structure and a metallic choke instead of the absorber choke, an isolation level improvement of about 13 dB is achieved over the suggested bandwidth. Table 5-1 summarizes the results.

The proposed hybrid isolator outperforms the hybrid isolator in [20], because the metallic choke supports the propagation of electric currents. These currents, when coupled from one antenna to the other, degrade the isolation level. Moreover, and as it will be shown later, the proposed isolator has less deviation on the radiation characteristics from the one in [20].

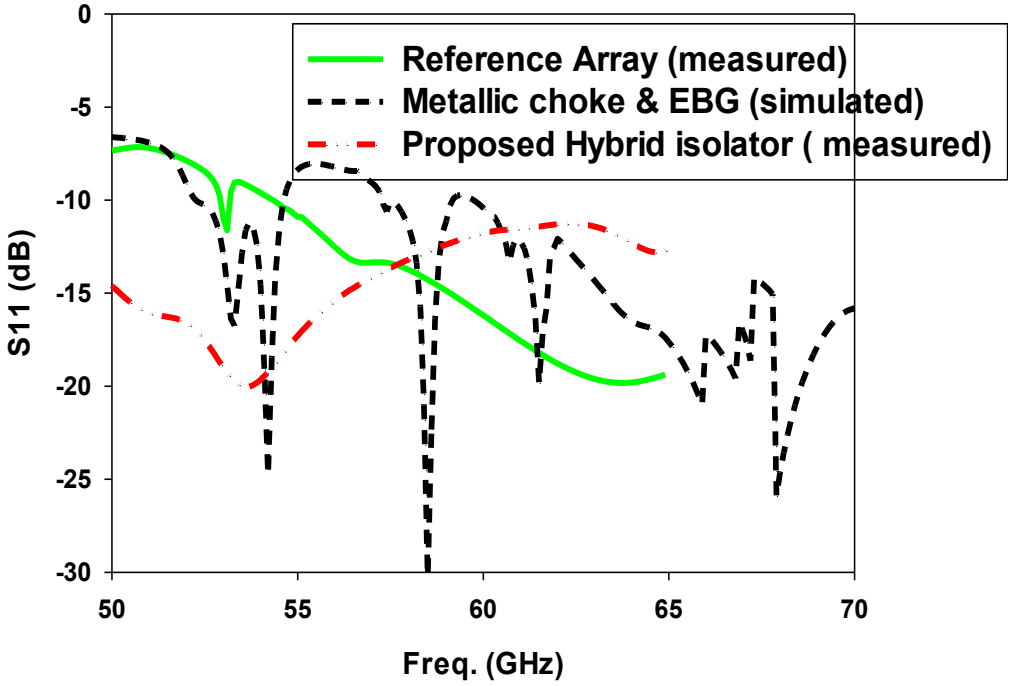

Fig.5-8. Simulated and measured reflection coefficients of the proposed and reference antenna arrays.

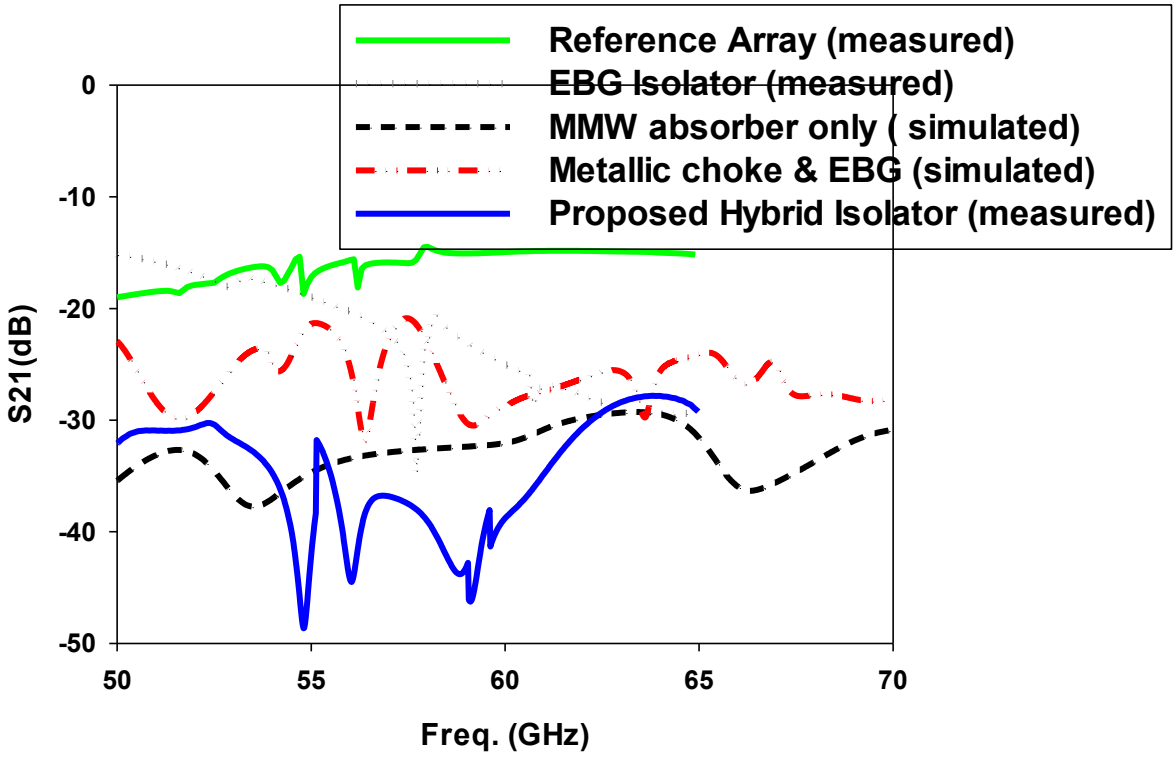

Fig.5-9. Simulated and measured transmission coefficients of the proposed and reference antenna arrays.

Table 5-2 Summary of the transmission coefficients for different isolation techniques.

Isolation Technique	*Avg. Mutual-coupling level reduction*
Reference Array(no isolation)	**16 dB(reference)**
EBG Isolator	**6-8 dB**
Hybrid: EBG+ Metallic Choke	**12-14 dB**
Absorber Choke only	**14-17 dB**
Proposed Hybrid Isolator	**22-24 dB**

The matching bandwidth is reduced by applying either the proposed hybrid isolator or the EBG and metallic choke isolator. This is due to close proximity between the EBG structure and the radiating elements, which yields near fields interactions, and hence changing the impedance of the radiating elements. Nonetheless, the array is still matched over the suggested bandwidth.

Fig. 5-10 and Fig. 5-11 show the E- and H- plane radiation patterns of an individual DR antenna for different isolation techniques. E-patterns reveal that, when the EBG isolator is used, the radiation along the substrate edge ($\theta = 270^o$) is significantly reduced by about 5 dB. This is due to the ability of the EBG structure to block surface wave propagation. In addition, for the case where metallic choke and EBG hybrid isolator is used, the pattern is pushed toward $\theta = 35^o$, with a little gain enhancement. However, the proposed hybrid isolator has a little effect on the E-plane radiation pattern. Less energy is radiated toward the $\theta = 270^o \sim 330^o$ region. Besides, gain loss of about 2 dB appeared in the main beam direction. This is due to the absorbed energy in this region. H- plane patterns, on the other hand, are less sensitive to different isolation techniques. Indeed, a little back radiation improvement is achieved when hybrid isolators are used.

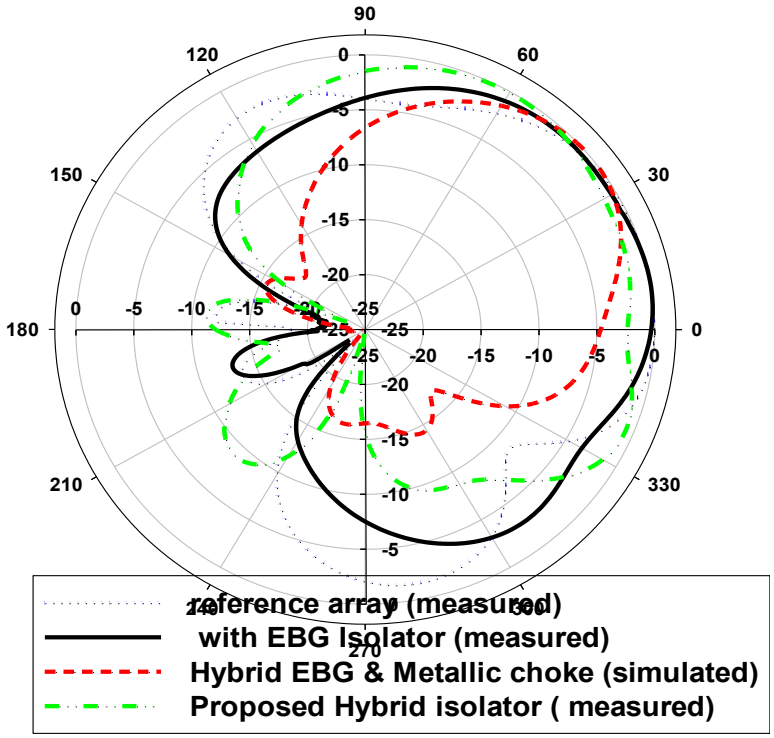

Fig.5-10. Normalized E- plane power patterns of an individual DR antenna for different isolation techniques.

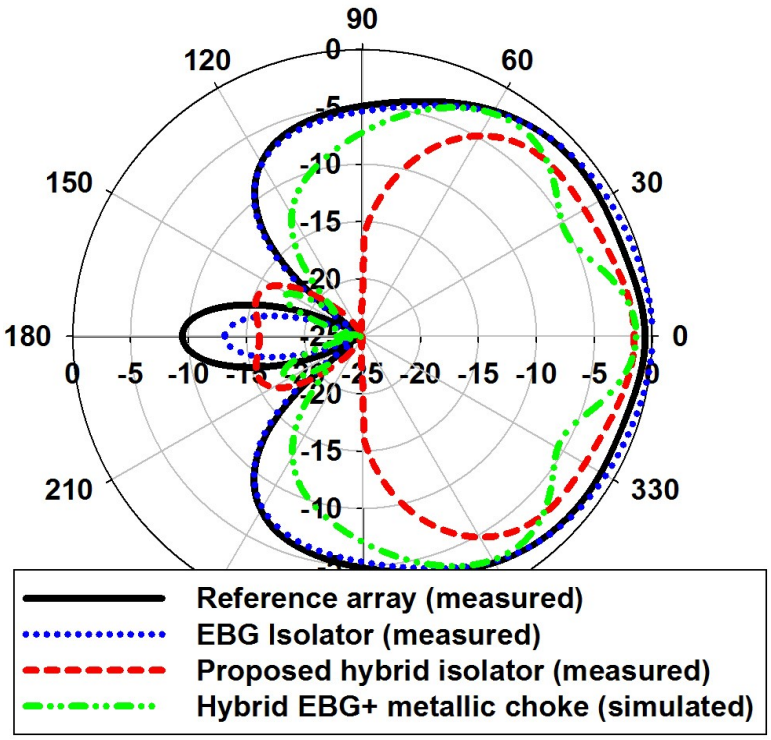

Fig.5-11. Normalized H- plane power patterns of an individual DR antenna for different isolation techniques.

5.4 References

[1] H. Farahani, M. Veysi, M. Kamyab, and A. Tadjalli, "Mutual coupling reduction in patch antenna arrays using a UC-EBG superstrate," IEEE Antennas Wireless Propag. Lett., vol. 9, pp. 57–59, Jan. 2010.

[2] J. Wallace and M. Jensen, "Mutual coupling in MIMO wireless systems a rigorous network theory analysis," IEEE Trans. Wireless Communications, vol. 3 no. 4, pp. 1317–1325, July 2004.

[3] E. Rajo-Iglesias, Ó. Quevedo-Teruel, and L. Inclán-Sánchez, "Planar soft surfaces and their application to mutual cupling reduction," IEEE Trans. Antennas Propag., vol. 57, no. 12, pp. 3852–3859, Dec. 2009.

[4] A. S. C. Svendsen and I. J. Gupta, "The effect of mutual coupling on the nulling performance of adaptive antennas," IEEE Antennas Propag. Mag., vol. 54, no. 3, pp. 17–38, Jun. 2012.

[5] L. Zhengyi, D. Zhengwei, M. Takahashi, K. Saito, and K. Ito, "Reducing mutual coupling ofMIMO antennas with parasitic elements for mobile terminals," IEEE Trans. Antennas Propag., vol. 60, no. 2, pp. 473–481, Feb. 2012M.

[6] J. Wallace and M. Jensen, "Mutual coupling in MIMO wireless systems a rigorous network theory analysis," IEEE Trans on Wireless Communications, vol. 3 no. 4, pp. 1317–1325, July 2004.

[7] R. J. Mailloux, "Phased Array Antenna Handbook". Dedham, MA: Artech House, 1993.

[8] Q. Lei, Z. Fei, X. Ke, C. Shun-Lian and M. Jun-Jie, "Transmit and receive isolation improvement of antenna arrays by using EBG structures," IEEE on Ant. and Wireless Propag. Lett., vol. 11, p.p. 93- 96, Jan. 2012.

[9] M. M. Bait-Suwailam, O. F. Siddiqui, and O. M. Ramahi, "Mutual coupling reduction between microstrip patch antennas using slotted-complementary split-ring resonators," IEEE Antennas Wireless Propag. Lett., vol. 9, pp. 876–878, 2010.

[10] L. Minz and R. Garg, "Reduction of mutual coupling between closely spaced PIFAs," Electron. Lett., vol. 46, no. 6, pp. 392–394, 2010.

[11] J. Ou Yang, F. Yang, and Z. M. Wang, "Reducing mutual coupling of closely spaced microstrip MIMO antennas for WLAN application," IEEE Antennas Wireless Propag. Lett., vol. 10, pp. 310–312, 2011.

[12] Z. Iluz, R. Shavit, and R. Bauer, "Microstrip antenna phased array with electromagnetic bandgap substrate," IEEE Trans. Antennas Propag., vol. 52, no. 6, pp. 1446–1453, Jun. 2004.

[13] T. Bertuch, "Comparative investigation of coupling reduction by EBG surfaces for quasi-static RCS measurement systems," IEEE Antennas Wireless Propag. Lett., vol. 5, pp. 231–234, 2006.

[14] M. J. Al-Hasan, T. A. Denidni, and A. Sebak, "Millimeter-wave EBG-Based Aperture-Coupled Dielectric Resonator Antenna ," IEEE Trans. Ant. and Propag., vol. 61, no. 8, pp. 4354-4357, August 2013.

[15] N. Sankaran, M. Swaminathan, and R. Tummala, "Synthesis of electromagnetic band gap structures using stepped impedance resonators," Microwave and optical technology letters., vol. 53, no. 10, pp., Oct. 2011.

[16] S. K. Sharma and L. Shafai, "Enhanced performance of an aperture coupled rectangular microstrip antenna on a simplified unipolar compact photonic bandgap (UC-PBG) structure," in IEEE Antennas and Propagation Soc. Int. Symp., vol. 2, pp. 498–501, Jul. 2001.

[17] Microwave Studio. (www.cst.com) .

[18] Behnam Zarghooni and Tayeb A. Denidni, "New compact Metamaterial unit-cell using SIR technique ," IEEE microwave and wireless components lett., vol. 24, no. 5, May 2014.

[19] Epoch Microelectronics, Inc. (www.epochmicro.com).

[20] M. N. Jazi, Tayeb A. Denidni, et al…"A Hybrid isolator to reduce electromagnetic interactions between Tx/Rx antenna," IEEE Antennas Wireless Propag. Lett., vol. 13, pp. 75-78, 2014.

CHAPTER SIX: MILLIMETER-WAVE EBG-BASED DIELECTRIC RESONATOR ANTENNA WITH RECONFIGURABLE RADIATION PATTERN

6.1 Introduction

Pattern reconfigurability is drawing an enormous attention due to their ability to produce diverse pattern configurations and beam steering [1, 2]. It is defined as the ability of the antenna to change/modify its basic pattern characteristics through electrical, mechanical, or other means [3].

Directional pattern can be used to reduce multipath effects, interferences, increase the spectral efficiency, and improve the energy efficiency. On the other hand, omni directional patterns are used to send and receive electromagnetic-wave (EM) waves from all directions. Moreover, in point-to-point communication systems, beam steering can be implemented to enhance the system performance, security, and increasing the capacity. Furthermore, beam steering is used in radar systems to scan the surrounding objects.

Pattern reconfigurability has the advantages of avoiding noisy environments and improving security and maneuver away from jamming. Moreover, it helps in power saving, size and cost reduction, and increasing the diversity gain [4]. Furthermore, in phased antenna arrays, pattern reconfigurability helps achieving wider scanning angles and grating nulls mitigation. Besides, it helps maintaining high quality communication systems in harsh and unpredictable conditions [5].

Reconfigurable-pattern antennas can be achieved by phased antenna arrays, Butler matrix, and leaky-wave antennas [6]. However, at millimeter-wave (MMW) bands, the feeding network, power components and phase shifters yield more complexity, higher cost, and larger physical size. In addition, the large bandwidths associated with MMW bands introduce difficulties in designing an impedance match in leaky-wave arrays.

Alternatively, electromagnetic band-gap (EBG) structures [7] have certain EM characteristics, when being incorporated with active devices, can be used to achieve

pattern diversity and beam steering. FSS structures are cheap, easy to fabricate and do not require any added components.

In this chapter, a millimeter-wave (MMW) electromagnetic bandgap (EBG)-based dielectric resonator (DR) antenna with beam steering capability is presented. Six EBG sectors of several cells are placed symmetrically around the DR antenna to achieve beam steering in the azimuth plane. Each sector is composed of twenty one circular-patch mushroom EBG unit cell. The vias in each sector are connected through thin metallic veins printed on a conductor-backed dielectric slab. The metallic veins are then connected to the ground plane through a switching diode. By switching the diode on and off, the EBG sector band-stop and band-pass properties are changed, yielding beam steering into that sector. Experimental results show flexible and effective beam steering capability in the azimuth plane using minimal number of diodes.

In this chapter, Millimeter-wave (MMW) electromagnetic bandgap (EBG)-based dielectric resonator (DR) antenna with beam steering capability is presented. Six EBG sectors of several cells are placed symmetrically around the DR antenna to achieve beam steering in the azimuth plane. Each sector is composed of twenty one circular-patch mushroom EBG unit cell. The vias in each sector are connected through thin metallic veins printed on a conductor-backed dielectric slab. The metallic veins are then connected to the ground plane through a switching diode. By switching the diode on and off, the EBG sector band-stop and band-pass properties are changed, yielding beam steering into that sector.

6.2 EBG Design and Switching Configuration

a) EBG Structure Design

The proposed EBG structure is shown in Fig. 6-1. It consists of circular patches printed on the top of a 0.254 mm thick substrate with a relative permittivity of 10.2. The patch diameter is 1.36 mm with a periodicity of 1.63 mm. Thin metallic veins printed on a conductor-backed, 0.127 mm thick substrate with a relative permittivity of 3.66. The centers of the patches are connected to the metallic veins through vias with 0.16 mm diameter. A switching diode is used to connect the veins to the ground plane.

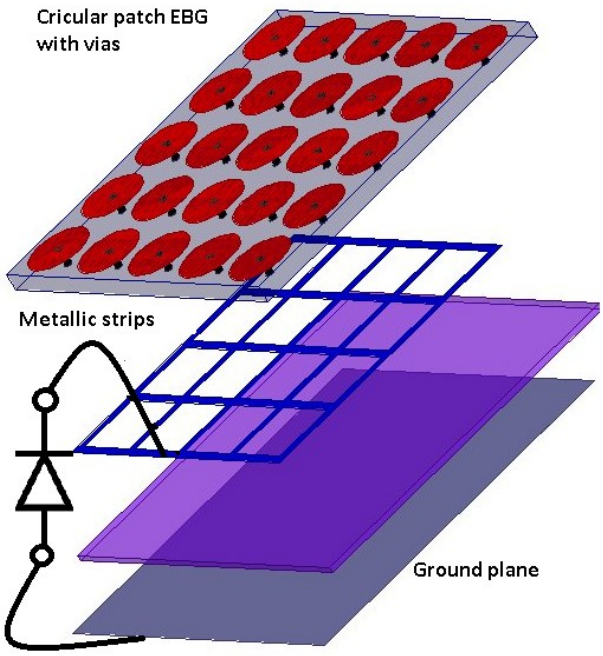

Fig.6-1 Exploded view of the proposed EBG structure.

The EBG structure is designed to have a stop-band around the 60 GHz band when the metallic veins are connected to the ground plane (diode is ON), and a pass-band around the same frequency band when the veins and the ground plane are disconnected (diode is OFF).

b) Diode Characterization

To ensure the applicability of switching PIN diodes at MMW bands, the transmission and reflection characteristics of MACOM (MA4AGFCP910) PIN diode [8] were tested and measured at the 60 GHz band. Measurements were carried out using TRL calibration kit, fixture, and VNA with built in bias-tee, as shown in Fig. 6-2.

Fig. 6-3 shows the measured reflection and transmission characteristics of the diode for the two different states. Apparently, the diode has a good conduction and isolation levels over the suggested bandwidth.

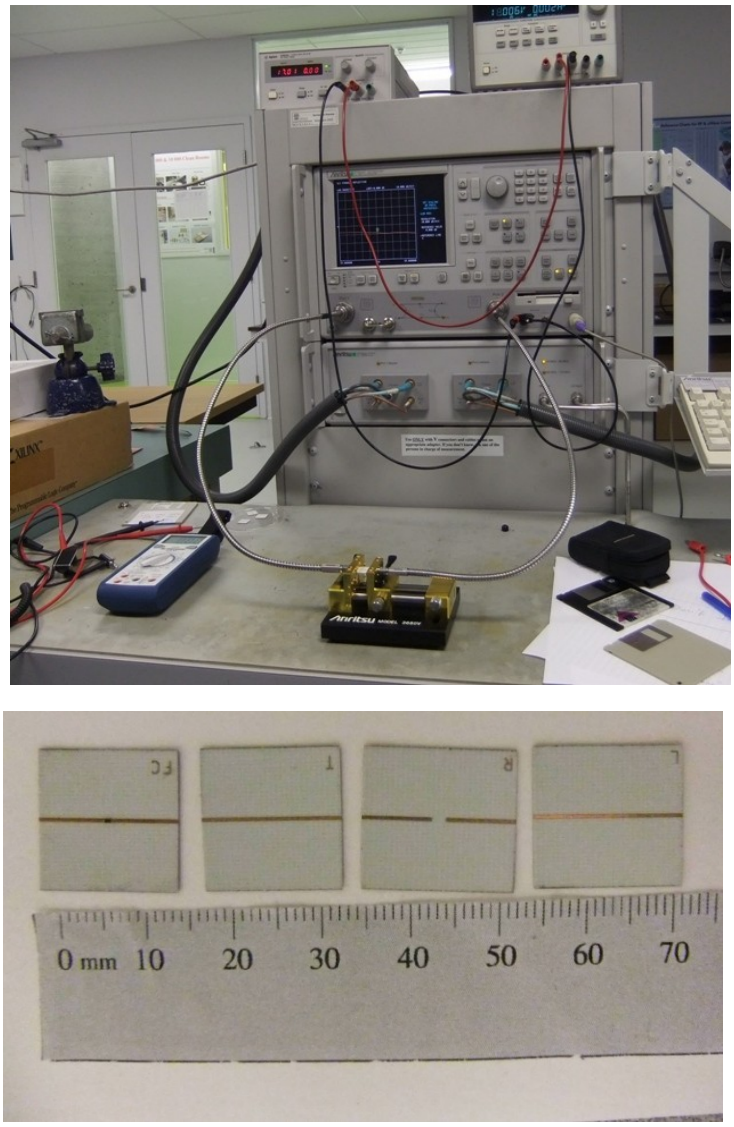

Fig.6-2 Measurement set-up.

a) Biasing Circuit

At millimeter-wave bands, the design of biasing circuit becomes very critical. This is due to the comparable dimensions between the biasing circuit and the radiator element. Moreover, the close proximity between electric components at MMW bands yields strong electromagnetic interactions and interferences. Therefore, practical considerations and fabrication limitations were taken into account during the design process.

Fig. 6-3 shows the suggested biasing circuit. The surface-mount resistor is used to limit the DC current going to the diode. The butterfly stub is used to perform AC open/short circuit over the suggested bandwidth (~57 GHz-64 GHz). The quarter-wave transformer prevents the AC

current from entering the DC source by transferring the low impedance point at the butterfly stub junction to a high impedance point at the other end. Since the suggested bandwidth spans the frequency from 57-63 GHz, the quarter-wave section cannot provide a good high impedance values across the complete bandwidth. Therefore, the quarter-wave section line is made a little bit narrower than the other 50 Ω transmission lines in order to further block AC signals from entering the DC source across the suggested bandwidth.

The distance between the ground plane and the EBG network of veins should be one guided wavelength (λg). However, and due to fabrication limitations, this distance was chosen to be double the guided wavelength. With this selection, the short circuit impedance value is probably transformed to the EBG structure when the diode is ON.

Nonetheless, for the case when the diode is OFF, the electrical length is no longer 2*λg, and hence, the open circuit value will not be transferred probably. This yields some impact on the EBG characteristics. However, adding another butterfly stub right after the diode will fix this problem, as shown in Fig. 6-6. Indeed, this idea came to the authors' minds after the fabrication was done, and therefore, they could not implement here. However, it will part of the future work.

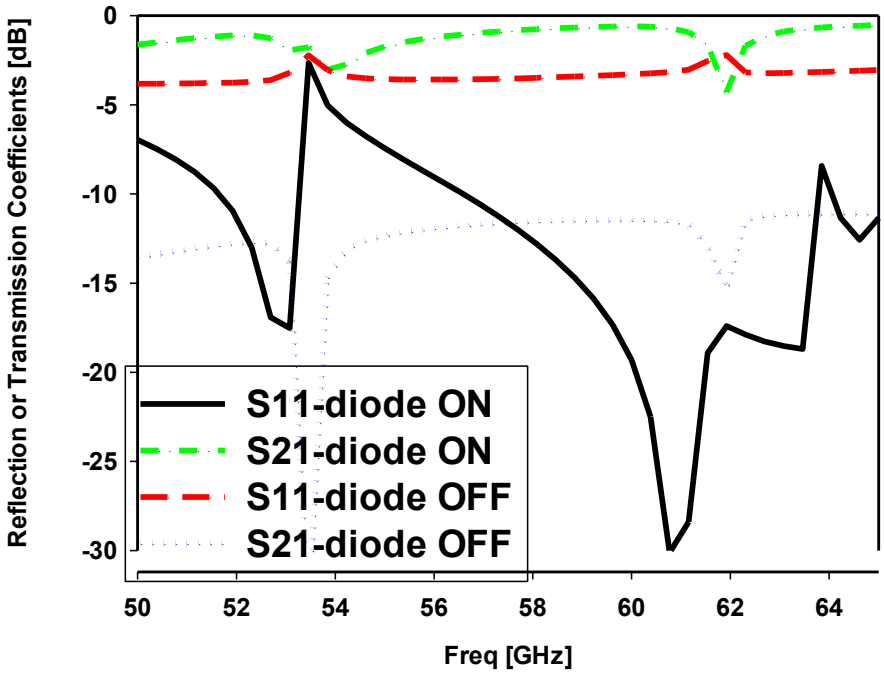

Fig.6-3 Reflection and transmission characteristics of the proposed EBG structure.

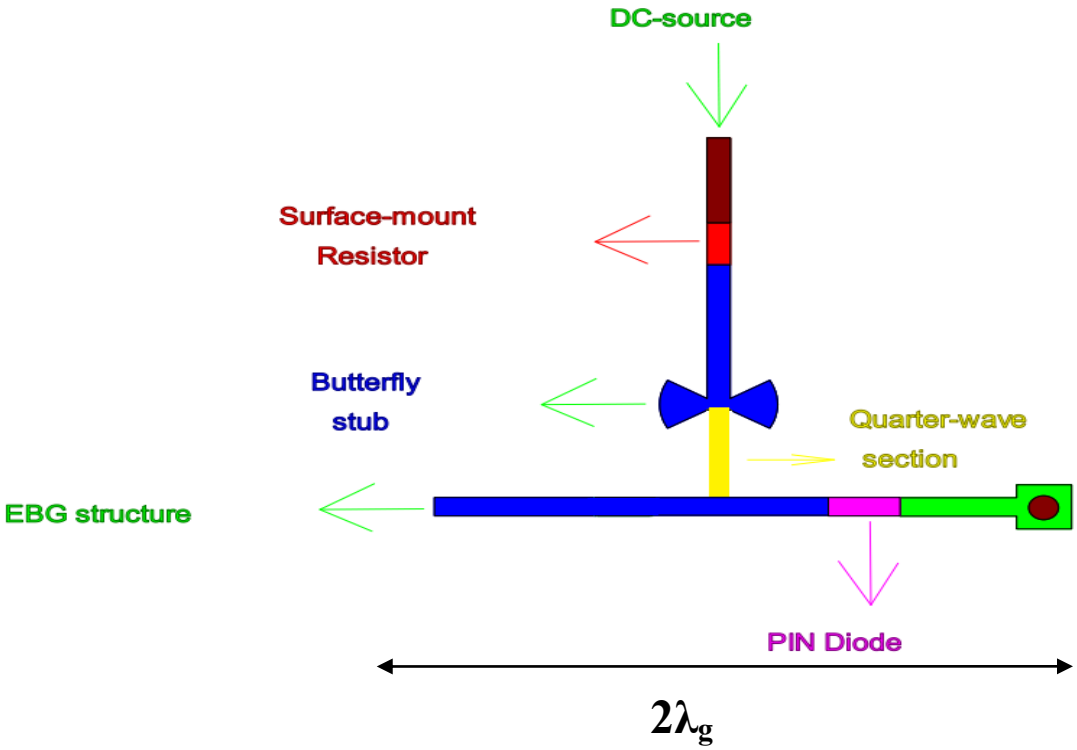

Fig.6-4 Biasing circuit of the proposed EBG structure.

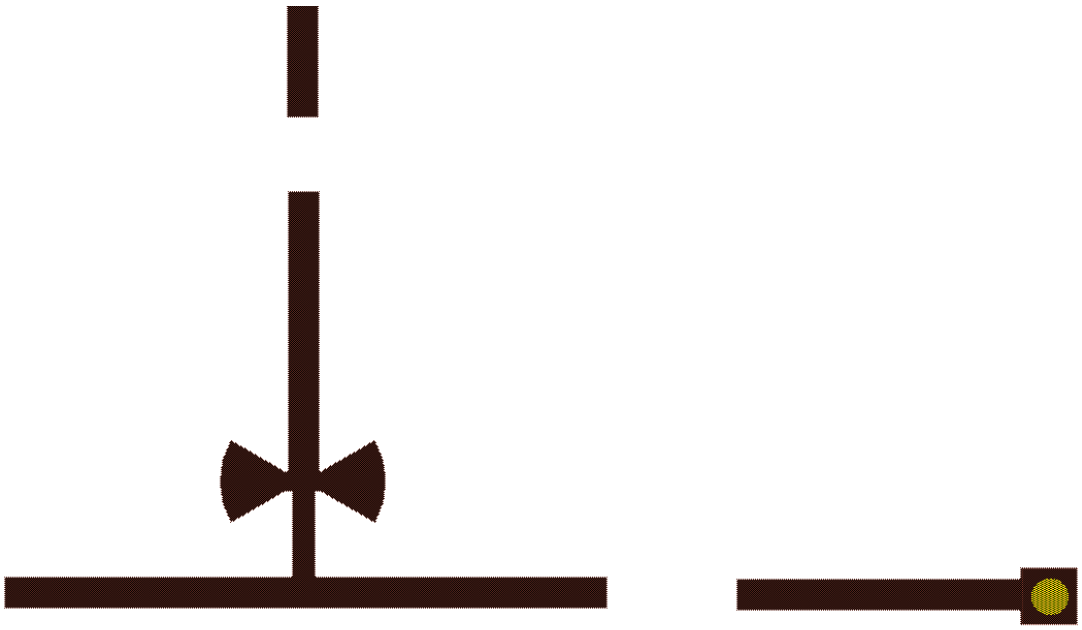

Fig.6-5 Layout of the proposed biasing circuit

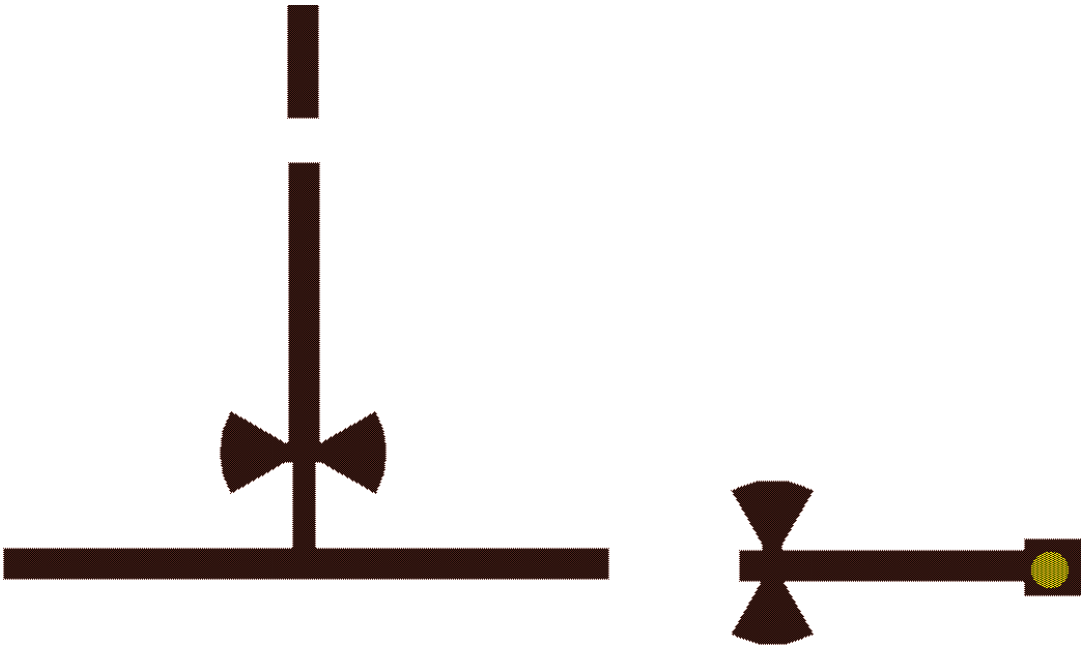

Fig.6-6 Layout of the biasing circuit with a butterfly stub added after the diode.

Fig. 6-7 shows a photo of the fabricated biasing circuit and EBG structure. The symmetric microstrip line method has been used to measure the transmission characteristics of the proposed EBG structure. This method is considered to be to be a strongly coupling technique, which reduces the influence of other parasitic propagation modes.

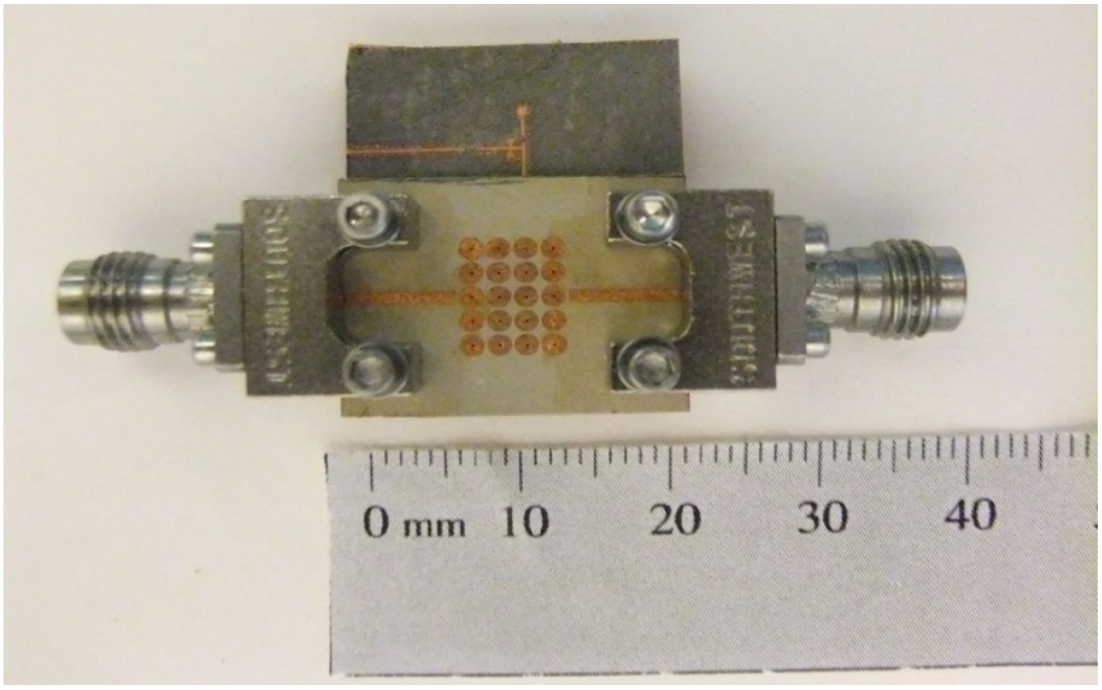

Fig.6-7 Photo of the fabricated EBG structure with the biasing circuit

Fig. 6-8 shows the measured transmission characteristics of the EBG structure. Clearly, n average of about 15 dB reduction of the transmission coefficient is obtained over the 57-64 GHz bandwidth.

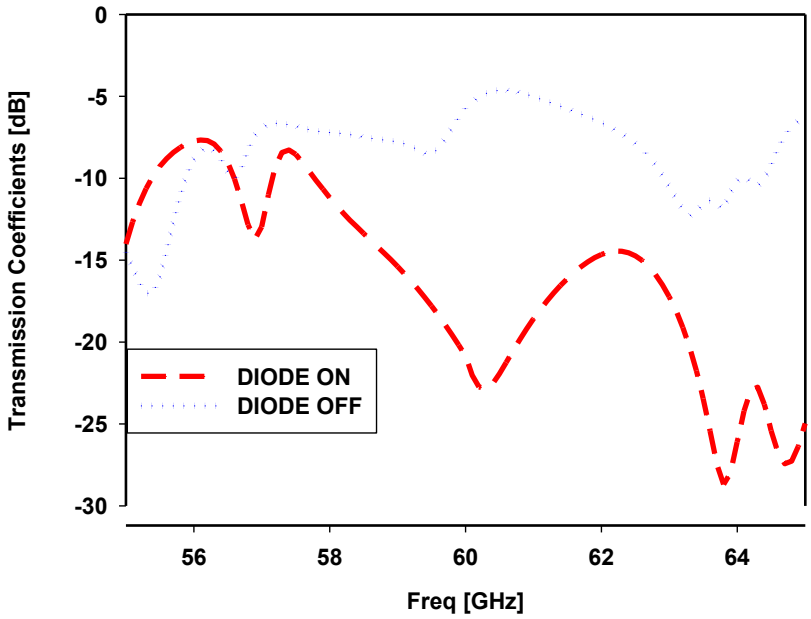

Fig.6-8 Measured Transmission characteristics of the proposed EBG structure.

6.3 Antenna Design

The geometry of the proposed antenna is shown in Fig. 3 . A 1.27 mm high cylindrical DR antenna with 1.02 mm diameter and relative permittivity of 10.2 is placed on the top of 0.254 mm thick hexagonal substrate with relative permittivity of 6.15. The cylindrical DR antenna is then slot-fed by a 50 Ω microstrip line of 0.57 mm width, printed on a 0.381 mm thick hexagonal substrate with a relative permittivity of 6.15. The energy is coupled from the micorstrip feedline to the cylindrical DR antenna through a slot in the ground plane.

Six sectors of the previously designed EBG structure, numbered from 1-6, are placed symmetrically around the cylindrical DR antenna. Each sector is composed of 26 EBG unit cell with 5-5-5-5-3-3 configuration. The metallic veins in each sector allowed the reduction of the number of diodes to six, one in each sector, and therefore, reducing the effect of the biasing circuit on the antenna characteristics, a big problem encountered at MMW bands where the

dimensions of the biasing circuit are comparable to those of the radiating element. Fig. 6-9 shows a photo of the fabricated antenna structure. DIP switch was used to switch the diodes.

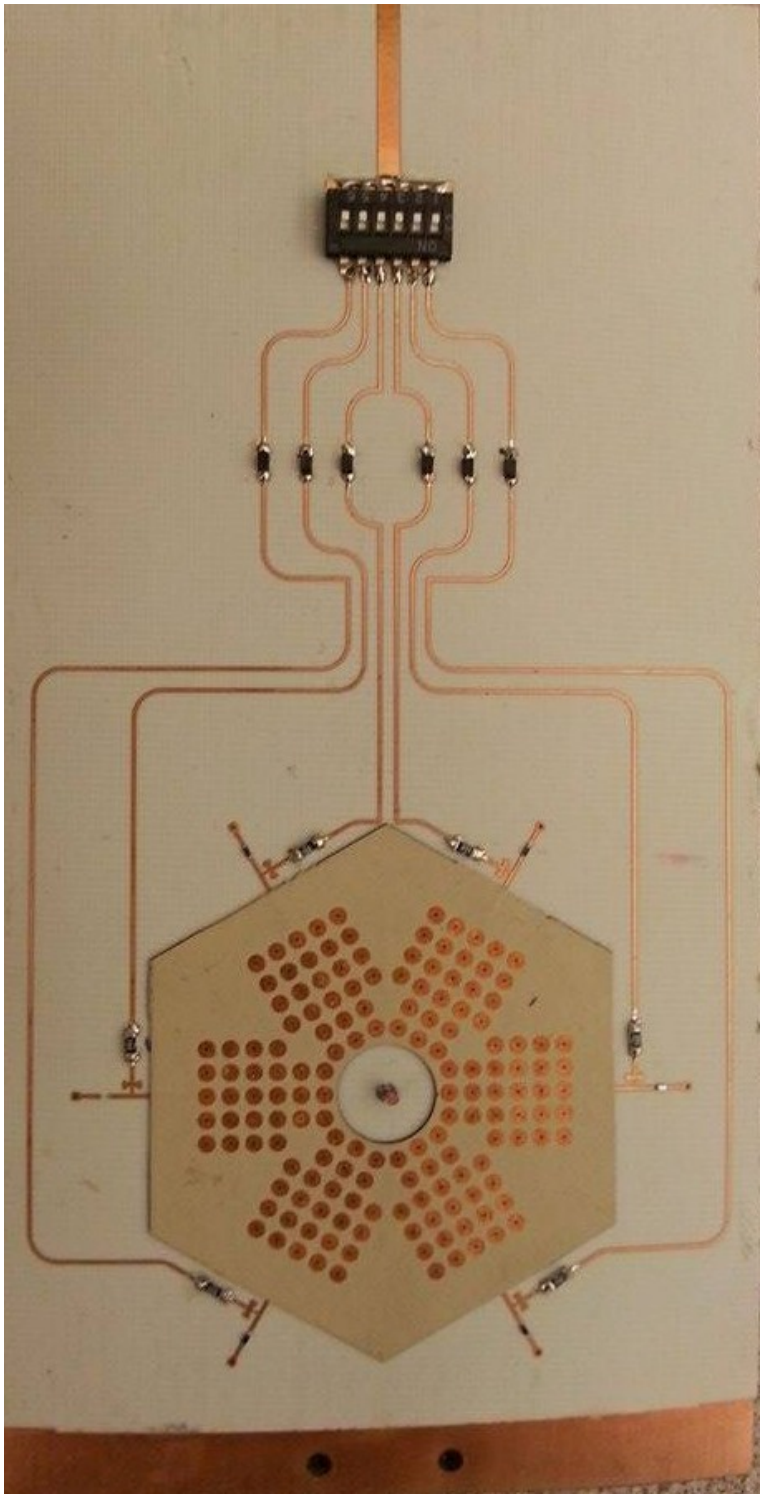

Fig.6-9 Photograph of the fabricated antenna structure

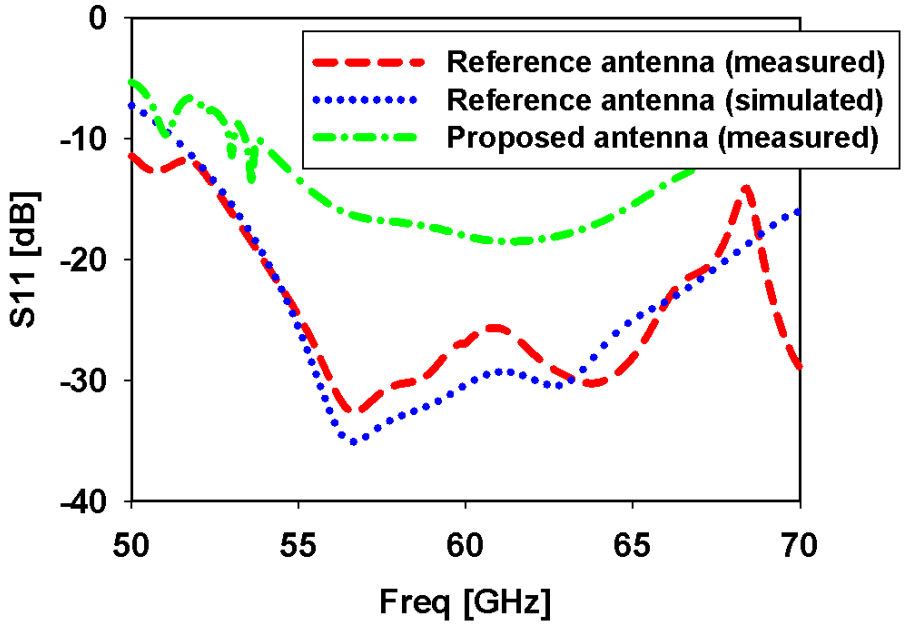

Fig.6-10 Measured reflection coefficient of the proposed (with EBG) and reference (without EBG) antennas

6.4 Results and discussions

Fig. 6-10 shows the measured reflection coefficients of the proposed antenna (with EBG) and reference antenna (without EBG). The EBG negatively affects the impedance bandwidth of the antenna by changing its input impedance. Therefore, the distance between the DR antenna and each EBG sector must be chosen carefully to keep the antenna tuned, while maintaining a high level of electromagnetic wave suppression.

The measured power patterns of the proposed antenna in the azimuth plane ($\theta = 90^{o}$) for different diodes status are shown in Fig. 6-11 to Fig. 6-13. For example, when the diodes in sectors 1 and 2 are OFF, and in sectors 3-6 are ON, the power is directed in the direction of 30^{o}, while for the case where the diodes are OFF in sectors 1 and 6, and ON in sectors 2-5, the power is directed along the 330^{o} direction. It is worth mentioning that other beam steering directions can be achieved through choosing other sectors' ON/OFF states combinations. With this feature, this antenna can provide an overall beam steering flexibility in the azimuth plane. The maximum gain of the antenna was measured in the elevation plain and found to be about 4.2 dBi.

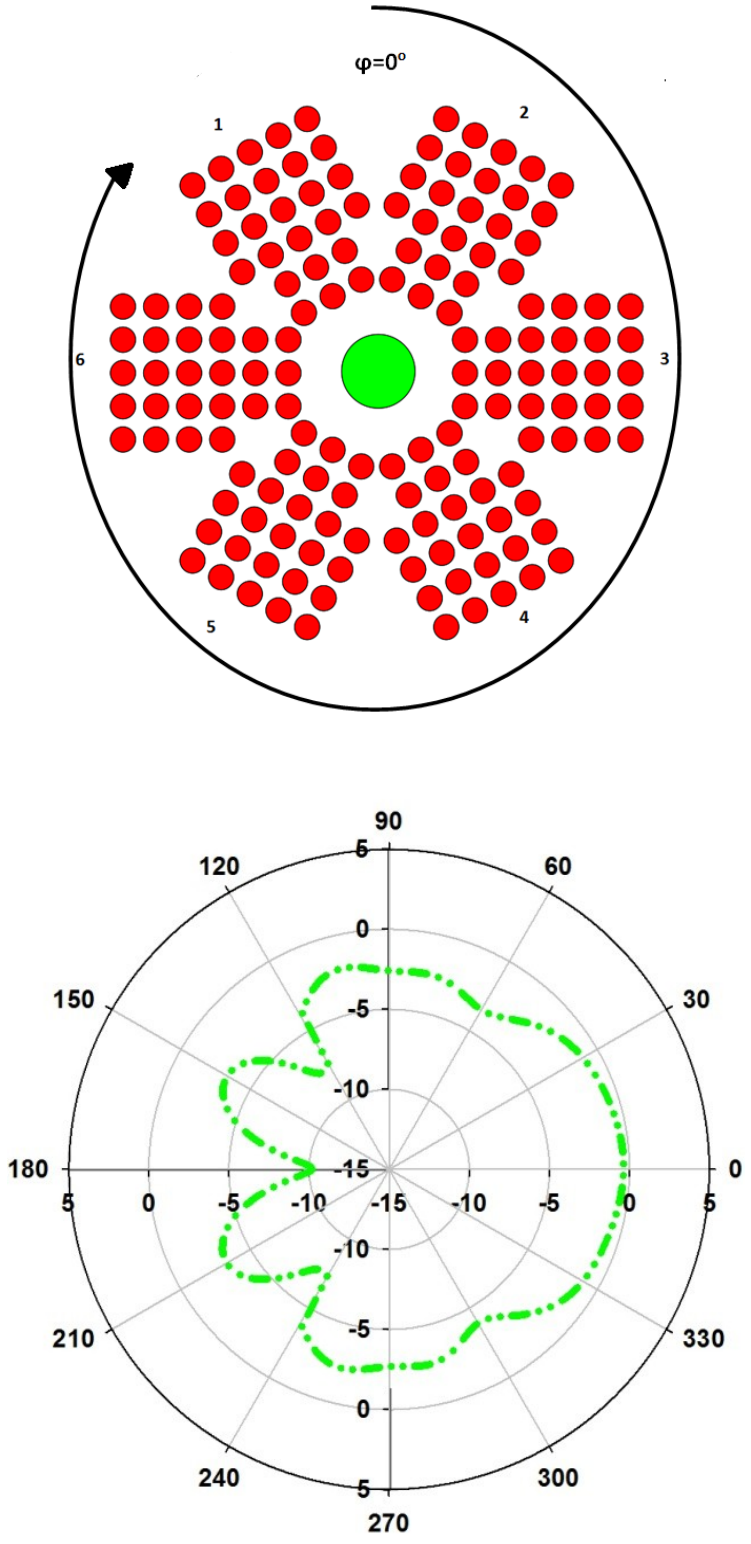

Fig.6-11 Measured radiation pattern in the azimuth plane when diodes 4,5 ON

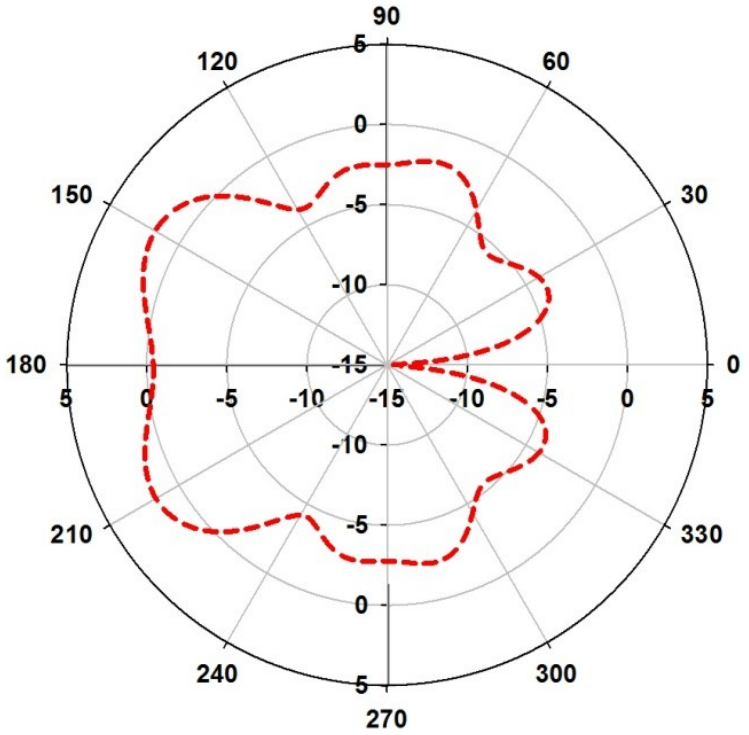

Fig.6-12 Measured radiation pattern in the azimuth plane when diodes 1,2 ON

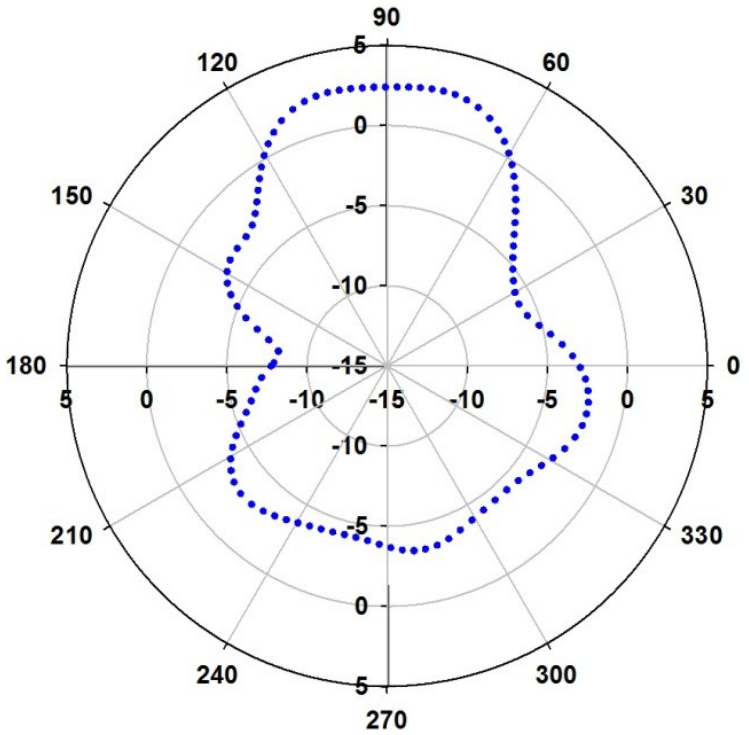

Fig.6-13 Measured radiation pattern in the azimuth plane when diodes 1,5,6 ON

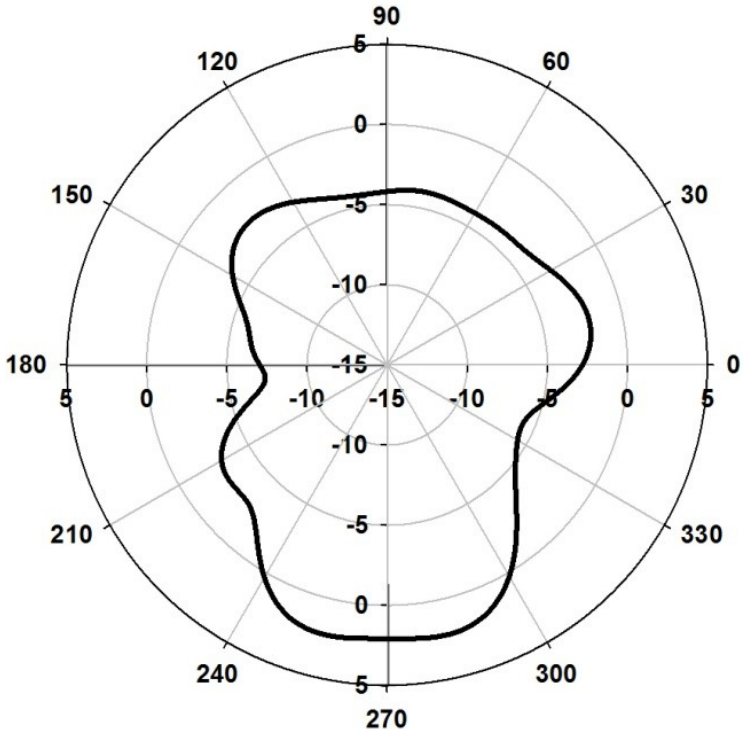

Fig.6-14 Measured radiation pattern in the azimuth plane when diodes 2,3,4 ON

6.5 References

[1] A. Forenza and R. W. Heath, Jr., "Benefit of pattern diversity via two element array of circular patch antennas in indoor clustered MIMO channels," IEEE Trans. Commun., vol. 54, no. 5, pp. 943–954, 2006.

[2] C. Ko , I. Tarn and S. Chung "A compact dual-band pattern diversity antenna by dual-band reconfigurable frequency selective reflectors with a minimum number of switches", IEEE Trans. Antennas Propag., vol. 61, no. 2, pp.646 -654, Jan. 2013.

[3] J. T. Bernhard, *Reconfigurable Antennas*, 1st ed. San Rafael, CA: Morgan & Claypool Publishers, 2007.

[4] D. Piazza, P. Mookiah, M. D'Amico, and K. Dandekar, "Experimental analysis of pattern and polarization reconfigurable circular patch antennas for MIMO systems," IEEE Trans. Veh. Technol., vol. 59, no. 5, pp. 2352–2362, Jun. 2010.

[5] J. Sarrazin, Y. Mahé, S. Avrillon, and S. Toutain, "Pattern reconfigurable cubic antenna," IEEE Trans. Antennas Propag., vol. 57, no. 2, pp. 310–317, Feb. 2009.

[6] Y.-L. Tsai, R.-B. Hwang, and Y.-D. Lin, A reconfigurable beam-switching antenna base on active FSS, In: 15th International Symposium Antenna Technology Application Electromagnetics (ANTEM), Toulouse, France, 2012, pp. 1–4.

[7] Sievenpiper, D., Lijun Zhang; Broas, R.F.J. Alexopolous, N.G. and Yablonovitch, E., "High-Impedance Electromagnetic Surfaces with a Forbidden Frequency Band", IEEE Trans. Microwave Theory and Techniques, vol. 47, no. 11, pp. 2059-2074, Nov. 1999.

[8] Macom Technologies (www.macomtech.com).

CHPATER SEVEN: CONCLUSION AND FUTURE WORK

7.1 Conclusion

In this thesis work, a comprehensive analysis, investigation, and applications of electromagnetic band-gap (EBG) structures in antenna and antenna arrays at millimeter-wave bands have been presented.

As the first objective of the work, mushroom-like EBG structure has been successfully used to enhance the radiation characteristics of aperture-coupled dielectric resonator (DR) antenna operating at the 60 GHz band. Significant gain enhancement was achieved without violating the antenna's other characteristics. Not only the proposed EBG structure mimics the behavior of artificial magnetic conductor around the suggested bandwidth, but it was shown that the proposed EBG structure has a stable in-phase reflection characteristics with respect to different angles of incidence and polarization. Moreover, full analytical model was derived, supported with simulation and experimental results.

A second approach has been introduced to increase the gain of millimeter-wave DR antenna. A millimeter-wave mushroom-like, circular patch EBG (CP-EBG) cell is designed and fabricated. The propagation characteristics of the proposed CP-EBG structure are measured using the asymmetric microstrip line method. A cylindrical DRA incorporating the developed CP-EBG structure is then designed and its performance is evaluated with and without the CP-EBG at the 60 GHz bandwidth. Measurements show a significant improvement in the antenna radiation characteristics when it is surrounded by CP-EBG structure while preserving the gain flatness over the suggested bandwidth .

The other objective of the thesis was to reduce the mutual-coupling between two 60 GHz DR antenna array elements separated by only half of the wavelength. Therefore, a new, compact, easy-to-fabricate uni-planar EBG structure was developed. The transmission characteristics of the proposed EBG structure were thoroughly investigated:

analytically, simulation, and experimentally. Results show the effectiveness of our proposed EBG structure in improving the isolation level. Furthermore, our proposed EBG structure surpasses the other EBG structures reported in the literature in term of both: compactness and effectiveness.

In order to further improve the isolation level between millimeter-wave antenna arrays, a new hybrid isolator was presented. The proposed hybrid isolator consists of an new-concept EBG structure based on stepped-impedance-resonance (SIR) technique, and a thin millimeter-wave choke absorber. It has been shown that with the new hybrid isolator, different sources of mutual-coupling can be delightedly controlled , and hence, significant improvement in the isolation level was achieved.

Finally, a new-concept millimeter-wave EBG-based antenna with pattern reconfigurability has been presented. The main challenge at millimeter-wave frequencies is the number of switching elements needed to achieve pattern reconfigurability. Therefore, the proposed antenna is based on the idea of dividing the EBG unit-cells into six sectors. After that, the EBG sectors are placed symmetrically around the antenna to achieve beam steering in the whole azimuth plane. Each sector is composed of twenty one circular-patch mushroom EBG unit cell. The vias in each sector are connected through thin metallic veins printed on a conductor-backed dielectric slab. The metallic veins are then connected to the ground plane through a switching diode. Each sector is controlled by one diode. The biasing circuit was designed and tested. By switching the diode on and off, the EBG sector band-stop and band-pass properties are changed, yielding beam steering into that sector. Results show flexible and effective beam steering capability in the azimuth plane using minimal number of diodes.

7.2 Future works

There are numerous opportunities for research on electromagnetic band structures applications for antenna applications, especially at millimeter-wave bands, in addition to the investigations presented in this dissertation. For example, antenna radiation topology can be a promising research avenue. In this dissertation, beam steering is achieved only in the azimuth plane. However, sweeping the radiation pattern in both planes; azimuth and elevation, at millimeter-wave bands has not yet been investigated. Three-dimensional beam steering yields more power savings, improve security and maneuver away from jamming.

Besides, the use of other periodic structures to achieve pattern reconfigurability is another possible research topic. Frequency selective surface and metamaterials are good candidates in this area. Furthermore, there is paucity on the design and practical considerations of biasing circuits at millimeter-wave bands. In this dissertation, PIN diodes were used to control the EBG clusters. However, other active devices can be also used, and may lead to better functionality.

Moreover, the experiments reported in this dissertation involved only the antenna/antenna array only. However, the performance of the antenna arrays in some different environments may be substantially different. For example, testing the proposed antenna arrays in multiple-input-multiple-output systems, and measuring the capacity and bit-error-rate of the channel, will give a better insight on the meaning of isolation improvement. Furthermore, it is desirable to understand the antenna array performance in multiple fading channels. This will help us determining the number of elements needed to operate a reliable communication systems in different environments, and the antenna array configuration yields to minimum interference.

Furthermore, the investigations presented in this dissertation considered arrays of two elements only with a simple feeding network and linear configuration. Moving toward

more complex antenna arrays' configurations, requires a careful and sophisticated design of the feeding network. This issue becomes more challenging at millimeter-wave frequencies. Carrying out full design of the antenna array subsystem would aid in more practical insight and functionality.

The continuous demand of higher data-rates and wider bandwidths for personal applications would definitely push the communication industry toward higher and higher frequency bands. Therefore, moving toward higher frequency bands will help us to put our feet in the future.

PUBLICATIONS

Journals

[J1] **M. J. Al-Hasan**, T. A. Denidni, and A. Sebak, "Millimeter-wave EBG-Based Aperture-Coupled Dielectric Resonator Antenna ," IEEE Trans. Antennas Propag vol. 61, no. 8, pp. 4354-4357, August 2013.

[J2] **M. J. Al-Hasan**, T. A. Denidni, and A. Sebak, "Millimeter-wave Compact EBG-Structure for Mutual Coupling Reduction Applications," IEEE Trans. Antennas Propag., vol. 63, no. 2, Feb. 2014.

[J3] **M. J. Al-Hasan**, T. A. Denidni, and A. Sebak, "New Millimeter-wave Hybrid Isolator for Mutual-Coupling reduction in Antenna Arrays," IEEE Trans. Antennas Propag, Accepted with minor revision.

[J4] **M. J. Al-Hasan**, T. A. Denidni, and A. Sebak, "60 GHz EBG-based Dielectric Resonator Antenna with Pattern Diversity,"

[J5] Amjad A. Omar and **M. J. Al-Hasan**, "A Dual-band Coplanar-waveguide fed Slot-coupled Dual Rectangular Dielctric Resonator Antennas," International Journal of Modeling and Simulation, Acta Press, Vol. 31, no. 1, 2011.

[J6] **M. J. Al-Hasan**, T. A. Denidni, A. Sebak, "Angular Stability and Surface-wave Suppression Properties of Millimeter-wave EBG Structure". IEEE Trans. Antennas Propag. Submitted.

Conferences

[C1] **M. J. Al-Hasan**, T. A. Denidni, and A. Sebak "Millimeter-wave FSS-based Dielectric Resonator Antenna with Resonfigurable Radiation Pattern," 2014 IEEE AP-S International Symposium on Antennas and Propagation. Memphis, USA.

[C2] **M. J. Al-Hasan**, T. A. Denidni, and A. Sebak "Millimeter-wave Hybrid Isolator for Mutual-Coupling Reduction Applications," 2014 IEEE AP-S International Symposium on Antenna Technology and Applied Electromagnetics, Victoria, BC, Canada.

[C3] **M. J. Al-Hasan**, T. A. Denidni, and A. Sebak "Millimeter-wave EBG-based Antenna Pattern Diversity," 2013 IEEE AP-S International Symposium on Antennas and Propagation. Orlando, USA.

[C4] **M. J. Al-Hasan**, T. A. Denidni, and A. Sebak "Millimeter-wave Compact EBG Structure for Mutual Coupling Reduction in Dielectric Resonator Antenna Arrays," 2013 IEEE AP-S International Symposium on Antennas and Propagation. Orlando, USA.

[C5] **M. J. Al-Hasan**, T. A. Denidni, and A. Sebak "EBG dielectric resonator antenna with reduced back radiation for millimeter-wave applications ," 2012 IEEE AP-S International Symposium on Antennas and Propagation. Illinios, USA.

[C6] **M. J. Al-Hasan**, T. A. Denidni, and A. Sebak "A UC-EBG base dielectric resonator antenna for millimeter-wave applications," 2011 IEEE AP-S International Symposium on Antennas and Propagation. Spokane, USA.

[C7] A.A. Omar, **M. J. Al-Hasan**, and T. A. Denidni, "Design of a new dual-band dielectric resonator antenna for wireless applications ," 2011 IEEE AP-S International Symposium on Antennas and Propagation. Spokane, USA.

[C8] A.A. Omar and **M. J. Al-Hasan**, "Dual-band Coplanar-waveguide fed Slot-coupled Rectangular Dielctric Resonator Antennas," 2011 ICFCC International Conference on Fututre Computer and Communication, Malysia, USA.